NUMERICAL STUDY ON THE DISPERSION AND DEPOSITION OF PARTICLES IN EVAPORATING SESSILE DROPLETS

A THESIS SUBMITTED TO
THE GRADUATE SCHOOL OF ENGINEERING AND SCIENCE
OF BILKENT UNIVERSITY
IN PARTIAL FULFILLMENT OF THE REQUIREMENTS FOR
THE DEGREE OF
MASTER OF SCIENCE
IN
MECHANICAL ENGINEERING

By
Ali Kerem Erdem
September 2022

NUMERICAL STUDY ON THE DISPERSION AND DEPOSITION OF PARTICLES IN EVAPORATING SESSILE DROPLETS

By Ali Kerem Erdem

September 2022

We certify that we have read this thesis and that in our opinion it is fully adequate, in scope and in quality, as a thesis for the degree of Master of Science.

Luca Biancofiore(Advisor)

Emine Yegân Erdem

Fabian Denner

Approved for the Graduate School of Engineering and Science:

Orhan Arıkan
Director of the Graduate School

ABSTRACT

NUMERICAL STUDY ON THE DISPERSION AND DEPOSITION OF PARTICLES IN EVAPORATING SESSILE DROPLETS

Ali Kerem Erdem
M.S. in Mechanical Engineering
Advisor: Luca Biancofiore
September 2022

Evaporating sessile droplets including dispersed particles are utilized in the coating, printing, and biomedical applications. Modeling this problem is a challenging process, therefore different assumptions are used in the literature. It is important to have a model which covers both pinned and moving contact line regimes for the droplet, thus whole evaporation process and deposition profile can be understood. Therefore, in this work, a numerical and mathematical model is derived to simulate two-dimensional symmetric thin evaporating sessile droplets whose contact line is firstly pinned and then moving. This model is derived by combining different models in literature with the help of lubrication theory and rapid vertical diffusion assumption. This model includes a temporal change in the droplet's surface height, contact line dynamics, particle dispersion, and deposition. The finite difference method is used in the numerical solution. Cases including pinned and moving contact lines in the literature are solved separately by different numerical algorithms developed in this work and these algorithms were combined. This new algorithm first solves a mathematical model in the pinned contact line regime. When the contact angle goes below the defined limit, the second part of the algorithm solves the mathematical model in the moving contact line regime until 95 percent of the total particle mass is deposited. A parametric study has been done with the developed algorithm. A set of parameters is defined and chosen parameters are changed to see their effects. It is observed that increasing the Marangoni number and Capillary number, increased particle accumulation near the center. Decreasing evaporation number and increasing Damkohler number result in more uniform particle deposition.

Keywords: evaporation, sessile droplets, dispersion, deposition, numerical model.

ÖZET

BUHARLAŞAN SAPSIZ DAMLACIKLARDA PARÇACIKLARIN DAĞILMASI VE BİRİKMESİ ÜZERİNE SAYISAL ÇALIŞMA

Ali Kerem Erdem
Makine Mühendisliği, Yüksek Lisans
Tez Danışmanı: Luca Biancofiore
Eylül 2022

Dağılmış parçacıklar içeren buharlaşan sapsız damlacıklar kaplama, baskı ve biyomedikal uygulamalarda kullanılır. Bu problemin modellenmesi zorlu bir süreçtir, bu nedenle literatürde farklı varsayımlar kullanılmaktadır. Damlacık için hem sabitlenmiş hem de hareketli temas hattı rejimlerini kapsayan bir modele sahip olmak önemlidir, böylece tüm buharlaşma süreci ve birikme profili anlaşılabilir. Bu nedenle, bu çalışmada, temas hattı önce sabitlenmiş ve sonra hareket eden iki boyutlu simetrik ince buharlaşan sapsız damlacıkları simüle etmek için sayısal ve matematiksel bir model türetildi. Bu model, literatürdeki farklı modellerin yağlama teorisi ve hızlı dikey difüzyon varsayımı yardımıyla birleştirilmesiyle elde edildi. Bu model, damlacık yüzey yüksekliğinin zamanla değişimini, temas hattı dinamiklerini, parçacık dağılımını ve birikimini içerir. Sayısal çözümde sonlu farklar yöntemi kullanıldı. Literatürde yer alan sabitlenmiş ve hareketli temas hatları içeren vakalar bu çalışmada geliştirilen farklı sayısal algoritmalar ile ayrı ayrı çözüldü ve bu algoritmalar birleştirildi. Bu yeni algoritma, önce sabitlenmiş temas hattı rejiminde bir matematiksel modeli çözer. Temas açısı tanımlanan sınırın altına düştüğünde, algoritmanın ikinci kısmı, toplam parçacık kütlesinin yüzde 95'i birikene kadar hareketli temas hattı rejimindeki matematiksel modeli çözer. Geliştirilen algoritma ile parametrik bir çalışma yapıldı. Bir dizi parametre tanımlandı ve etkilerini görmek için seçilen parametreler değiştirildi. Marangoni sayısı ve Kapiler sayısının artmasının merkeze yakın parçacık birikimini arttırdığı gözlemlendi. Azalan buharlaşma sayısı ve artan Damkohler sayısı, daha düzgün parçacık birikimi ile sonuçlandı.

Anahtar sözcükler: buharlaşma, sapsız damlacık, dağılma, birikme, sayısal model.

Acknowledgement

This work is completed with many people's direct and indirect contributions. First of all, I would like to thank my supervisor Dr. Biancofiore. During this research period, he was always supportive, respectful, and understanding to me. It was a great opportunity for me to work with him and gain experience in my research field.

I would like to thank Dr. Denner for his support and recommendations.

I would like to thank all my colleagues, my research group, and Bilkent Mechanical Engineering Department. Gülce Bayram shared her workstation with me, therefore I am very grateful to her. I had a beneficial discussion with Humayun Ahmed, Omair Mohammed, Hammam Mohammed, Umar Rauf, and Mert Yusuf Çam. I am thanking all of them for their support. I would like to thank Onur Vardar for helping us in terms of improving the speed of our code.

I would like to thank my all family for supporting and encouraging me in doing research. I could not come to this point without their support.

Finally, I acknowledge that this work was supported by The Scientific and Technological Research Council of Turkey (TUBITAK) under project number 120N695.

Contents

List of Figures

List of Tables

Chapter 1

Introduction

Droplets can be seen in different aspects of a daily life and have many application areas in industry and science. The shape of the droplet and its interaction with the environment causes different physical phenomenons and mechanisms. Droplets can sit on solid surfaces which can have different properties. Because of environmental effects, the droplet will evaporate and when it totally dries out, dispersed particle will be deposited on the surface. This mechanism can be useful in different application areas. Therefore, many researchers studied on inner physical mechanisms of the droplets and deposition of solute particles.

One of the famous example of this phenomenon can be called as coffee-ring effect which is emphasized by Deegan et al. [2]. When a droplet of coffee or tea is spilled to some surface, remaining stain's shape is like a ring, because of the inner flow explained by Deegan et al. [2]. Another example will be related to printing technology. In ink-jet printing, ink with solute particles is ejected to the surface and evaporation of ink droplet deposits solute particles on it [3]. Evaporating droplets are also used in biomedical application. In DNA mapping, DNA molecules are deposited into coated solid surface in order to do gene analysis, with the help of evaporation in droplet [4]. The last example will be related to academic research field. In Ni et al. [5], modified version of the capillarity-assisted particle assembly method also uses particle deposition mechanism inside colloidal

droplets.

Mentioned application areas shows that it is important to understand the mechanism inside droplet. Mathematically modeling and numerically simulating evaporating droplets can give important insight about this process. This is a challenging work, because many different physical phenomena must be modeled, and geometry of droplet creates issues at some points. Droplet has contact line which is outer boundary where solid surface, liquid droplet and vapor or gas meets. Modeling this part of the droplet which can also move is quite challenging. In addition, modeling free interface surface where liquid droplet and gas meet is also challenging, because there is a phase change in this part.

There are several mechanisms which control flow inside droplet, contact line movement and deposition of solute particles to surface. Therefore, in the upcoming sections, related important phenomenons will be mentioned briefly.

1.1 Evaporation

Evaporation has important impact on dynamics inside droplet. This physical mechanism affects inner flow and deposition pattern of solute particles. Therefore, different models, assumptions and simplifications related to evaporation will be presented.

In the modeling of evaporation, thermodynamic situation of liquid-gas interface is important. Murisic and Kondic [6] mentions that two assumptions can be made and these are equilibrium and nonequilibrium. These assumptions will affect modeling of relation between pressure and temperature [6]. Property of gas above the liquid droplet is also another important parameter in the modeling of evaporation [6]. The gas above the liquid can be only vapor of the droplet or some gas mixture which includes also vapor [6].

Modeling and solving all phases of problem is hard and challenging, therefore,

different simplification can be made [6]. First one can be ignoring convection of vapor and limiting its movement with diffusion [6]. If there is also dominance of liquid properties to vapor's one, instead of modeling both phases, only liquid phase and diffusion of vapor can be modeled [6]. With some further simplification, diffusion of vapor can be considered as steady-state [6]. If contact line of droplet is pinned, mass flux of evaporation will have certain form [6]. Murisic and Kondic [6] mentions form in Deegan et al. [7] which is interpreted as $J \sim 1/h^{\psi}$. Where, J is mass flux of evaporation, and h is interface height of the droplet.

When contribution of gas phase is almost neglected and only liquid droplet phase is focused this model is named as one-sided model by Burelbach et al. [8]. In this model, nonequilibrium state of interface is used and J will be in the form of $1/(h + B)$, where B is some constant [6]. This model assumes rapid vapor diffusion when there is vapor and some gas mixture, or vapor above the droplet interface does not affect or limit J [6]. This model can be used when some material contaminates liquid-gas interface of droplet or there is only vapor of the droplet above mentioned interface [6].

As a result, both mentioned model indicates that evaporation rate is increasing from center of droplet to contact line for given cases which can be faced in daily life. This behavior will be important for understanding other mechanism in droplet.

1.2 Capillary and Thermo-Capillary Flow

Understanding flow inside the droplet is crucial, because it affects the shape of droplet and the deposition profile of solute particles. For thin droplets, viscous effects, surface tension and evaporation are quite important because, these phenomenon affect the flow inside droplet. Sometimes, competition between different flows affects the deposition pattern of the dispersed particles. Therefore in this part, two major flow regime related to case of this thesis will be explained.

In the previous part, nonuniform evaporation in the droplet was explained. In some cases contact line of droplet is pinned because of some surface irregularities or properties [2]. Deegan et al. [2] showed that higher evaporation rate near the contact line causes more fluid loss in this region which must be replenished to ensure contact line as pinned. In this case, fluid will move from center to contact line [2]. This situation causes some kind of capillary flow and deposits particle to region near contact line [2].

Surface tension in the liquid-gas interface of droplet gives its circular shape. This phenomenon is caused by unbalanced forces in the mentioned interface [9]. Surface tension can depend on temperature, therefore, changes of it in this interface will cause surface tension change or gradient which will cause the inner mechanism called as thermocapillary or Marangoni flow [1, 9, 10]. In the droplet, Marangoni flow will start from from high temperature area, going to low temperature area and again return to high temperature area in a circulatory manner [1]. Temperature difference in the liquid-gas interface of droplet can be caused by nonuniform evaporation along surface, because this situation can create nonuniform cooling along the interface [10].

1.3 Wetting Behaviors and Contact Line Dynamics

Interaction of droplet with surface below it and gas above it affects its geometrical properties. How droplet's contact line will spread is also related to this interaction. Spreading of droplet depend on interfacial tensions between liquid-gas, liquid-solid and solid-gas [11]. In the book of De Gennes et al. [11], this relation is stated as following:

$$S = \gamma_{SA} - (\gamma_{SL} + \gamma_{LA}) \tag{1.1}$$

Where S is spreading parameter, and γ_{SA}, γ_{SL} and γ_{LA} are interfacial tensions

between solid-air, solid-liquid and liquid-air [11]. If S is bigger than 0, droplets spreads and wets surface totally in order to decrease its surface energy [11]. On the other hand, if S is smaller than 0, liquid droplet will partially spreads on the surface and create some equilibrium shape with non-zero contact angle which can be defined as angle between liquid-gas interface of droplet and solid surface at point, where all phases meet [11].

Value of contact angle is a good indicator of surface property about spreading of droplet. The surface will be hydrophilic, when contact angle of droplet is smaller than 90°, otherwise it will be hydrophobic [12]. Wetting of surface will depend on its roughness and chemical composition [12].

With experiments, it is indicated that there is a relation between contact line speed and contact angle [13]. By looking at the contact angle vs contact line speed profile, advancing and receding contact angles can be found [13]. Advancing contact angle is limit, and above it, droplet spreads or advance [13]. Receding contact angle is another limit, and below it, droplet recedes [13]. However, these two contact angle limit will not always be same. If there is a difference between them, this situation is called contact angle hysteresis and in this interval contact line is not moving [13].

By fitting experimental data, some models are used to describe movement of contact line. One of the model used by Ehrhard and Davis [14] is as following:

$$\frac{\partial a}{\partial t} = \kappa(\theta - \theta_A)^m \tag{1.2}$$

Where left hand side is velocity of contact line or temporal derivative of radius of droplet, κ is some constant, m is mobility exponent, θ and θ_A are current contact angle and advancing contact angles [14].

1.4 Particle Deposition

When droplet is evaporating, solute particle inside of it will move with convective and diffusive effects. In addition some of the solute particles can attach to solid surface during this process. Spielman and Friedlander [15] mentions that the effects of London-van der Waals attraction and repulsion of electrical double layer can be used to define interaction between deposition surface and deposited particles. If mentioned interactions are restricted to close enough region of deposition surface, deposition flux (J_{dep}) can be modeled with first order reaction and this can be simply expressed as particle concentration multiplied (c) by some constant related to rate of reaction (k') [15]:

$$J_{dep} = k'c \tag{1.3}$$

1.5 Literature Review For Different Numerical Studies

In previous sections, some brief information about the different mechanisms and the related models in the literature were presented. In this section, numerical and experimental studies about evaporating droplet will be mentioned.

Spreading of volatile and nonvolatile pure droplet is studied by different researchers. Dussan [13, 16] worked on slip boundary condition and relation between contact angle and speed of contact line for pure liquids. Ehrhard and Davis [14] studied spreading of droplet which is nonvolatile, thin and Newtonian. Their model includes, gravity, capillarity and thermocapillarity. To describe contact line motion, they used a constitutive relation derived from experimental results between contact angle and droplet radius speed [14]. Governing equations are simplified with the help of lubrication approximation [14]. They worked on isothermal and non-isothermal cases. They realized that thermocapillarity affects the spreading of droplet in a non-isothermal case [14].

Anderson and Davis [1] studied the steady-state and transient change of droplet interface height profile with the help of lubrication approximation. They looked at the competition between viscous spreading and evaporation [1]. They also proposed a new model related to change of droplet radius [1]. In their article [1], effect of vapor recoil and thermocapillarity is also included. They looked at different cases in terms of capillary number and evaporation constant [1]. They also worked on contact line hysteresis [1].

Ajaev [17] worked on thin evaporating droplet which spreads or recedes on plate heated uniformly. In his mathematical model, there are disjoining pressure, evaporation, thermocapillarity, capillarity and gravity [17]. He run simulation for fully and partially wetting droplets. In the modeling of contact line movement, he used precursor thin film, thus he eliminated many problem about this topic [17].

Nguyen et al. [18] studied theoretically and experimentally the evaporating sessile droplet of water on different surfaces which are made hydrophobic. They got results for droplets with wide and narrow contact angles [18]. They showed the effects of surface properties and contact angle hysteresis to evolution of contact angle, droplet radius, volume of droplet and evaporation [18]. Their experimental and theoretical results [18] are matching with the observation that droplet contact line is pinned initially and after some contact angle value, it is moving. They observed that for the sessile droplet with small contact angle, change of droplet volume can be considered as constant [18]. On the other hand, this situation is not the case when contact angle is large [18].

Amini and Homsy [19] studied moving and pinned contact line for thin evaporating droplet. In their study [19], there are two configuration which are fixed contact line with changing contact angle and moving contact line with fixed contact angle. For moving contact line, they developed algorithm which modifies droplet interface height profile according to changing contact line [19].

Evaporation on droplets and its effects to inner flow field is another interesting research field. Hu and Larson [20, 21] worked on this field. In one of their

article [21], they conducted an experiment and found that water droplet on a glass surface is pinned until 2° to 4° . By referring to this experimental finding, they expressed evaporation of pinned droplet in two regimes [20]. Firstly, pinned droplet is evaporating and contact angle decreases [20]. After reaching some contact angle value, its contact line starts to recede [20]. In this kind of droplets, they studied analytical solution of velocity field inside the droplet with help of Lubrication theory [20]. They assumed that droplet is axisymmetric, pinned and they used small Capillary and Reynolds number [20]. Evaporation is modeled with Laplace equation [20]. In the formulation, they assumed that shear stress is zero at droplet interface, thus, they eliminated Marangoni effect in the flow [20]. They also compared their analytical velocity field results with Finite Element Method (FEM) results [20].

Murisic and Kondic [6] worked on numerical and experimental investigation of evaporation process on sessile droplet. Solid plate under the sessile droplet is smooth enough, therefore contact line of the droplet is not pinned for their case [6]. They got results with two different evaporation models which can be shortly described as equilibrium and non-equilibrium models which are used in research field frequently and compared them with the help of experimental results [6]. They found that suitability of these models is related to used material and how this material is evaporating [6]. They showed that in their experimental setup, non-equilibrium model is more suitable for water droplet, on the other hand, equilibrium model is more suitable for isopropanol droplet which is more volatile [6]. They also evaluated effect of Marangoni [6]. They demonstrated that thermal effects are also important for their case [6].

Some researchers studied about particle concentration, its effects on contact line and different particle deposition patterns. Deegan [7] worked on particle deposition pattern of evaporating pinned droplet. Experiments were done to show pinning process in the evaporating droplet [7]. He also showed that pinning can affect the particle deposition pattern [7]. In other article, Deegan et al. [22] studied accumulation of particle near the contact line experimentally and numerically. They observed that evaporation in pinned droplet causes outward flow to contact line and this situation results in occurrence of ring-like particle

deposition in contact line [22]. They also showed that to keep droplet as pinned, loss of fluid near the contact line region must be compensated, therefore, fluid must be transferred from center to contact line and as a result of this, outward flow is occurring [22]. They observed that this outward flow is moving particles to contact line of droplet and causes accumulation of particle in this region [22].

Fischer [23] studied fluid flow inside axisymmetric droplet with pinned contact line for different evaporation models and effect of evaporation on particle concentration distribution. In his article [23], thermocapillarity and vapor recoil is ignored. In the solution of particle concentration, effect of diffusion is ignored [23]. For different evaporation models, various results emerged. He observed that, deposition place of particles are related to evaporation model because evaporation affects direction of flow inside the droplet [23].

Popov [24] studied evaporating sessile droplet and deposition pattern of particles. They stated that volume of the particles, which is ignored in some other previous work, should also be concerned and this can affect the particle movement [24]. Therefore, particle deposited close to contact line will have some thickness [24]. They did numerical and analytical work on this topic and they compared these results with experimental ones [24].

Hu and Larson [10] studied experimentally and numerically effect of Marangoni flow to particle deposition and flow inside droplet. In experimental part, they measured flow inside droplet and deposition of particle [10]. In numerical simulation, they looked at same phenomena and used Brownian dynamic simulation [10]. As a result of this work, they showed that temperature difference in droplet interface surface causes surface tension gradient and this situation creates circulatory Marangoni flow inside droplet [10]. However, contamination of droplet interface surface is also important [10]. Octane droplet exhibits strong Marangoni flow because of its resistance to surface contamination, on the other hand, water demonstrates weak Marangoni flow because its droplet surface can be easily contaminated [10]. Lastly, they observed that strong Marangoni flow caused particle deposition near the center of octane droplet, on the contrary, weak Marangoni flow did not inhibit coffee-ring deposition and particles mostly deposited near the

contact line of water droplet [10].

Widjaja and Harris [25] studied numerical solution of evaporation of sessile droplet with solute particle deposition to solid plate. In their model, flow inside droplet is modeled with Stokes flow and continuity equation, particle concentration change is model with advection-diffusion equation where both of the term is included and particle deposition is modeled with first order chemical reaction equation [25]. They assumed deposited particle will not return back to sessile droplet [25]. Their numerical results show that particle deposition pattern is affected by evaporation, movement of particle caused by advection-diffusion and particle deposition rate to solid plate [25]. Therefore, arranging necessary parameter related to mentioned physical phenomenon changes the particle deposition pattern [25].

Tarasevich et al. [26] studied gelation of evaporating colloidal droplet. They used similar model as Fischer [23], however, viscosity depends on particle concentration in their model [26]. They modified evaporation model according to gelation of droplet and when particle concentration reaches to gelation limit, evaporation stops [26]. They observed that shape of droplet at the end of simulation depends on initial particle concentration profile, capillary and evaporation numbers [26].

Thokchom et al. [27] worked on numerical and experimental analysis of evaporating sessile droplet which is heated with the help of Infrared light and deposition of dispersed particle in it. In their numerical model, they studied steady-state flow of pinned droplet and included effect of Marangoni and buoyancy on flow inside droplet [27]. In the experimental study, they measured profile of particle concentration and the velocity of fluid [27]. They observed that particle deposition pattern can be changed with external heating of Infrared light, because droplet interface temperature is changing [27].

Karapetsas et al. [28] studied the effect of surfactant adsorbed on the liquid-air interface of droplet. Their model includes lubrication and rapid-vertical diffusion approximations, thus, particle concentration and droplet interface height only

depends on x coordinate and time [28]. They have evolution equations for surfactant, particle concentration and droplet interface height [28]. They showed that surfactant can affect the capillary and Marangoni flow inside droplet [28]. Surfactant can decrease the evaporation rate because it decreases the effective area of droplet's outer interface [28].

Wang et al. [29] studied how particle deposition pattern on confined droplet is affected by confining environment and competition between rate of particle deposition and speed of contact line. They showed that increase in temperature and geometric properties of confining environment affect final particle deposit pattern [29].

Zhang and Akcora [30] studied contact line dynamics for polymer droplet which is colloid, with nano particles in it for different evaporation conditions. They completed some experiment about this topic and measured parameters related to dynamics of contact line [30]. They showed that speed of contact line and contact angle effect deposition characteristic of particles [30].

Pham and Kumar [31] studied numerically evaporating colloidal droplets on surface with considerable roughness. In order to model contact line dynamics, they used disjoining pressure and precursor thin film approach [31]. They showed that even without colloidal particles, irregularity in surface can pin contact line of droplet [31].

1.6 Aim and Layout of Thesis

After literature review, it was realized that, for one dimensional model, getting evolution equation with the help of lubrication theory and combining it with advection-diffusion equation for dispersed particle is popular and there are many findings about it. In most of these cases, the contact line is either assumed pinned or moving. For moving case, it is observed that the precursor thin film and constitutive equation derived from experimental data are used frequently. Most of

the results observed in literature are focusing on one part of the problem in detailed. Combining these approaches and deriving a model which considers all of droplet's life without constraining contact line movement to one regime and depositing particle during evaporation process can be beneficial. Therefore, the main aim of this thesis is developing numerical model for dispersed particle deposition in evaporating thin sessile droplet and conducting some parametric study about deposition pattern. For this purpose, different models in literature will be merged in order to develop both a mathematical and a numerical model which will govern the droplet behaviors about contact line movement, which includes both pinned and moving approach, droplet interface height change, particle dispersion and deposition.

The layout of thesis will be as following. In chapter 2, the governing equations, constitutive relations, boundary conditions, scaling and assumptions will be explained to present mathematical model. In chapter 3, the solutions of equation and necessary numerical algorithm will be described to explain numerical modeling. In chapter 4, results of validation cases and new numerical algorithm will be presented and discussed. In chapter 5, conclusion will be made and future works will be described.

Chapter 2

Mathematical Modeling

In this chapter, mathematical modeling of incompressible, two dimensional, symmetric droplet, which is on solid surface which has uniform temperature, will be presented. Its vapor is above the droplet. Cartesian coordinates will be used in this modeling. Explanatory scheme of problem can be seen in Figure 2.1:

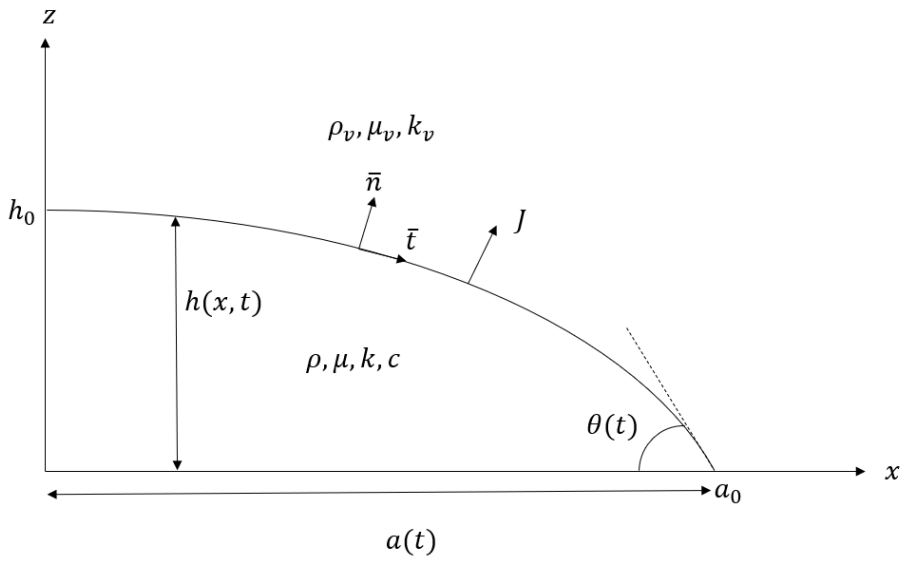

Figure 2.1: Explanatory Scheme of Problem

In Figure 2.1, ρ, μ, k, c are density, dynamic viscosity, thermal conductivity

and particle concentration of droplet. Subindices v indicates that this properties belong to vapor of the droplet. $a(t), h(x,t),$ and θ are radius, interface height, and contact angle of droplet. J represents evaporative mass flux. $\bar{n}$ and $\bar{t}$ are unit normal and tangential vector on droplet interface surface.

A general practical application contains liquid and vapor phases. Solving and modeling both of them are hard processes. Therefore, one-sided model [8] will be used. In this model, it is assumed that viscosity, density and conductivity of liquid droplet are much bigger than same properties of vapor [8]. Therefore, contribution of physical properties of vapor can be ignored and only liquid phase can be modeled [8]. As in Burelbach et al. [8], density of vapor will be kept, because multiplication of vapor density and velocity can be considerable due to possibility of large vapor velocity.

Main aim of modeling droplet is observing how liquid-vapor interface, contact line, solute particle concentration and deposition profiles are changing with time. Therefore, equations for temporal evolution of droplet's interface height, particle concentration and contact line will be derived. In derivation and modeling of these equations, common methodology used by different researchers [28, 8, 1, 14] will be followed.

Governing equations for mathematical modeling of thin droplet will be simplified with lubrication theory and it will be assumed that $\frac{h_0}{a_0} = \epsilon << 1$. This will allow to get partial differential equation that models the droplet interface height change in time. The contact line speed will be modeled, according to methodology in Anderson and Davis [1].

Motion of solute particle inside the droplet will be modeled with advection-diffusion equation. For this purpose, methodology in Karapetsas et al. [28] will be followed. In addition, rapid vertical assumption in same article [28] will be used. With this assumption, advection-diffusion equation can be simplified more and component of particle concentration which only depends on x and t, will be solved in numerical simulation. Lastly, methodology in Widjaja and Harris [25] for solute particle deposition to solid surface will be adopted to particle

concentration equation.

2.1 Governing Equations and Boundary Conditions

In this section, all governing equations, constitutive relations and boundary conditions related to problem will be presented. These equations, relations and conditions are adopted from different articles in literature [1, 8, 14, 25, 28].

Firstly, flow and thermodynamics inside the droplet will be modeled. Navier-Stokes continuity, momentum and energy Equations will be used for this purpose. In the modeling, two dimensional Cartesian x and z coordinates will be used. Therefore, y components of related parameters will be ignored. Effect of gravity will be not considered in this modeling. As a result, governing equations with mentioned assumptions will be following:

$$\rho\frac{\partial\bar{U}}{\partial t} + \rho\bar{U}.\nabla\bar{U} = \nabla.\bar{T} \tag{2.1}$$

$$\nabla.\bar{U} = 0 \tag{2.2}$$

$$\rho c_p\left(\frac{\partial T}{\partial t} + \bar{U}.\nabla T\right) = k\nabla^2 T \tag{2.3}$$

In these equations, $\bar{U} = (u, w)$ is velocity vector where u and w are x and z components of velocity. t, T and c_p are time, temperature and specific heat. $\bar{T}$ is stress tensor and version of it in Burelbach et al. [8] will be followed:

$$\bar{T} = -p\bar{I} + 2\mu\bar{\tau} \tag{2.4}$$

Where p is pressure, $\bar{I}$ is identity tensor and $\bar{\tau}$ is rate of deformation tensor of liquid droplet [8]. μ will depend on c and can be modeled as following [32, 33]:

$$\mu = \mu_0 \left(1 - \frac{c}{c_\infty}\right)^{-2} \tag{2.5}$$

In equation 2.5, μ_0 is dynamic viscosity of droplet without particle concentration and c_∞ is maximum packing value of solute particles. c_∞ depends on shape and size of particles [28]. In addition, configuration of solute particles packing, can also affect this parameter [28]. From equation 2.5, it can be seen that dynamic viscosity goes to infinity, when the solute particle concentration approaches to maximum packing limit, therefore as indicated in Karapetsas et al. [28], this model works well in dilute solutions where c is small.

As indicated before, temporal change of solute particle concentration inside droplet will be modeled with advection-diffusion equation and it will be as following, where D_c is diffusion coefficient [28]:

$$\frac{\partial c}{\partial t} + \bar{U}.\nabla c = D_c \nabla^2 c \tag{2.6}$$

After mentioning governing equation related to flow, thermodynamics and particle concentration change, model about contact line of the droplet can be described. As indicated before, methodology used in Anderson and Davis [1] will be followed. In this model, radius of droplet is affected by contact angle and evaporation at contact line. For the contribution of contact angle, Anderson and Davis [1] used constitutive relation between contact angle and fluid velocity at contact line based on experimental data. For the contribution of evaporation, mass balance at contact line is used by them [1]. These two effects are superposed and as a result of this, expression for droplet contact line speed will be as following [1]:

$$\frac{\partial a}{\partial t} = -\frac{J(a)}{\rho sin\theta} + \eta f(\theta) \tag{2.7}$$

In equation 2.7, η is constant and $f(\theta)$ is a piece-wise function which shows contribution of contact angle to contact line speed [1]. This function is defined

as following [1]:

$$f(\theta) = \left\{ \begin{array}{ll} (\theta - \theta_A)^m, & \text{if } \theta > \theta_A \\ 0 \quad , & \text{if } \theta_A > \theta > \theta_R \\ (\theta - \theta_R)^m, & \text{if } \theta_R > \theta \end{array} \right\} \tag{2.8}$$

In this function, θ_A and θ_R are advancing and receding contact angles, m is mobility exponent and η is constant [1]. As in Anderson and Davis [1], m will be equal to 3. This function is expanded version of equation 1.2 where receding and contact angle hysteresis effects are also included. In equation 2.7, effect of evaporation contributes to receding of contact line. Second term in right hands will contribute to advancing or receding of droplet, according to contact angle.

After presenting governing equations for different phenomenons in droplet, surface tension, evaporative mass flux and particle deposition flux to solid surface must be also defined. For this purpose, constitutive relations related to mentioned parameters will be explained. Solute particle deposition will be exception, its constitutive relation will be explained at the end of this section with related boundary condition. In the first chapter, relation between temperature and surface tension is explained. To model this relation, constitutive equation commonly used in literature [1, 8, 14], will be followed. In this model, there is linear relationship between surface tension and local droplet interface temperature:

$$\sigma = \sigma_0 - \gamma(T_I - T_S) \tag{2.9}$$

In equation 2.9, T_I and T_S are local temperature at liquid-vapor interface of droplet and saturation temperature [1]. Surface tension value at T_S is called as σ_0 [8]. γ is constant and positive [1].

For evaporative mass flux, constitutive relation in Burelbach et al. [8] will be used. In this equation, there is similar linear relation between evaporative mass flux and local droplet interface temperature:

$$J = \left(\frac{\alpha \rho_v L}{T_s^{3/2}}\right)\left(\frac{M_w}{2\pi R_g}\right)^{1/2}(T_I - T_S) \tag{2.10}$$

Where α is accommodation coefficient, L is latent heat, R_g is universal gas constant and M_w is molecular weight [8]. Following the same approach in Anderson and Davis [1], $\left(\frac{T_s^{3/2}}{\alpha \rho_v L}\right)\left(\frac{2\pi R_g}{M_w}\right)^{1/2}$ will be named as K^*. As a result of this, constitutive equation will be as following:

$$K^* J = (T_I - T_S) \tag{2.11}$$

Boundary conditions are needed for deriving temporal evolution of h and c. Therefore, in this section, relevant boundary condition of problem will be explained. These conditions are taken from different resources in the literature [1, 8, 14, 28]. For two dimensional geometry, boundary conditions at $x = 0$, $x = a(x,t)$, $z = 0$ and $z = h(x,t)$ will be presented. Droplet is symmetric and smooth at $x = 0$, therefore following boundary condition will be used:

$$\frac{\partial h}{\partial x} = \frac{\partial^3 h}{\partial x^3} = \frac{\partial c}{\partial x} = 0 \tag{2.12}$$

Following boundary condition will be used in contact line where $x = a(t)$:

$$\frac{\partial h}{\partial x} = -\theta, \quad h = 0, \quad c = 0 \tag{2.13}$$

There will be several boundary conditions for liquid-vapor interface where $z = h(x,t)$. First one will be related to kinematic boundary condition and dimensional version of it according to Burelbach et al. [8] will be used:

$$\left(w - \frac{\partial h}{\partial t} - \frac{\partial h}{\partial x}u\right)\left(\frac{1}{\sqrt{1 + \left(\frac{\partial h}{\partial x}\right)^2}}\right) = \frac{J}{\rho} \tag{2.14}$$

Next one will be related to balance between gradient of surface tension and jump of shear stress [8]. Following shear stress boundary condition will be used:

$$\bar{T}.\bar{n}.\bar{t} = \nabla\sigma.\bar{t} \tag{2.15}$$

Following normal and tangential unit vectors will be used in relevant boundary conditions [8]:

$$\bar{n} = \left(\frac{-\frac{\partial h}{\partial x}}{\sqrt{1 + \frac{\partial h}{\partial x}^2}}, \frac{1}{\sqrt{1 + \frac{\partial h}{\partial x}^2}} \right) \tag{2.16}$$

$$\bar{t} = \left(\frac{1}{\sqrt{1 + \frac{\partial h}{\partial x}^2}}, \frac{\frac{\partial h}{\partial x}}{\sqrt{1 + \frac{\partial h}{\partial x}^2}} \right) \tag{2.17}$$

Next boundary condition will be related to balance between jump of normal stress and surface tension multiplied by two times curvature [8]. Following normal stress boundary will be used [8]:

$$-\frac{J^2}{\rho_v} - \bar{T}.\bar{n}.\bar{n} = 2H\sigma \tag{2.18}$$

$$2H = \nabla.\bar{n} \tag{2.19}$$

Following Jump energy boundary condition will be used [8] at liquid-gas interface:

$$J(L + \frac{1}{2}\left(\frac{J}{\rho_v}\right)^2) = -k\nabla T \tag{2.20}$$

For particle concentration, following form of boundary condition will be used [28]:

$$D_c(\bar{n}.\nabla c) = \frac{J}{\rho}c \tag{2.21}$$

At solid-liquid interface, slip boundary condition will be used for x component of velocity because with moving contact line, no-slip boundary condition will cause force singularity [16]. Slip boundary condition will be as following [14]:

$$u = \beta^* \frac{\partial u}{\partial z} \tag{2.22}$$

Where β^* is slip coefficient [1].

Z component of velocity will be zero and temperature will be uniform at liquid-solid interface:

$$w = 0 \quad T = T_P \tag{2.23}$$

Dispersed particle will be deposited solid substrate. For this purpose, dimensional of version it in Widjaja and Harris, will be used [25]:

$$D_c(\bar{n}.\nabla c) = -k_d c \tag{2.24}$$

Where k_d is deposition rate constant [25]. In Widjaja et al. [25], there is nondimensional version of this boundary condition. According to their parameter, it became dimensional, and written here in this format.

In Widjaja and Harris [25], dimensional version of constitutive equation for particle deposition is not presented. By looking at their methodology, particle deposition flux ($J_p(x,t)$) is assumed as nondimensional version of right hand side of equation 2.24 in their paper [25]. Although, their methodology [25] will be used, constitutive relation will be a little bit different in terms of expression because scaling will be different for this thesis and extra assumption for c will be made.

2.2 Lubrication Theory and Scaling

Modeled sessile droplet is thin enough therefore ratio of its maximal interface height to its radius will be small. In this case, $\epsilon << 1$, and to simplify governing equations, frequent application of lubrication theory in different articles [1, 14] will be followed. To make parameter nondimensional, general viscous scales for lubrication theory mentioned in different articles [1, 28] will be followed.

x, z, h and θ will become nondimensional with initial radius of droplet (a_0), and initial maximum droplet height (h_0):

$$x^* = \frac{x}{a_0}, \quad z^* = \frac{z}{h_0}, \quad h^* = \frac{h}{h_0}, \quad \Theta = \frac{\theta}{\epsilon} \tag{2.25}$$

Velocity components are nondimensionalized with characteristic velocity $u_c = \frac{\nu_0}{h_0}$, where ν_0 is kinematic viscosity in the absence of particle concentration and time is nondimensionalized with ratio of initial radius to characteristic velocity:

$$u^* = \frac{u}{u_c}, \quad w^* = \frac{w}{u_c \epsilon} \quad t^* = \frac{t}{\frac{a_0}{u_c}} \tag{2.26}$$

Pressure, evaporative mass flux, temperature and particle concentration will be scaled in following way:

$$p^* = \frac{p}{\frac{\rho \nu_0 u_c a_o}{h_0^2}}, \quad J^* = \frac{J}{\frac{k \Delta T}{h_0 L}}, \quad T^* = \frac{T - T_S}{\Delta T} \quad c^* = \frac{c}{c_i} \tag{2.27}$$

Where c_i is initial particle concentration and $\Delta T = T_P - T_S$. By using mentioned scales and lubrication theory, governing equations and boundary conditions will be simplified. Detailed explanation of this process can be found in Appendix A. Superscript "*" will be abandoned to ease writing and after this point written parameters will be nondimensional:

$$-\frac{\partial p}{\partial x}+\frac{\partial}{\partial z}\left(\tilde{\mu}\frac{\partial u}{\partial z}\right)=0 \qquad \left(\tilde{\mu}=\left(1-\frac{c_i}{c_\infty}c\right)^{-2}\right) \tag{2.28}$$

$$-\frac{\partial p}{\partial z}=0 \tag{2.29}$$

$$\frac{\partial u}{\partial x}+\frac{\partial w}{\partial z}=0 \tag{2.30}$$

$$\frac{\partial^2 T}{\partial z^2}=0 \tag{2.31}$$

$$\frac{\partial c}{\partial t}+u\frac{\partial c}{\partial x}+w\frac{\partial c}{\partial z}=\frac{1}{Pe}\left(\frac{\partial^2 c}{\partial x^2}+\frac{1}{\epsilon^2}\frac{\partial^2 c}{\partial z^2}\right) \qquad \left(Pe=\frac{u_c a_0}{D_c}\right) \tag{2.32}$$

In equation 2.32, Pe is Peclet number and it measures ratio of convection to diffusion for particle concentration [28].

$$\frac{da}{dt}=-\frac{EJ(a)}{\Theta}+\eta^* f(\Theta) \tag{2.33}$$

Where $\eta^*=\frac{\eta h_0 \epsilon^3}{\nu_0}$ and $E=\frac{k\Delta T}{\epsilon\rho\nu_0 L}$. E is evaporation number which can be considered as ratio between slow viscous time scale and evaporative time scale. It is a measure about power of evaporation on droplet [1]. In $f(\Theta)$, scaled versions of advancing and receding contact angles will be $\Theta_A=\frac{\theta_A}{\epsilon}$ and $\Theta_R=\frac{\theta_R}{\epsilon}$.

Scaled boundary conditions at $x=0$ will be as following:

$$\frac{\partial h}{\partial x}=\frac{\partial^3 h}{\partial x^3}=\frac{\partial c}{\partial x}=0 \tag{2.34}$$

Scaled boundary conditions at $x=a(t)$ will be as following:

$$\frac{\partial h}{\partial x}=-\Theta, \quad h=0, \quad c=0 \tag{2.35}$$

Scaled boundary conditions at $z=0$ will be as following:

$$u = \beta \frac{\partial u}{\partial z}, \quad \left(\beta = \frac{\beta^*}{h_0}\right) \quad w = 0, \quad T = 1, \quad \frac{\partial c}{\partial z} = Da\epsilon c \left(Da = \frac{k_d a_0}{D_c}\right) \tag{2.36}$$

Da is Damkohler number which shows the ratio of particle deposition rate to particle diffusion rate [25].

Scaled boundary conditions at $z = h$ will be as following:

$$w - \frac{\partial h}{\partial t} = \frac{\partial h}{\partial x} u + EJ \tag{2.37}$$

$$p = \frac{E^2}{\tilde{\rho}} J^2 - Ca^{-1} \frac{\partial^2 h}{\partial x^2} \tag{2.38}$$

$$\frac{\partial u}{\partial z} = -\frac{M}{\tilde{\mu}} \left(\frac{\partial T}{\partial x} + \frac{\partial T}{\partial z} \frac{\partial h}{\partial x}\right) \tag{2.39}$$

$$J = -\frac{\partial T}{\partial z} \tag{2.40}$$

$$D_c \left(-\frac{\partial h}{\partial x} \frac{\partial c}{\partial x} + \frac{1}{\epsilon^2} \frac{\partial c}{\partial z}\right) = \frac{1}{\epsilon^2} \frac{k \Delta T}{\rho L} Jc \tag{2.41}$$

Scaled constitutive equation for J at $z = h$ will be as following:

$$T = KJ \tag{2.42}$$

In equations 2.37-2.42, $\tilde{\rho}$ is ratio of vapor density to liquid density, Ca is Capillary number which measures ratio between viscous stress to surface tension stress [9], M is Marangoni number and K is nonequilibrium parameter which is a degree of nonequilibrium in liquid-air interface [8]. Their expressions are as followings:

$$\tilde{\rho} = \frac{1}{\epsilon^3} \frac{\rho_v}{\rho} \tag{2.43}$$

$$Ca = \frac{1}{\epsilon^3} \frac{\rho \nu_0^2}{h_0 \sigma_0} \tag{2.44}$$

$$M = \epsilon \frac{\gamma \Delta T h_0}{\mu_0 \nu_0} \tag{2.45}$$

$$K = \frac{K^* k}{h_0 L} \tag{2.46}$$

2.3 Rapid Vertical Diffusion Assumption

Karapetsas et al. [28] assumed rapid vertical diffusion for their particle concentration equation. This will be followed to eliminate two dimensional dependence of particle concentration. According to rapid vertical diffusion, particle concentration is written with two components. One of them does not depend on z and other one is fluctuation [34, 35]:

$$c(x, z, t) = c_0(x, t) + \epsilon^2 Pe c_1(x, z, t) \tag{2.47}$$

In this assumption $\epsilon^2 Pe << 1$ and height averaged fluctuations is equal to zero [35]:

$$\bar{c_1} = \frac{1}{h} \int_0^h c_1 dz = 0 \tag{2.48}$$

If this expansion applied to equation 2.32 with particle concentration boundary conditions 2.36,2.41 and indicated equation is averaged in height, then, following equation will be derived:

$$\frac{\partial c_0}{\partial t} + \bar{u} \frac{\partial c_0}{\partial x} = \frac{1}{Pe} \frac{\partial^2 c_0}{\partial x^2} + \frac{1}{h} \left(\frac{1}{Pe} \frac{\partial h}{\partial x} \frac{\partial c_0}{\partial x} + EJ c_0 - \frac{Da}{\epsilon Pe} c_0 \right) \tag{2.49}$$

Derivation of equation 2.49 can be found in Appendix A. With this assumption, z component of particle concentration is eliminated, thus, c_0 is solved in advection-diffusion equation. Equation 2.47 is also substituted to viscosity and by assuming $\epsilon^2 Pe << 1$, it becomes:

$$\tilde{\mu} = \left(1 - \frac{c_i}{c_\infty} c_0\right)^{-2} \tag{2.50}$$

As a result of this $\tilde{\mu}$ will only depend on x. Therefore, in scaled x-momentum equation 2.28, derivative of $\tilde{\mu}$ in terms of z will be canceled, and its final form will be as following:

$$-\frac{\partial p}{\partial x} + \tilde{\mu}\frac{\partial u^2}{\partial z^2} = 0 \tag{2.51}$$

For deposition of particle concentration to solid plate, equation at Widjaja et al. [25] is followed. However, with different scaling and rapid vertical diffusion, instead of using only multiplication of Da and c terms, equation has changed. While applying rapid vertical diffusion, extra terms are added in decomposition of c. Therefore, particle deposition flux becomes following expression:

$$J_p(x,t) = \frac{Da}{\epsilon Pe} c_0 \tag{2.52}$$

After this point, c_0 will be written as c to ease writing the equations and it will depend on x and t. Another important topic is related to particle deposition term ($\frac{Da}{h\epsilon Pe}c$) in equation 2.49. In order to cancel c_1 term, it is assumed that Da is same order of magnitude as ϵPe. Mathematical derivation of equation 2.49 can be found in Appendix A and this derivation shows why mentioned assumption is made.

2.4 Derivation of The Droplet Interface Height Equation

In the derivation of h equation, method used by different sources [1, 14] in literature is followed. Firstly, by integrating equation 2.31 two times, and substituting

relevant boundary conditions in 2.36 and 2.40, analytical expression for temperature is found:

$$T = 1 - Jz \tag{2.53}$$

J can be found by evaluating equation 2.53 at $z = h(x,t)$ and using constitutive equation 2.42:

$$J = \frac{1}{K + h} \tag{2.54}$$

After finding J and T, continuity equation 2.30 can be integrated from 0 to h and z component of velocity can be found at $z = h$:

$$\int_0^h \frac{\partial w}{\partial z} dz = -\int_0^h \frac{\partial u}{\partial x} dz \tag{2.55}$$

$$w|_{z=h} - w|_{z=0} = -\int_0^h \frac{\partial u}{\partial x} dz \tag{2.56}$$

From relevant boundary condition 2.36, $w|_{z=0} = 0$, therefore:

$$w|_{z=h} = -\int_0^h \frac{\partial u}{\partial x} dz \tag{2.57}$$

Substitute equation 2.57 to kinematic boundary condition 2.37:

$$-\int_0^h \frac{\partial u}{\partial x} dz - \frac{\partial h}{\partial t} = u\frac{\partial h}{\partial x} + EJ \tag{2.58}$$

According to Leibniz's theorem about differentiation in integral [9]:

$$\int_0^h \frac{\partial u}{\partial x} dz = \frac{\partial}{\partial x}\left(\int_0^h u dz\right) - u|_{z=h}\frac{\partial h}{\partial x} \tag{2.59}$$

Equation 2.59 can be applied to integration in equation 2.58 and equation becomes:

$$-\frac{\partial}{\partial x}\left(\int_0^h u dz\right) + u\frac{\partial h}{\partial x} - \frac{\partial h}{\partial t} = u\frac{\partial h}{\partial x} + EJ \tag{2.60}$$

After doing cancellations, droplet interface height equation is :

$$\frac{\partial h}{\partial t} + EJ + \frac{\partial}{\partial x}\left(\int_0^h u dz\right) = 0 \tag{2.61}$$

Equation 2.61 can be written with height averaged velocity $\bar{u}$:

$$\frac{\partial h}{\partial t} + EJ + \frac{\partial}{\partial x}\left(h\bar{u}\right) = 0 \tag{2.62}$$

$\bar{u}$ can be found by deriving u and averaging. Method in Ehrhard et al. [14] is followed to derive u. Detailed mathematical derivation is explained in Appendix A:

$$\bar{u} = 2\frac{\partial h}{\partial x}\frac{E^2 h\left(\frac{h}{3}+\beta\right)}{\tilde{\mu}\tilde{\rho}(K+h)^3} + \frac{\partial^3 h}{\partial x^3}\frac{h\left(\frac{h}{3}+\beta\right)}{\tilde{\mu}Ca} + \frac{\partial h}{\partial x}\frac{MK\left(\frac{h}{2}+\beta\right)}{\tilde{\mu}(K+h)^2} \tag{2.63}$$

Without particle concentration, equation 2.62 will be exactly same as h equation in Anderson and Davis [1]. This situation is not coincidence because most of the model is taken from Anderson and Davis [1], only particle concentration dependent viscosity is added. As in Anderson and Davis [1], in height averaged x-component of velocity, term with $\frac{E^2}{\tilde{\rho}}$ will be named as vapor recoil term, term with $\frac{1}{Ca}$ will be named as curvature term, and term with M will be named as thermocapillarity term.

Anderson and Davis [1] mentions important equation related to mass of the droplet. The droplet should only loses mass because of evaporation and mathematical expression of this argument is as following [1]:

$$\int_0^{a(t)} \left(\frac{\partial h}{\partial t} + EJ \right) dx = 0 \tag{2.64}$$

Summation of total temporal change along x in h and total change along x caused by evaporation should be zero, therefore, droplet will only lose mass by evaporation. In this chapter, mathematical modeling is described. In the next chapter, numerical methodology, which will solve the set of equations, will be introduced.

Chapter 3

Numerical Method

In this chapter, methodology for numerically solving the derived equation for different parameters will be explained. There are three temporal evolution equation, one criterion and deposition of solute particles. Therefore, this chapter is divided to sections for presenting numerical methods for different part of the problem.

Firstly, numerical methodology will be described for solution of equations related to main parameters. Temporal evolution of h and c are formulated as partial differential equations. Change of droplet radius in time is described with ordinary differential equation in which contact angle is main variable. These equations will be solved with Finite Difference Method (FDM). Time and space discretization of equations in FDM will be presented.

Secondly, integration of boundary conditions to discretization of equation in space will be explained. Derived equations for h and c are one dimensional and therefore boundary condition in x direction must be considered. For this purpose, numerical implementation of boundary conditions at symmetry and contact line will be explained.

Lastly, numerical methodology about simultaneous solution of all equations will be explained. Height averaged velocity is utilized in temporal change of h and c. It contains nondimensional viscosity, therefore, it depends on both c

and h. In this case, equations for h and c are coupled. Temporal evolution of droplet radius depends on contact angle which depends on h. Therefore, h affects calculation of a. In the mean time, criterion related to mass of droplet and deposition of particle must be concerned. While solving all the mentioned equation, changing mesh through the time must also be considered. Therefore, this process is quite hard and challenging. How all these calculations are made together will be presented for different cases of the problem.

3.1 Discretization

As a reminder, partial and ordinary differential equations for main parameters are as following:

$$\frac{\partial h}{\partial t} + EJ + \frac{\partial}{\partial x}\left(h\bar{u}\right) = 0 \tag{3.1}$$

$$\frac{\partial c}{\partial t} + \bar{u}\frac{\partial c}{\partial x} = \frac{1}{Pe}\frac{\partial^2 c}{\partial x^2} + \frac{1}{h}\left(\frac{\frac{\partial h}{\partial x}\frac{\partial c}{\partial x}}{Pe} + EJc - \frac{Da}{\epsilon Pe}c\right) \tag{3.2}$$

$$\frac{da}{dt} = -\frac{EJ(a)}{\Theta} + \eta^* f(\Theta) \tag{3.3}$$

Geometrical domain of problem must be discretized to solve equation 3.1 - 3.3. h and c are one dimensional parameters, therefore, domain is divided point-wise in x direction to establish mesh. Figure 3.1 shows discretization process of droplet.

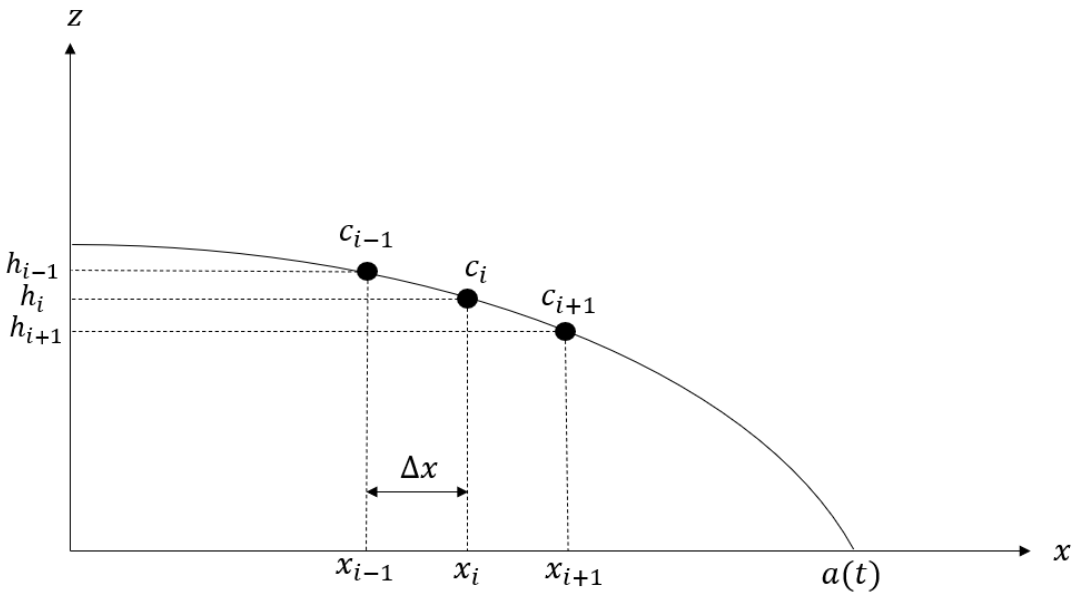

Figure 3.1: Numerical Scheme of Problem

In Figure 3.1, i is label of point in domain and it is used in subscript to indicate that parameters belong to specified point. Points are located in liquid-vapor interface for display purposes, problem is still one dimensional for c and h. n will represent number of subdomain in current configuration, therefore there will be $n+1$ points. Parameters for discretized geometry will be $[h_0, h_1, h_2, ..., h_{n-1}, h_n, h_{n+1}]$, $[c_0, c_1, c_2, ..., c_{n-1}, c_n, c_{n+1}]$ and $[x_0, x_1, x_2, ..., x_{n-1}, x_n, x_{n+1}]$. Δx will be distance between two consecutive point in the x direction. Δx will be constant through geometry because domain is divided uniformly. Following equations related to h and c can be written for each point in the problem domain:

$$\frac{\partial h_i}{\partial t} + EJ + \frac{\partial}{\partial x}\left(h_i \bar{u}\right) = 0 \tag{3.4}$$

$$\frac{\partial c_i}{\partial t} + \bar{u}\frac{\partial c_i}{\partial x} = \frac{1}{Pe}\frac{\partial^2 c_i}{\partial x^2} + \frac{1}{h}\left(\frac{\frac{\partial h}{\partial x}\frac{\partial c_i}{\partial x}}{Pe} + EJc_i - \frac{Da}{\epsilon Pe}c_i\right) \tag{3.5}$$

J and $\bar{u}$ are evaluated at h_i and c_i in given equations. If these equations are written for all points in the domain, there will be system of initial value problems which contains $n+1$ equation for h and c. Equations 3.4 and 3.5 will be solved

in time and spatial domain with FDM. Time domain will be discretized with Runge-Kutta 4th Order Method (RK4). Spatial domain will be discretized with Central Difference and Backward Difference Method.

3.1.1 Time Discretization

Numerical method textbook [36] will be followed in the implementation of RK4. In order to apply this method, equations 3.4 and 3.5 will be written in following format:

$$\frac{\partial h_i}{\partial t} = f(h_i(x,t), c_i(x,t)) \tag{3.6}$$

$$\frac{\partial c_i}{\partial t} = f(h_i(x,t), c_i(x,t)) \tag{3.7}$$

In equations 3.6 and 3.7, functions at right-hand sides depend on $h(x,t)$ and $c(x,t)$. Therefore, these equations are coupled. Before, implementing RK4, they will be decoupled with following approach: In equation 3.6, c_i values and its derivatives will be considered as constant and current time step value of particle concentration (c_i^t) will be used. Superscript represents time step. In equation 3.7, $h(x,t)$ and its derivatives will be considered as constant and next time step value of droplet interface height ($h_i^{t+\Delta t}$) will be used, because these values have already been calculated. Δt represents time step size.

After decoupling the equations, according to RK4 [36], following discretized forms will be used:

$$h_i^{t+\Delta t} = h_i^t + \frac{(k_{1,h} + 2k_{2,h} + 2k_{3,h} + k_{4,h})\Delta t}{6} \tag{3.8}$$

$$c_i^{t+\Delta t} = c_i^t + \frac{(k_{1,c} + 2k_{2,c} + 2k_{3,c} + k_{4,c})\Delta t}{6} \tag{3.9}$$

Where $k_{1,h}, k_{2,h}, k_{3,h}, k_{4,h}$ will be [36]:

$$
\begin{aligned}
k_{1,h} &= f(h_i(t)) \\
k_{2,h} &= f(h_i(t) + \frac{1}{2}k_{1,h}\Delta t) \\
k_{3,h} &= f(h_i(t) + \frac{1}{2}k_{2,h}\Delta t) \\
k_{4,h} &= f(h_i(t) + k_{3,h}\Delta t)
\end{aligned}
\tag{3.10}
$$

With similar approach, $k_{1,c}, k_{2,c}, k_{3,c}, k_{4,c}$ will be [36]:

$$
\begin{aligned}
k_{1,c} &= f(c_i(t)) \\
k_{2,c} &= f(c_i(t) + \frac{1}{2}k_{1,c}\Delta t) \\
k_{3,c} &= f(c_i(t) + \frac{1}{2}k_{2,c}\Delta t) \\
k_{4,c} &= f(c_i(t) + k_{3,c}\Delta t)
\end{aligned}
\tag{3.11}
$$

For equation about a, similar RK4 approach will be used. It will be written in following format:

$$
\frac{\partial a}{\partial t} = f(\Theta(t)) \tag{3.12}
$$

Function in right-hand side of equation 3.12 depends on Θ. Therefore, intermediate time step values of contact angle must be calculated for RK4. h profiles of intermediate time steps is calculated, as indicated in Equation (3.10), therefore, necessary Θ values can be calculated with following boundary condition:

$$
\frac{\partial h}{\partial x} = -\Theta \tag{3.13}
$$

According to this approach, discretized equation is as following:

$$
a^{t+\Delta t} = a^t + \frac{(k_{1,a} + 2k_{2,a} + 2k_{3,a} + k_{4,a})\Delta t}{6} \tag{3.14}
$$

Superscript represents time step and $k_{1,a}, k_{2,a}, k_{3,a}, k_{4,a}$ will be:

$$\begin{aligned}
k_{1,a} &= f(\Theta_{1,a}) = f(-\frac{\partial h(x,t)}{\partial x}\big|_{x=a}) \\
k_{2,a} &= f(\Theta_{2,a}) = f(-\frac{\partial (h(x,t) + \frac{1}{2}k_{1,h}\Delta t)}{\partial x}\big|_{x=a}) \\
k_{3,a} &= f(\Theta_{3,a}) = f(-\frac{\partial (h(x,t) + \frac{1}{2}k_{2,h}\Delta t)}{\partial x}\big|_{x=a}) \\
k_{4,a} &= f(\Theta_{4,a}) = f(-\frac{\partial (h(x,t) + k_{3,h}\Delta t)}{\partial x}\big|_{x=a})
\end{aligned} \tag{3.15}$$

3.1.2 Spatial Discretization

Equation 3.4 and 3.5 includes derivatives of h and c in terms of x. In FDM, these partial derivatives will be approximated with some schemes. For this purpose, 4th order central difference scheme will be used. 4th order accuracy is chosen because even with less number of point, desired accuracy level can be achieved. In addition, with decreasing Δx, accuracy will increase faster. For mentioned schemes, the numerical methods book [37] will be followed:

$$\begin{aligned}
\frac{\partial h}{\partial x} &= \frac{-h_{i+2} + 8h_{i+1} - 8h_{i-1} + h_{i-2}}{12\Delta x} + O(\Delta x^4) \\
\frac{\partial^2 h}{\partial x^2} &= \frac{-h_{i+2} + 16h_{i+1} - 30h_i + 16h_{i-1} - h_{i-2}}{12\Delta x^2} + O(\Delta x^4) \\
\frac{\partial^3 h}{\partial x^3} &= \frac{-h_{i+3} + 8h_{i+2} - 13h_{i+1} + 13h_{i-1} - 8h_{i-2} + h_{i-3}}{8\Delta x^3} + O(\Delta x^4) \\
\frac{\partial^4 h}{\partial x^4} &= \frac{-h_{i+3} + 12h_{i+2} - 39h_{i+1} + 56h_i - 39h_{i-1} + 12h_{i-2} - h_{i-3}}{6\Delta x^4} + O(\Delta x^4)
\end{aligned} \tag{3.16}$$

For derivatives of particle concentration, following equations will be used:

$$\frac{\partial c}{\partial x} = \frac{-c_{i+2} + 8c_{i+1} - 8c_{i-1} + c_{i-2}}{12\Delta x} + O(\Delta x^4)$$

$$\frac{\partial^2 c}{\partial x^2} = \frac{-c_{i+2} + 16c_{i+1} - 30c_i + 16c_{i-1} - c_{i-2}}{12\Delta x^2} + O(\Delta x^4) \tag{3.17}$$

Near the contact line, different scheme is applied because there is not enough boundary condition for applying 4th order central difference scheme. Near this point, 4th order backward difference will be used. This scheme is derived by following the book for finite difference method [38]. In the upcoming section, the derivation of this scheme will be presented.

3.1.3 Derivation of The 4th Order Backward Difference Schemes for Uniform Mesh

Undetermined coefficient method is used for derivation of 4th order backward difference scheme, and for this derivation, finite difference book [38] is followed. First derivative of h in terms of x can be written in following format:

$$h'_i = ah_i + bh_{i-1} + ch_{i-2} + dh_{i-3} + eh_{i-4} \tag{3.18}$$

Coefficients in equation 3.18 can be found by writing Taylor-Series expansions of $h_i, h_{i-1}, h_{i-2}, h_{i-3}, h_{i-4}$:

$$
\begin{aligned}
h_i' = a h_i + & b h_i - b h_i' \Delta x + \frac{b}{2} h_i'' \Delta x^2 - \frac{b}{6} h_i''' \Delta x^3 + \frac{b}{24} h_i^{(4)} \Delta x^4 \\
& + c h_i - 2c h_i' \Delta x + \frac{4c}{2} h_i'' \Delta x^2 - \frac{8c}{6} h_i''' \Delta x^3 + \frac{16c}{24} h_i^{(4)} \Delta x^4 \\
& + d h_i - 3d h_i' \Delta x + \frac{9d}{2} h_i'' \Delta x^2 - \frac{27d}{6} h_i''' \Delta x^3 + \frac{81d}{24} h_i^{(4)} \Delta x^4 \\
& + e h_i - 4e h_i' \Delta x + \frac{16e}{2} h_i'' \Delta x^2 - \frac{64e}{6} h_i''' \Delta x^3 + \frac{256e}{24} h_i^{(4)} \Delta x^4 \\
& + (b + c + d + e) O(\Delta x^5)
\end{aligned} \tag{3.19}
$$

Only coefficients of h_i' will remain, therefore, summation of other parameter's coefficients will be equal to 0. Summation of coefficients can be written in more organized way:

$$
\begin{aligned}
& a + b + c + d + e = 0 \\
& (-b - 2c - 3d - 4e)\Delta x = 1 \\
& (b + 4c + 9d + 16e)\frac{\Delta x^2}{2} = 0 \\
& (-b - 8c - 27d - 64e)\frac{\Delta x^3}{6} = 0 \\
& (b + 16c + 81d + 256e)\frac{\Delta x^4}{24} = 0
\end{aligned} \tag{3.20}
$$

$\frac{\Delta x^2}{2}, \frac{\Delta x^3}{6}, \frac{\Delta x^4}{24}$ will be canceled and matrix form of equations in 3.20 will be in following format:

$$
\begin{bmatrix}
1 & 1 & 1 & 1 & 1 \\
0 & -1 & -2 & -3 & -4 \\
0 & 1 & 4 & 9 & 16 \\
0 & 1 & 8 & 27 & 64 \\
0 & 1 & 16 & 81 & 256
\end{bmatrix}
\begin{bmatrix} a \\ b \\ c \\ d \\ e \end{bmatrix}
=
\begin{bmatrix} 0 \\ \frac{1}{\Delta x} \\ 0 \\ 0 \\ 0 \end{bmatrix} \tag{3.21}
$$

After solving matrix equation 3.21, coefficients will be as followings:

$$a = \frac{50}{24\Delta x}, b = \frac{-96}{24\Delta x}, c = \frac{72}{24\Delta x}, d = \frac{-32}{24\Delta x}, e = \frac{6}{24\Delta x}$$

As a result of this:

$$h'_i = \frac{50h_i - 96h_{i-1} + 72h_{i-2} - 32h_{i-3} + 6h_{i-4}}{24\Delta x} + O(\Delta x^4) \tag{3.22}$$

In the equation 3.19, there is $(b+c+d+e)O(\Delta x^5)$ term. This term becomes $O(\Delta x^4)$ in the equation 3.22, because $(b+c+d+e)$ is $O(\frac{1}{\Delta x})$. As a result of this, approximation of first derivative will be following with error $O(\Delta x^4)$:

$$\frac{\partial h_i}{\partial x} \approx \frac{50h_i - 96h_{i-1} + 72h_{i-2} - 32h_{i-3} + 6h_{i-4}}{24\Delta x} \tag{3.23}$$

Similar method shown in equations 3.18 - 3.21 can be applied also for second, third and fourth derivatives and the approximations are as followings:

$$\frac{\partial^2 h_i}{\partial x^2} \approx \frac{450h_i - 1540h_{i-1} + 2140h_{i-2} - 1560h_{i-3} + 610h_{i-4} - 100h_{i-5}}{120\Delta x^2} \tag{3.24}$$

$$\frac{\partial^3 h_i}{\partial x^3} \approx \frac{4410h_i - 20880h_{i-1} + 41490h_{i-2} - 44640h_{i-3} + 27630h_{i-4} - 9360h_{i-5} + 1350h_{i-6}}{720\Delta x^3} \tag{3.25}$$

$$\frac{\partial^4 h_i}{\partial x^4} \approx \frac{ah_i + bh_{i-1} + ch_{i-2} + dh_{i-3} + eh_{i-4} + fh_{i-5} + gh_{i-6} + jh_{i-7}}{5040\Delta x^4} \tag{3.26}$$

Where $a = 47040, b = -279720, c = 715680, d = -1023960, e = 887040, f = -466200, g = 137760, j = -17640$. To check found schemes, polynomial expression $1 - x^5$ can be used and its derivatives at $x = 1$ can be compared with numerical approximations. Δx is taken as 0.01:

	4th Order Backward Difference Result	Analytical Result
$\frac{\partial h}{\partial x}$	-4.999999760	-5.000000000
$\frac{\partial^2 h}{\partial x^2}$	-20.000000000	-20.000000000
$\frac{\partial^3 h}{\partial x^3}$	-59.999999996	-60.000000000
$\frac{\partial^4 h}{\partial x^4}$	-119.999996341	-120.000000000

Table 3.1: Derivative Comparison of $1 - x^5$ at $x = 1$ for 4th Order Backward Difference and Analytical Result

Table 3.1 shows that derived 4th order backward difference schemes are good enough and there is no error in the derivation. For derivatives of particle concentration, found approximations will be used:

$$\frac{\partial c_i}{\partial x} \approx \frac{50c_i - 96c_{i-1} + 72c_{i-2} - 32c_{i-3} + 6c_{i-4}}{24\Delta x} \tag{3.27}$$

$$\frac{\partial^2 c_i}{\partial x^2} \approx \frac{450c_i - 1540c_{i-1} + 2140c_{i-2} - 1560c_{i-3} + 610c_{i-4} - 100c_{i-5}}{120\Delta x^2} \tag{3.28}$$

3.2 Boundary Conditions

h and c depend on only x in spatial domain. Therefore, boundary conditions on x coordinate will be applied to numerical calculation. Boundary condition at $x = 0$ are as following:

$$\frac{\partial h}{\partial x} = \frac{\partial^3 h}{\partial x^3} = \frac{\partial c}{\partial x} = 0 \tag{3.29}$$

4th Order Central Difference will be used for derivatives near the symmetry boundary conditions. At $x = 0$, where sub-index $i = 0$, first and third derivative of h are as following:

$$\frac{\partial h(x=0,t)}{\partial x} = \frac{-h_2 + 8h_1 - 8h_{-1} + h_{-2}}{12\Delta x} = 0$$

$$\frac{\partial^3 h(x=0,t)}{\partial x^3} = \frac{-h_3 + 8h_2 - 13h_1 + 13h_{-1} - 8h_{-2} + h_{-3}}{8\Delta x^3} = 0 \tag{3.30}$$

h_{-1}, h_{-2}, h_{-3} are ghost nodes and Figure 3.2 shows the location of ghost nodes in domain:

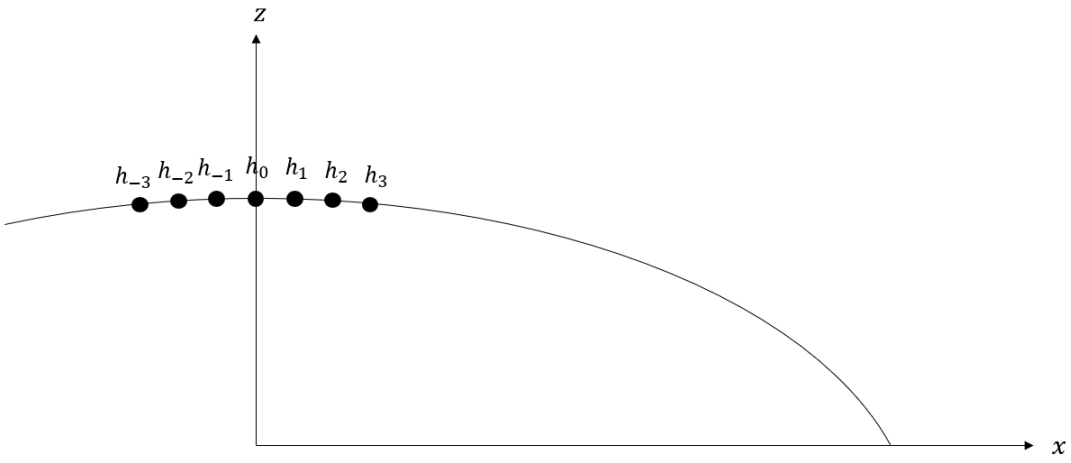

Figure 3.2: Location of Ghost Nodes in Domain

These ghost nodes are out of calculation domain, however, they can still be calculated. According to symmetry, there is solution for 3.30 when:

$$h_1 = h_{-1}, \quad h_2 = h_{-2}, \quad h_3 = h_{-3}$$

This assumption will be also applied the particle concentration at symmetry boundary because x derivative of particle concentration is 0 at this point. As a result of this:

$$c_1 = c_{-1}, \quad c_2 = c_{-2}$$

Boundary conditions at $x = a(t)$:

$$\frac{\partial h}{\partial x} = -\Theta, \quad h = 0, \quad c = 0 \tag{3.31}$$

Because 4th order backward difference will be used near the contact line, there is no need for special treatment near the contact line. Boundary conditions at this point implies that h and c values are constant, therefore numerical calculations will be not made for mentioned variables.

3.3 Particle Deposition

In this section, two dimensional numerical particle deposition will be explained. Particle mass flux is known for each point in the domain. Figure 3.3 shows geometrical configuration of deposition.

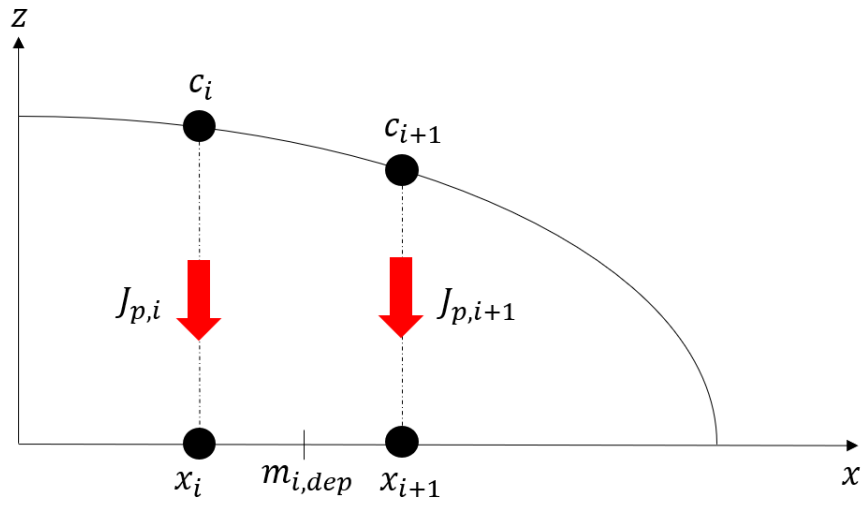

Figure 3.3: Explanatory Scheme for Numerical Particle Deposition Mechanism

In Figure 3.3, particle deposition flux represented with red arrows to points on solid surface. Subscript i of J_p shows that it belongs to point i. $m_{i,dep}$ is deposited particle mass per unit length, and its deposition location is in the middle of point i and $i+1$ in solid surface line. Mathematical formulation of deposition is inspired by method in Widjaja and Harris [25]. Some modification are done, because their coordinates and particle concentration definitions are different. Solid surface is taken as one dimensional. Therefore, line integration is used to find deposited mass per unit length and time. After this process, as in Widjaja and Harris [25], this integration is multiplied with time step size to find deposited particle mass per unit length :

$$m_{i,dep} = \left(\int_{x_i}^{x_{i+1}} J_p dx \right) \Delta t \tag{3.32}$$

Integration can be done numerically with trapezoidal method, and to implement it, numerical method book [36] will be followed:

$$\int_{x_i}^{x_{i+1}} J_p dx \approx \frac{Da}{\epsilon Pe} \left(\frac{c_{i+1} + c_i}{2} \right) (x_{i+1} - x_i) \tag{3.33}$$

As a result, numerical calculation of deposited particle for one time step will be following:

$$m_{i,dep} = \frac{Da}{\epsilon Pe} \frac{c_{i+1} + c_i}{2} \Delta x \Delta t \tag{3.34}$$

3.4 Algorithms

In the previous sections, application of FDM for given case and dispersed particle deposition were described. Main goal is developing numerical algorithm which considers both pinned and moving contact line regimes. Indicated process is quite challenging. Therefore, two validation case will be used for developing

different parts of final algorithm and after these, final numerical algorithm will be presented.

The first validation scenario will be the simulation of evaporating sessile droplet with moving contact line. In this scenario, there is no dispersed particle. Numerical algorithm will be set for h profile adjustment according to changing mesh through time and mass criterion. Results of Anderson and Davis [1] will be used for comparison.

Second validation scenario will be simulation of evaporating sessile droplet with pinned contact line and particle concentration equation. In this case, there is no need for readjusting h and c profile, because mesh will not change. Results of Fischer [23] and Tarasevich et al [26] will be used for comparison. These two articles have similar configuration, however, viscosity and evaporative flux are different. Tarasevich et al. [26] has particle concentration depended viscosity, on the other hand, viscosity in Fischer [23] is constant. Indicated articles [23, 26] use polar coordinates and same form of equations for temporal change of h and c which are derived with approaches and assumptions similar to those used in this thesis:

$$\frac{\partial h}{\partial t} = -\frac{1}{r}\frac{\partial}{\partial r}(rh\bar{u}) - EJ \tag{3.35}$$

$$\frac{\partial}{\partial t}(hc) = -\frac{1}{r}(rh\bar{u}c) \tag{3.36}$$

As indicated before, evaporative mass flux and height averaged velocity are different. Although model in this thesis uses Cartesian coordinates, validation of the algorithm for polar coordinates can still be utilized, because it is important to validate solution methodology of solving h and c together, which is not dependent on type of coordinates. If solution methodology gives similar results as reference results in polar coordinates, same situation can also be expected in Cartesian coordinate cases. In final algorithm, equations in Cartesian coordinates will be solved, however same solution methodology will be used to solve h and c together.

3.4.1 Numerical Algorithm for Evaporating Droplet with Moving Contact Line

For given scenario, h will be calculated with explained FDM then it will be corrected according to criterion related to mass loss, and changing radius of droplet. In Figure 3.4, brief flow chart of algorithm can be found:

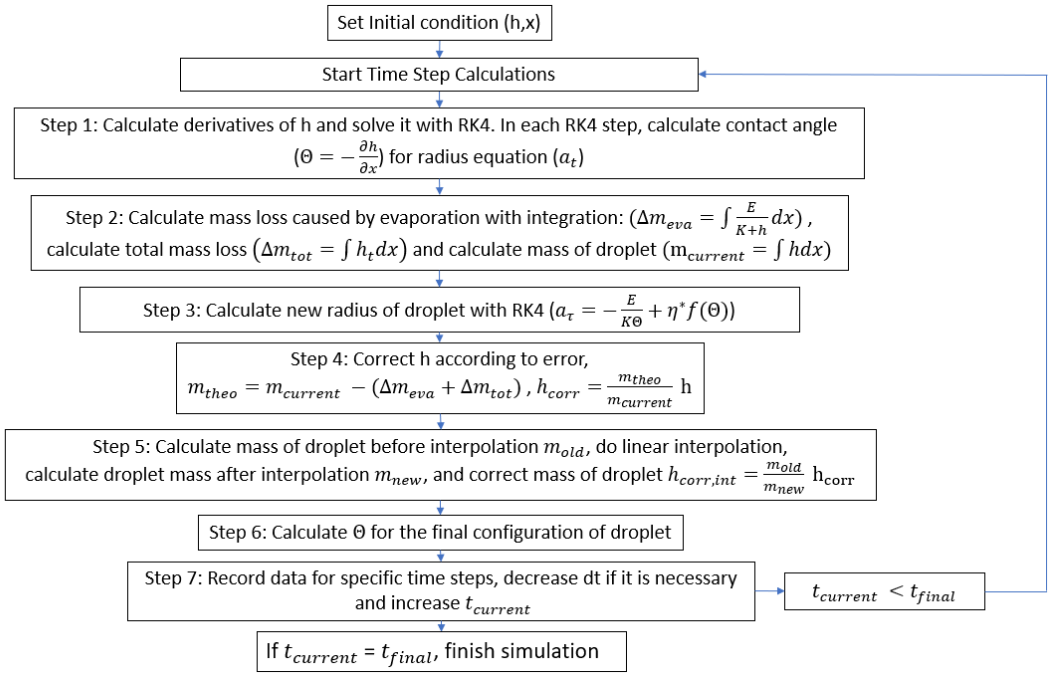

Figure 3.4: Flow Chart of Numerical Algorithm For Moving Contact Line Case

In Figure 3.4, $t_{current}$ and t_{final} are current time and final time values. Algorithm has loop and it will run until final time. After initial conditions are set, temporal evolution of h will be calculated. After this step, necessary calculations will be done for equation 2.64 which is mass loss criterion. Integrals will be calculated along x until a. For this process, Simpson's 1/3 rule will be applied by following numerical methods book [36]:

$$\int_{x_i}^{x_{i+1}} \frac{\partial h}{\partial t} dx = \frac{x_{i+1} - x_i}{6} \left(\frac{\partial h(x_i)}{\partial t} + 4 \frac{\partial h(\frac{x_i + x_{i+1}}{2})}{\partial t} + \frac{\partial h(x_{i+1})}{\partial t} \right) \tag{3.37}$$

$$\int_{x_i}^{x_{i+1}} \frac{E}{K+h} dx = \frac{x_{i+1}-x_i}{6} \left(\frac{E}{K+h(x_i)} + \frac{4E}{K+h(\frac{x_i+x_{i+1}}{2})} + \frac{E}{K+h(x_{i+1})} \right) \tag{3.38}$$

Where parenthesis after h means this parameter is evaluated at given coordinate. Equation 3.38 represents total mass loss caused by evaporation and it will be named as Δm_{eva}. Equation 3.37 represents total temporal height change and it will be named as Δm_{tot}. After calculating temporal change of h, $m_{current}$, which is nondimensional mass of droplet, will be calculated.

Temporal change of droplet radius will be calculated, thus value of it for next time step will be found. In this calculation, contact angle values calculated from intermediate h profiles found by RK4, will be used.

After this process, mass loss criterion can be checked. In theory, $\Delta m_{eva}+\Delta m_{tot}$ will be equal to 0, if all mass loss is caused by evaporation. While temporal change of h is calculated, this summation may not be 0 and it will be considered as error. Current nondimensional mass, $m_{current}$ is calculated and must be corrected according to error. This correction can be done by simply subtracting error from current mass.

$$m_{theo} = m_{current} - (\Delta m_{eva} + \Delta m_{tot}) \tag{3.39}$$

Where m_{theo} is expected mass value in theory according to evaporation loss. Error is subtracted because, in the case of negative error, droplet will lose more mass than expected value according to evaporation. Therefore, absolute value of error must be added for compensation. Same logic must also followed in the case of positive error, because droplet will gain more mass than expected value according to evaporation.

According to new corrected mass, h profile must be adjusted. For this adjustment, ratio of corrected mass to current mass can be utilized:

$$f_{corr} = \frac{m_{theo}}{m_{current}} \tag{3.40}$$

If h profile is multiplied by this ratio, it will be corrected:

$$h_{corr}(x,t) = f_{corr} h(x,t) \tag{3.41}$$

Main reasoning behind this idea is related to nature of numerical integration methods which usually contain summation. If all components of this summation, is multiplied by some constant, it will be common factor to all summation. Therefore, if all h profile is multiplied by f_{corr}, in numerical integration used in this thesis, it will be common factor and $m_{current}$ which is numerical integration of h profile along x, will become m_{theo}, due to $m_{current}\frac{m_{theo}}{m_{current}}$.

With this approach, mass loss criterion can be satisfied numerically. Last remark about this topic, will be related to mass loss situation in contact line. Boundary condition states that h is 0 at this point. This situation will affect the integration. h equation at $x = a$ is as following:

$$\left(\frac{\partial h}{\partial t}\right)_{x=a} + EJ(a) + \frac{\partial}{\partial x}\left(h(a,t)\bar{u}(h(a,t))\right) = 0 \tag{3.42}$$

$h(a,t)$ is 0, thus, term $\frac{\partial}{\partial x}\left(h(a,t)\bar{u}(h(a,t))\right)$ will also be 0. Therefore, equation 3.42 will be following:

$$\left(\frac{\partial h}{\partial t}\right)_{x=a} + EJ(a) = 0 \tag{3.43}$$

Equation 3.43 shows that calculation at contact line will not contribute to integration demonstrated in equation 2.64 because it is 0 at this point. Therefore, in numerical integration of this criterion, contact line is not included in calculation by equating both term to 0 in equation 3.43.

After satisfying mass loss criterion, another correction is needed for h profile. Radius of droplet is changed in the calculation, therefore, mesh is changed and h profile must be adopted to new radius of droplet. For this, linear interpolation is used. According to new x coordinates of the points, new h values are found by interpolating corrected h profiles. At $x = 0$, h value is not changing and at $x = a$, $h = 0$, because of boundary condition. As a result of this, h profile is only changing near the contact line. According to advancing or receding contact line, droplet gains or losses mass artificially. This should also be corrected. Similar approach as in mass loss criterion, is used to correct h profile last time. Before interpolation, mass of droplet (m_{old}) is calculated. Then, linear interpolation is applied. After interpolation, mass of droplet (m_{new}) is calculated again with new radius. Because, desired mass of the droplet is m_{old}, h profile is corrected with following calculation:

$$h_{corr,int} = \frac{m_{old}}{m_{new}} h_{corr} \tag{3.44}$$

As a result of all the mentioned calculation, final form of h is calculated and after calculation of contact angle of new profile, new time step calculation can be started. This loop will continue, until t_{final} is reached.

After running some simulations, it was realized that when error ($\Delta m_{eva} + \Delta m_{tot}$) becomes too high, correction of h causes divergence. Therefore, time step size is decreased, when error goes above some limit. For this case, limit is chosen as 10^{-10} and, when limit is exceeded, time step size is multiplied by 0.96. Limit and multiplication factor was found by trying and running different simulations. According to different cases, these values can be rearranged.

3.4.2 Numerical Algorithm for The Fixed Contact Line Case with Particle Concentration

In this case, h equation and c equation must be solved simultaneously. Contact line is assumed to be fixed, therefore, radius of droplet will not change. Thus, h will not be corrected because of moving radius. Although, mass loss criterion can still be investigated, it will not be considered in the calculations, because results of Tarasevich et al. [26] and Fischer [23] are numerical and they do not include this criterion. Flow chart in Figure 3.5 summarizes general algorithm of given case:

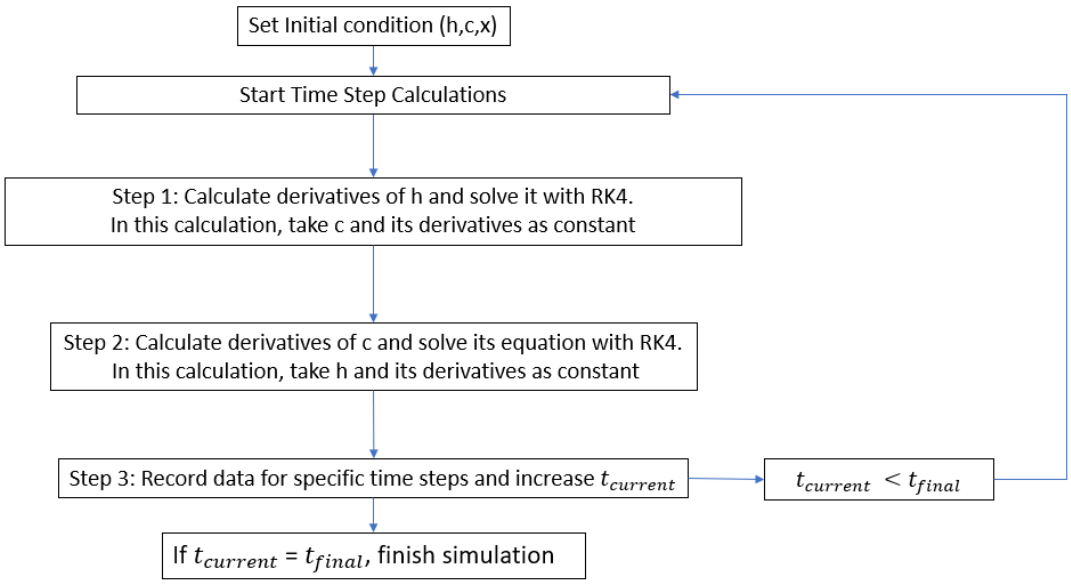

Figure 3.5: Flow Chart of Numerical Algorithm For Fixed Contact Line Case with Particle Concentration

Method about solving h and c equations were already mentioned in Time Discretization part. A further remark should be made about h equation. In both of the article [23, 26], h equation is in polar coordinates. Therefore, there is $1/r$ term which will go to infinity at $r = 0$. r is radial coordinate. h equation in Fischer [23] is as following:

$$\frac{\partial h}{\partial t} = -\frac{1}{r}\frac{\partial}{\partial r}(rh\bar{u}) - EJ \tag{3.45}$$

Special treatment is needed at $r = 0$. Tarasevich et al. [26] equating $\bar{u}$ to 0 at $r = 0$. Equation 3.45 will be as following, if derivative term is expanded:

$$\frac{\partial h}{\partial t} = -\frac{h\bar{u}}{r} - \frac{\partial h}{\partial r}\bar{u} - h\frac{\partial \bar{u}}{\partial r} - EJ \tag{3.46}$$

$-\frac{h\bar{u}}{r}$ and $-\frac{\partial h}{\partial r}\bar{u}$ will be 0 at $r = 0$, because $\bar{u} = 0$. However, $-h\frac{\partial \bar{u}}{\partial r}$ will not be 0 and it must be calculated. $\frac{\partial \bar{u}}{\partial r}$ can not be calculated analytically because it has $1/r$ which will go to infinity when $r = 0$. Therefore, this term will be calculated numerically. In this calculation, second order forward difference will be used [37]:

$$\left(\frac{\partial \bar{u}}{\partial r}\right)_{r=0} = \frac{-\bar{u}_2 + 4\bar{u}_1 - 3\bar{u}_0}{2\Delta r} \tag{3.47}$$

Where Δr is spacing between two consecutive points, $\bar{u}_2$ is $\bar{u}$ value at $r = 2\Delta r$, $\bar{u}_1$ is $\bar{u}$ value at $r = \Delta r$ and $\bar{u}_0$ is $\bar{u}$ value at $r = 0$. Particle concentration equation will be following in polar coordinates where there is no diffusion and deposition [23]:

$$\frac{\partial}{\partial t}(hc) = -\frac{1}{r}(rh\bar{u}c) \tag{3.48}$$

With necessary substitutions and simplifications:

$$\frac{\partial c}{\partial t} = -\frac{\partial c}{\partial r}\bar{u} + \frac{EJ}{h}c \tag{3.49}$$

With boundary condition $\bar{u} = 0$ at $r = 0$, particle concentration equation will become:

$$\left(\frac{\partial c}{\partial t}\right)_{r=0} = \left(\frac{EJ}{h}c\right)_{r=0} \tag{3.50}$$

How main equations will be solved at $r = 0$ is mentioned in previous paragraphs. At contact line where $r = a$, Tarasevich et al. [26] assumes $h = h_f$, where h_f is nonzero height at contact line. Fischer [23] assumes $h = 0$, at this point. Therefore, h equations for both cases will not be solved at this point. For particle concentration, Tarasevich et al. [26] assumes $\bar{u} = 0$ at $r = a$ and $J(a) = 0$. For Fischer [23] evaporative mass flux is also 0 at contact line and $\bar{u}$ will be following at contact line:

$$(\bar{u})_{r=a} = \frac{1}{3Ca}h(r = a, t)^2 \frac{\partial}{\partial r}\left(\frac{1}{r}\frac{\partial}{\partial r}\left(r\frac{\partial h(r = a, t)}{\partial r}\right)\right) = 0 \tag{3.51}$$

Where Ca is capillary number. Height averaged velocity is 0 because h is 0 at contact line. When $\bar{u}$ and J are 0 for both articles [23, 26], temporal change of particle concentration at contact line will be following:

$$\left(\frac{\partial c}{\partial t}\right)_{r=a} = 0 \tag{3.52}$$

Therefore, c will not change at contact line.

For the simulation about comparing results of Tarasevich et al. [26], spatial and temporal schemes are changed at some points, because in the simulation it was seen that with current configuration, results are diverging for particle concentration. Therefore, for the points, whose indices are [n-7,...,n-3], first derivative of particle concentration is calculated with first order forward difference [37]:

$$\frac{\partial c}{\partial x} = \frac{c_{i+1} - c_i}{\Delta x} \tag{3.53}$$

Indicated points are chosen, because simulation was starting to diverging from this part. In addition, this modification applied to only particle concentration

equation, because in the calculation of h equation, there is no problem. With this modification, divergence issue is fixed. In addition, in the calculation of particle concentration equation, temporal scheme is change to explicit Euler method and it is calculated in following way [36]:

$$c_i^{t+\Delta t} = c_i^t + f(c_i(t))\Delta t \tag{3.54}$$

Main reason of this modification is decreasing the computational time of simulation.

3.4.3 Combining the Two Algorithms: Moving Contact Line Plus Particle Concentration

To validate different results in literature, algorithms were explained in previous sections. In this section, numerical algorithm for combined case which includes both pinned and moving contact line with particle dispersion and deposition will be explained. Features of previous algorithms are merged in this algorithm, and some additional features will also be needed.

In combined case, droplet will be pinned until some contact angle value for specific scenario. After some point, its contact line will start to move and it will continue in this situation until 95 % of total initial particle mass is deposited. Pinned part will be very similar to explained algorithm for pinned validation case. Only particle deposition and mass loss criterion check will be added. For moving contact line part, h, c and deposition profiles must be arranged according to changing mesh. Following figures show flow chart of algorithms for both cases:

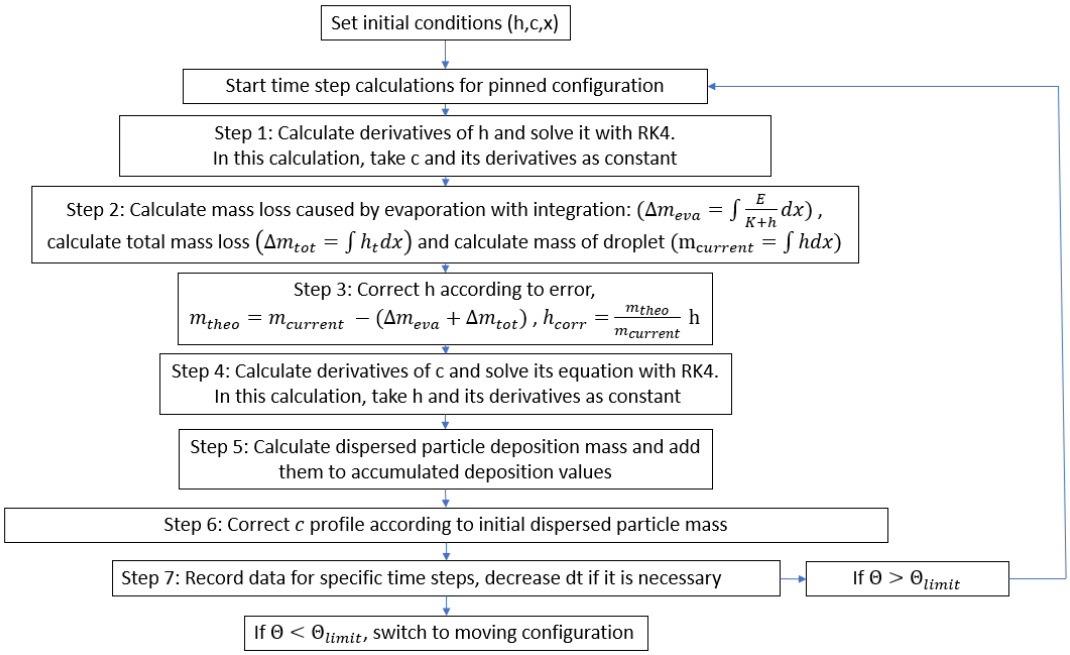

Figure 3.6: Flow Chart for Pinned Part of Combined Numerical Algorithm

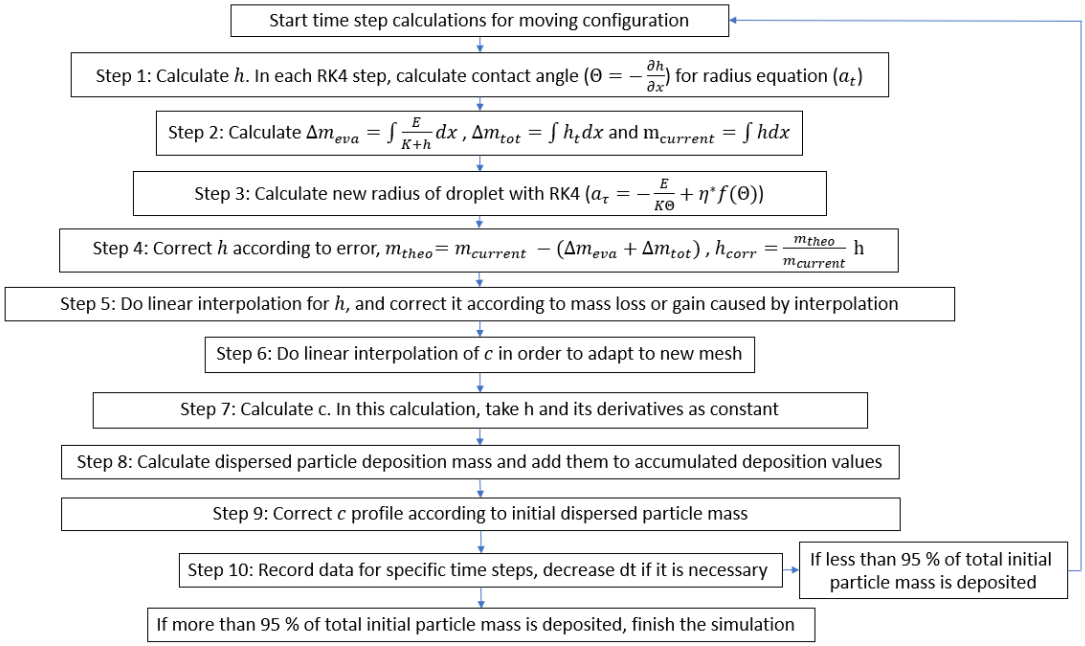

Figure 3.7: Flow Chart for Moving Part of Combined Numerical Algorithm

In Figure 3.6, most of the parts are explained in previous sections, only dispersed particle deposition and correction of c profile are new. Dispersed particle deposition points on surface will be fixed and not change through time. After this process, total mass correction of deposited particle can be evaluated. At the beginning, droplet will have total nondimensional particle mass ($m_{c,tot,init}$), which will be calculated as following:

$$m_{c,tot,init} = \int_0^{a_0} \int_0^{h} c(x, t = 0) dz dx \tag{3.55}$$

$$m_{c,tot,init} = \int_0^{a_0} c(x, t = 0) h(x, t = 0) dx \tag{3.56}$$

In the calculation of particle mass, Karapetsas et al. [28] is followed. In Equation 3.56, intergral will be calculated with Simpson's 1/3 rule. Current total particle mass ($m_{c,tot,current}$) will be summation of total particle mass in droplet ($m_{c,drop,current}$), total mass which will be deposited ($m_{c,dep,inst,current}$) and total accumulated deposited mass ($m_{c,dep,acc}$):

$$m_{c,tot,current} = m_{c,drop,current} + m_{c,dep,inst,current} + m_{c,dep,acc} \tag{3.57}$$

Error($m_{c,error}$) in particle mass will be related to difference between initial total mass and current total mass:

$$m_{c,error} = m_{c,tot,init} - m_{c,tot,current} \tag{3.58}$$

This error will be used in correction of c profile. Accumulated deposition value will not be corrected, because deposited particle cannot return back to droplet and in some cases, correction can cause this situation. Also, mass value for instantaneous deposition in one time step will not be corrected, because total particle mass in droplet is far bigger than it. As a result of this, corrected total particle mass value ($m_{c,drop,corrected}$) in droplet will be:

$$m_{c,drop,corrected} = m_{c,drop,current} + m_{c,error} \tag{3.59}$$

After knowing theoretically correct mass, same approach as in h will be followed for c profile. Correction ratio ($f_{c,drop,corr}$) will be calculated and all c profile will be multiplied with this value to find corrected value ($c_{corrected}$).

$$f_{c,drop,corr} = \frac{m_{c,drop,corrected}}{m_{c,drop,current}} \tag{3.60}$$

$$c_{corrected}(x,t) = f_{c,drop,corr}c(x,t) \tag{3.61}$$

Last step of pinned part will be recording necessary values, doing time step size decrease if it is necessary and checking contact angle for limit. If it is below the limit, then code will switch to moving part.

For the moving part, algorithm in Figure 3.7 will be followed. In this algorithm, until step 6, familiar process in old algorithms will be applied. In step 6, linear interpolation is done for c, because radius of droplet and mesh changed. Thus, c profile for new points can be found. After this, c equation can be calculated. Similar approach in previous section will be followed for this process. After calculation of c, deposition must be done. Changing droplet radius make this process challenging. The particle deposition points will be fixed. When radius of the droplet moves, related deposition points under current droplet will be chosen and the deposition will be done on these points. In this process following steps will be followed. Firstly, deposited particle mass for one time step will be found for current mesh configuration. Secondly, by looking at coordinates of these points, their deposition values will be added to nearest fixed deposition point. In other words, if distance between newly deposited point and fixed deposition point is smaller than $\Delta x/2$, then this deposition value will be added to indicated fixed point.

After deposition, correction of c profile, which is mentioned in pinned part, will

be done. After this correction, necessary values will be recorded for indicated time steps and time step size will be decreased if it is necessary. This loop will end, when 95 percent of initial total particle mass is deposited.

Further notice will be needed for given case. After doing some simulation for this case, it was seen that near the contact line 4th Order Backward difference usage for derivatives of c in terms of x, can cause divergence of c in some cases. Therefore, for the combined code, derivatives of c in point near the contact line is calculated with 2nd Order Central Difference [37]:

$$\frac{\partial c}{\partial x} = \frac{c_{i+1} - c_{i-1}}{2\Delta x}, \qquad \frac{\partial^2 c}{\partial x^2} = \frac{c_{i+1} - 2c_i + c_{i-1}}{\Delta x^2} \tag{3.62}$$

Chapter 4

Results and Discussion

In this chapter, numerical results will be presented. In the first part, validation of numerical algorithm will be demonstrated and discussed. For this purpose, results of different articles [1, 23, 26] will be used. In the second part, results of derived model will be presented and parametric study will be done for different parameters. Selection process for set of parameters will be explained and current configuration will be described.

Simulations in this chapter, were executed in C++ platform and the codes for numerical algorithms were written by the author.

4.1 Validation of The Numerical Algorithms

In this section, validation of different aspects of numerical algorithm will be done. In the previous section, two different special case were chosen and numerical algorithms were explained for them. These two cases will be used for validation. These cases were chosen because, in literature, there are results for comparison.

First case was moving contact line without particle concentration. Results of Anderson and Davis [1] will be used for this case. Because main aim is validating

numerical algorithm, parameters and equations of Anderson and Davis [1] will be used. Their parameters and equations are very similar to mathematical model explained in this report. Their model [1] does not include particle concentration depended viscosity.

Second case was fixed contact line with particle concentration. Results of Fischer [23] and Tarasevich et al. [26] will be used for this case. Because main aim is validating numerical algorithm, parameters and equations of Fischer [23] and Tarasevich et al. [26] will be used. The models used in these articles are similar to mathematical model explained in this report. The main difference is related to coordinates and included physical phenomenons. In both of these articles, there is no Marangoni and Vapor recoil effects. Viscosity in Tarasevich et al. [26] depends on particle concentration. On the other hand, viscosity used in Fischer [23] does not depend on particle concentration and is constant. Both of these articles do not include diffusion, and particle deposition in their particle concentration equation. However, these are included in the presented model in this report. Although both of these articles use polar coordinates, main aim is validation of solving h and c together, as indicated before. If numerical algorithm gets similar results as reference results in polar coordinates, this solution methodology can also be used in solving h and c equations together in Cartesian coordinates.

Although given articles do not include all the physical phenomenon in the presented model in this report, combination of these articles are still covering moving contact line, h and c equations.

4.1.1 Validation for The Moving Contact Line without Particle Concentration

In the previous part, it was mentioned that results of Anderson and Davis [1] will be used. In this article, there are results for small capillary number. Anderson and Davis [1] assumed h is expansion of capillary number in following way:

$$h = h_0 + Cah_1 + ... \tag{4.1}$$

Leading order solution gives following expression for h_0 [1]:

$$h_0 = \frac{\Theta}{2a}(a^2 - x^2) \tag{4.2}$$

They have also solution for h_1 with $O(Ca^2)$ error [1], however it is not mentioned here. Using radius equation, global mass balance which is named as mass loss criterion in this thesis, and h expansion up to $O(Ca)$ results in relation between contact angle and radius of droplet [1]. This relation is solved with Runge-Kutta algorithm in article of Anderson and Davis [1] and they got graphs for temporal change of radius and contact angle.

Instead of using expansion of h, mathematical model in Anderson and Davis [1] are solved with numerical algorithm explained in previous chapter and results are compared with results of Anderson and Davis [1]. As it is mentioned before, their equations, parameters and boundary conditions are used. In this part, for all the results, following parameters in Anderson and Davis [1] are used:

$$Ca_A = 0.1,\ K_A = 0.1,\ \eta_A^* = 0.1,\ \Theta_A = \Theta_R = 0.1,\ m_A = 3, \beta_A = 0.5,\ E_A = 0.5$$

Subscript "A" indicates these are parameters of Anderson and Davis [1]. For validation of proposed numerical algorithm, different cases from Anderson and Davis [1] will be used. Marangoni number (M) and density ratio ($\tilde{\rho}$) will be chosen according to these cases.

In Case 1, thermocapillarity and vapor recoil terms are ignored. In Case 2 only thermocapillarity term is ignored. In Case 3, only vapor recoil term is ignored.

In the most of the report, time is showed with t. However, in this part, τ will be used for time which is a result of scaling with $\frac{t_v}{\epsilon}$, where $t_v = \frac{h_0^2}{\nu_0}$ in Anderson

Case	M_A	$\tilde{\rho}_A$
Case 1	0.0	∞
Case 2	0.0	10.0
Case 3	1.0	∞

Table 4.1: M_A and $\tilde{\rho}_A$ values for different cases in Anderson and Davis [1]

and Davis [1]. Reference results are taken from article with the help of plot digitization. Initial condition of h for numerical calculation is taken as leading order solution of h in Anderson and Davis [1]:

$$h(x, t = 0) = \frac{\Theta(0)}{a(0)}(a^2 - x^2) \tag{4.3}$$

Where $\Theta(0) = 2$ and $a(0) = 1$ [1]. Figure 4.1 - 4.3 show comparison of results for temporal change of droplet radius and contact angle. Contact angle depends on first derivative of h in contact point, and in the calculation of it 4th Order Backward Difference will be used.

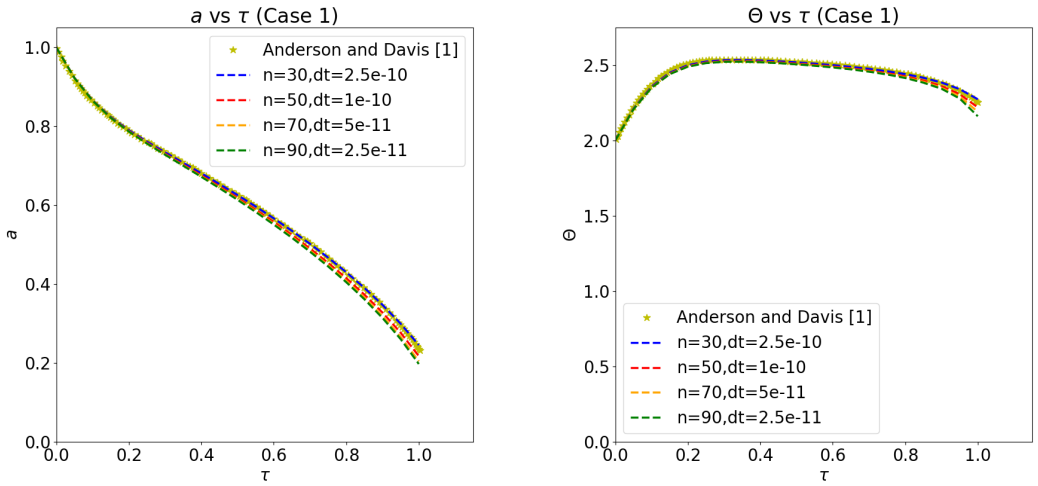

(a) Radius vs Time

(b) Contact Angle vs Time

Figure 4.1: Result Comparison for Case 1

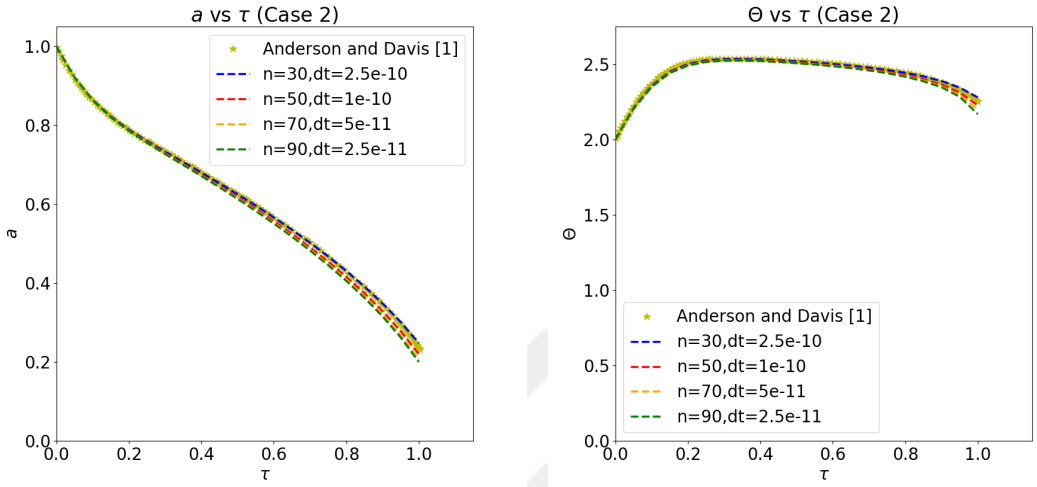

(a) Radius vs Time (b) Contact Angle vs Time

Figure 4.2: Result Comparison for Case 2

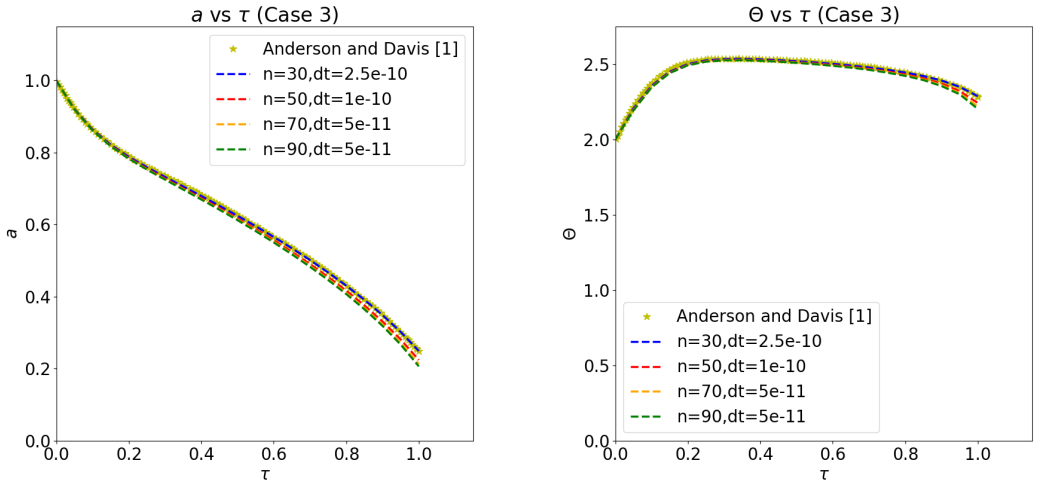

(a) Radius vs Time (b) Contact Angle vs Time

Figure 4.3: Result Comparison for Case 3

In Figure 4.1 - 4.3, four different mesh configuration is used to show simulation is converging to some result. After $n = 90$, number points in the system were not increased, because in the early and mid time step, results are not changing

considerably after $n = 70$. In the legends of figure, dt corresponds to assigned initial time step size. According to error in mass loss criterion, this time step size is decreased and this process is already explained in the numerical section.

In all of the presented results, there is a good agreement in the early and mid time steps. In final stages of simulation, there is a deviation from the reference value of Anderson and Davis [1]. Reason of this issue can be related to solution methodology. Anderson and Davis [1] uses expansion of h in terms of Capillary number to find relations for radius and contact angle and solves numerically. However, numerical algorithm in this report solve h and radius equation directly without doing any expansion. Only initial condition for h is taken as leading order solution of Anderson and Davis [1]. These reasons can cause the difference between two results. However, agreement between given results can still validate numerical algorithm developed for this case.

4.1.2 Validation for Fixed Contact Line with Particle Concentration

In this section, contact line is not moving, however particle concentration equation is solved with h equation. Firstly, result comparison will be done for results of Fischer [23]. Following parameters will be used from Fischer [23]:

$$E_F = 0.1, \quad Ca_F = 0.01, \quad K_F = 1.0, \quad A = 250$$

Subscript "F" shows that these are parameters of Fischer [23]. There is extra parameter "A", because Fischer [23] modified his evaporation model in a following way:

$$J = \frac{1}{K + h}(1 - e^{-A(r-1)^2}) \tag{4.4}$$

Where r is radial component in polar coordinates. With this modification,

evaporative mass flux at contact point will be zero [23]. Equations of Fischer with boundary conditions were solved with the numerical method proposed in the relevant section of previous chapter. h and c values are compared. Reference values are taken from article with the help of plot digitization. Initial conditions for h and c are as following [23]:

$$h(r, t = 0) = 1 - r^2 \quad c(r, t = 0) = 1.0 \tag{4.5}$$

In Figures 4.4 and 4.5, different colors are indicating different time steps and they are demonstrated in the legend. Solid line is result of Fischer [23] and result with star markers are calculated numerical result with algorithm explained before. Same color indicates same time step. For this case, numerical result are calculated with $n = 70$ and $dt = 10^{-10}$. In Figure 4.5, particle concentration is compared. Fischer [23] demonstrates results of P vs r in his article, where P is [23]:

$$P = V_{drop}c \tag{4.6}$$

Where, V_{drop} is volume of droplet, whose temporal change is also given in article [23]. According to these values in the article, P is converted to c and in Figure 4.5, these converted values are compared.

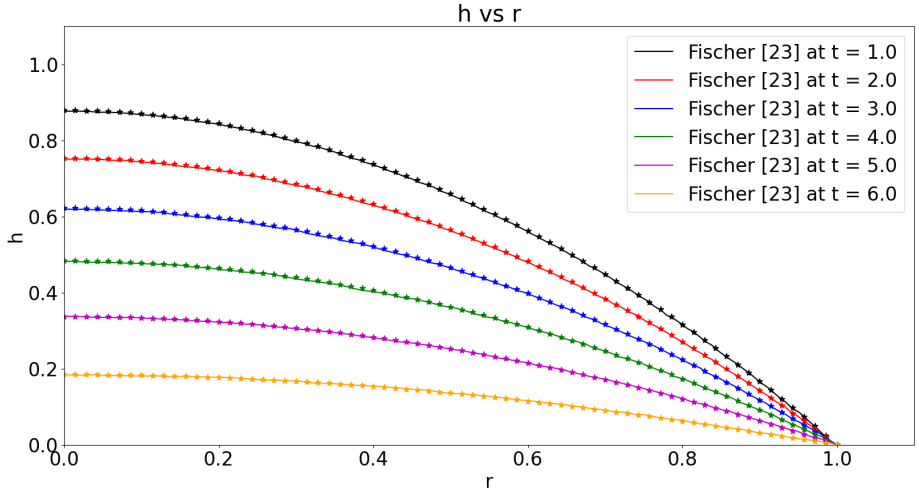

Figure 4.4: Result Comparison for h

Figure 4.4 shows that calculated and article's results are in good agreement through different time steps. Therefore, it can be concluded that numerical algorithm works fine in solving h equation.

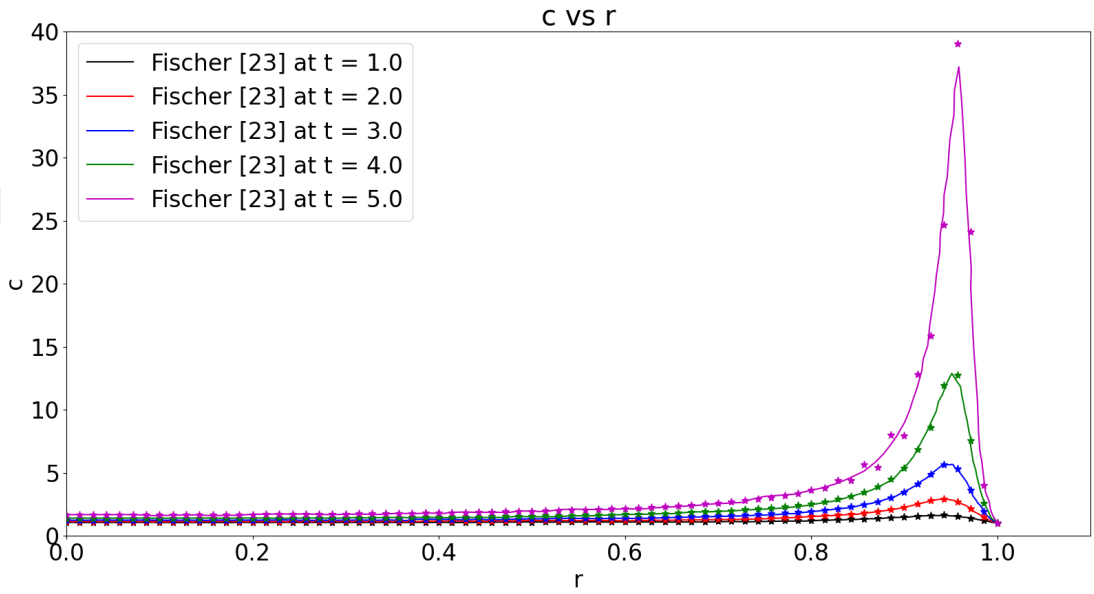

Figure 4.5: Result Comparison for c

Figure 4.5 shows that article results and calculated results are matching well until $t = 4$. At $t = 5$, there is a small deviation in the peak point of particle concentration. In addition, around $r = 0.85$, there is irregularity in these points. Until peak point, first derivative of c is either zero or positive, however this is not the case for the mentioned point and there is small zigzag on this area. This situation can be related to spatial schemes. 4th Order Central difference is used. This may cause the problem in the final stages of simulation. However, during the big portion of simulation, results are matching and this problem occurs at the final stage of simulation. Therefore, numerical scheme was not changed for this case. If same problem occurs in the future simulations, using lower order central difference or forward difference scheme can locally be a solution.

After numerical simulation with Fischer's results [23], result comparison with Tarasevich et al. [26] will be demonstrated in the following part of this section. In the article of Tarasevich et al. [26], particle concentration dependency of viscosity

couples h and c equations. Proposed solution methodology for this problem was explained in the relevant section of previous chapter. Following parameters of Tarasevich et al. [26] will be used in the comparison:

$$Ca_T = 0.1, E_T = 0.1, c_0 = 0.2, K_T = 0.01, h_f = 0.01$$

Subindice "T" shows that these are parameters of Tarasevich et al. [26].Their evaporative mass flux is as following [26]:

$$J = \frac{1 - c^2}{K + h} \tag{4.7}$$

Initial nondimensional h profile is as following [26]:

$$h(r, t = 0) = h_f + \left(1 - \left(\frac{r}{a_0}\right)^2\right) \tag{4.8}$$

Where a_0 is initial radius of droplet. Initial particle concentration is as following [26]:

$$c(r, t = 0) = 2 - c_0 + 2\frac{c_0 - 1}{1 + e^{w(r-1)}} \tag{4.9}$$

Where w is a constant and equals to 10 [26]. c is height average particle concentration in Tarasevich et al. [26] and when it reaches to 1, it becomes gelation concentration [26]. At this point, evaporation also stops. In the Figure 4.6, temporal change of droplet mass is compared. Result of Tarasevich et al. [26] is taken from article with the help of plot digitizing. For numerical result where $n = 120$ and $dt = 5 \times 10^{-11}$, h profile is calculated through time and after this, the area under the h profile for corresponding time step is used as mass in Figure 4.6. In Figure 4.7, particle concentration profiles in r are compared through different time steps. In the article [26], ϕ vs r graph is digitized and used in these graphs. ϕ is volume fraction of particle and by looking at article

results and initial condition about particle concentration, it is assumed that ϕ and c can be used interchangeably, therefore in Figure 4.7, title is c vs r, rather than ϕ vs r. Also for initial condition, it is assumed that $\phi_0 = c_0$.

In the article [26], for given parameters, particle concentration results are not presented with exact nondimensional time step value but instead scaled value of t in terms of t_{max} is used. t_{max} is maximum time when whole droplet becomes like a solid, therefore, h is not changing and evaporation stops in all droplet [26]. Because, exact value of t_{max} is not mentioned in the article [26], this value is predicted from temporal change of mass graph in the article and it is assumed that $t_{max} = 3.0$. According to this, results are compared for $\frac{t}{t_{max}} = 0.25$ where $t = 0.75$, $\frac{t}{t_{max}} = 0.5$ where $t = 1.5$, $\frac{t}{t_{max}} = 0.75$ where $t = 2.25$, and $\frac{t}{t_{max}} = 1.0$ where $t = 3.0$.

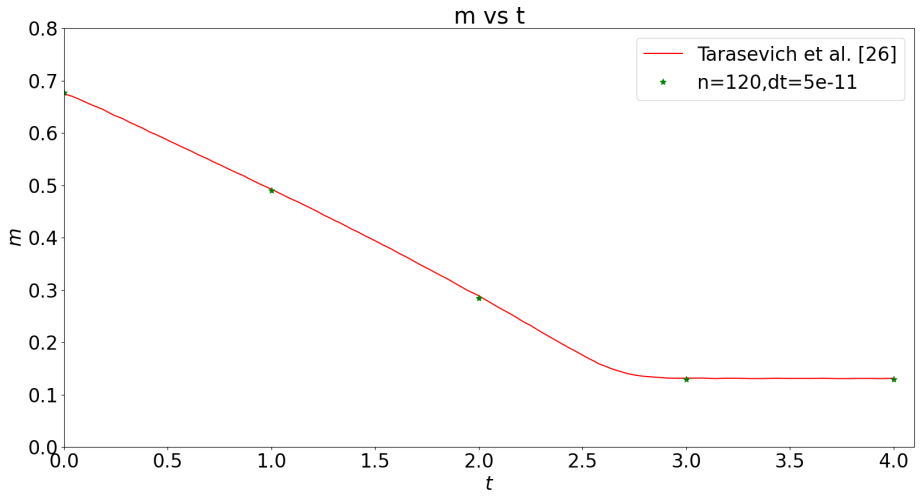

Figure 4.6: Comparison of Temporal Change of Droplet Mass

Temporal change of mass for article's result and result where $n = 120$ and $dt = 5 \times 10^{-11}$ are matching well. This situation shows that numerical algorithm calculates h profile through the time works well in given configuration.

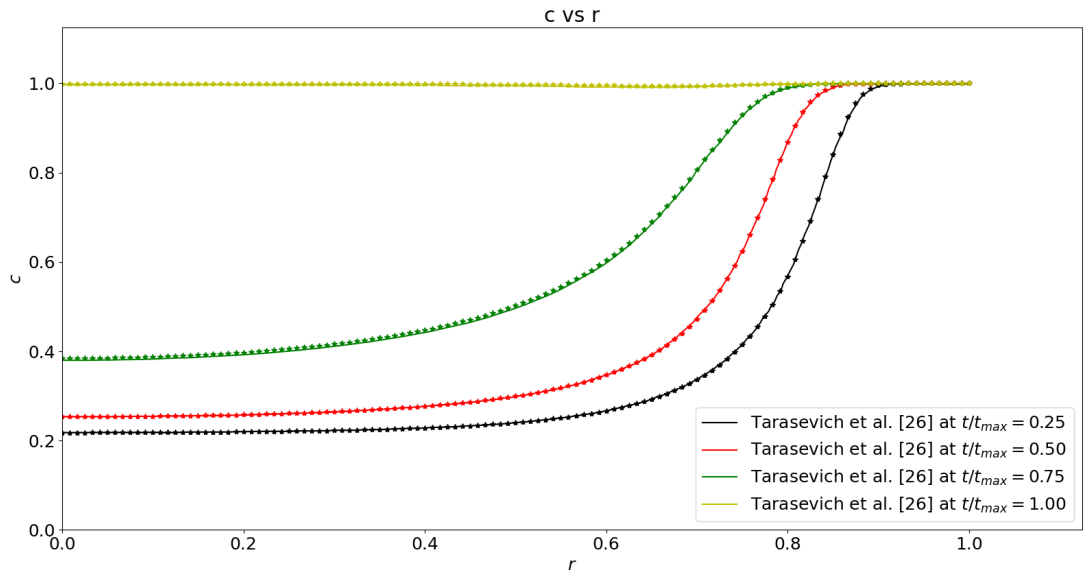

Figure 4.7: Particle Concentration Profile Comparison for Different Time Steps

In Figure 4.7, same color indicates same time step. Solid lines are results of Tarasevich et al. [26] and stars are result of numerical algorithm explained in this work. Results are well matching until $t/t_{max} = 0.75$. At this point, results are deviating a little bit from the reference result. The reason can be related to assumption of t_{max}. By looking at Figure 4.6, it is predicted as 3, however this can be any value between 2.9 to 3. This uncertainty may affect results at later time steps. However in the majority of time, results are close to each other, therefore, this situation shows that numerical algorithm works well in this case.

4.2 Numerical Simulations

In this section, numerical results of combined algorithm will be presented. Firstly, selection process of different parameters in temporal evolution equations of h, c, and a will be explained. After this, initial condition will be stated and results of chosen parameter set will be presented. This parameter set will be considered as base and by changing different parameter in this set, effect of them will be observed.

4.2.1 Parameter Selection

Temporal evolution of h, c, and a depend on various constant parameters which are E, Ca, M, K, $\tilde{\rho}$, Da, Pe, χ, β, η^*, θ_A and θ_R. These constants affect inner flow, evaporation, contact line movement, particle dispersion and deposition. According to material choice of droplet, solid surface type and experimental configuration, indicated constants can change. In the choice of these parameters, it will be influenced by values in literature. Constant parameters in Anderson and Davis [1], Fischer [23], Tarasevich et al. [26] and Karapetsas et al. [28], are either same or similar to constant parameter used in this thesis. Therefore, mostly these articles will be followed. Table 4.2 shows possible options for mentioned constants:

Constant	Possible Values	References
E	0.01 - 1.00	[23]
Ca	0.0015, 0.01 - 10.00	[1], [23]
M	1.0 , 85.0	[1]
K	0.001,0.002, 0.01 , 1.0	[1], [23], [26]
$\tilde{\rho}$	1.0 - 1000.0	[28]
Pe	0.01 - 100.0	[28]
χ	0.01 - 0.1	[28]
β	0.01	[1]
η^*	0.03	[1]
Θ_A	0.1	[1]
Θ_R	0.1	[1]

Table 4.2: Possible Values of Constants Used in Literature

For evaporation and capillary number, parameter range mentioned in Fischer [23] is presented in table. For capillary number, values in Anderson and Davis [1] is also mentioned because for water, they present values of different constants where $\epsilon = 0.1$. For Marangoni number, values in Anderson and Davis [1] are mentioned. In their simulation, they used $M = 1.0$, and they mentioned $M = 85.0$ for water where $\epsilon = 0.1$. For nonequilibrium parameter, 3 different articles [1, 23, 26] was analyzed and it is shown that there is a broad usable range of K. For the ratio of densities, values in Karapetsas et al. are mentioned. Although physical

description exactly same, there is following difference between two parameters:

$$\tilde{\rho} = \frac{\tilde{\rho}_{karapetsas}}{\epsilon} \tag{4.10}$$

Therefore, their $0.1 - 100$ range [28] is taken as $1.0 - 1000$. For Peclet number, following comparison is followed. Formulation is same for both parameter in terms of characteristic velocity. However, characteristic velocities are different. Therefore, ratio between Peclet number of this thesis (Pe) to Peclet number of Karapetsas et al. [28] ($Pe_{karapetsas}$) will be as following:

$$Pe = Pe_{karapetsas} \frac{u_c}{u_{c,karapetsas}} \tag{4.11}$$

$u_c = \frac{\nu_0}{h_0}$ and $u_{c,karapetsas} = \frac{\epsilon\sigma_0}{\mu_0}$ [28]. Therefore,

$$Pe = Pe_{karapetsas} \frac{\mu_0^2}{\epsilon^2 \rho \sigma_0 a_0} \tag{4.12}$$

From Karapetsas et al. [28], $\mu_0 = 10^{-3}$, $a_0 = 10^{-}3$, $\rho = 10^3$, $\sigma_0 = 0.07$ and $\epsilon = 0.1$:

$$Pe = Pe_{karapetsas} \frac{1}{700} \tag{4.13}$$

From end result, it can be said that for given conditions, there is approximately 3 order of magnitude difference, therefore, their $10 - 100000$ range [28] will be taken as $0.01 - 100$. For Damkohler number, there is criterion, that it can be same or lower order of magnitude of ϵPe, therefore it will be arranged according to Pe number. χ is taken as it is from Karapetsas et al. [28]. Parameters related to contact line movement is taken as it is from Anderson and Davis [1].

4.2.2 Initial Condition

Initial condition for h and c will be as following:

$$h(x, t = 0) = 1 - x^2 \tag{4.14}$$

$$c(x, t = 0) = tanh(100(1 - x)) \tag{4.15}$$

Initial a will be 1.0 as scaling indicates and contact angle will be 2.0 which can be deducted from equation 4.14. Initial conditions for h and c are presented in Figure 4.8:

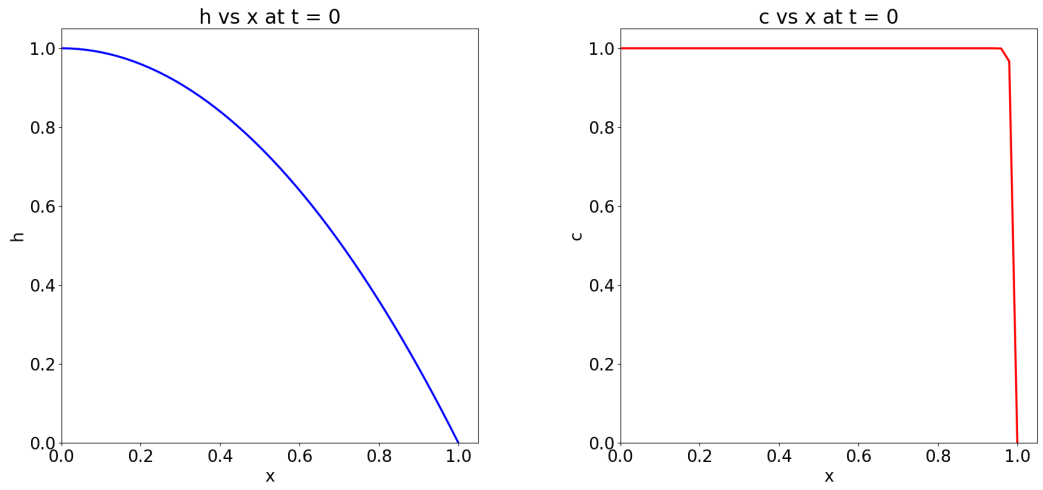

(a) Initial Droplet Interface Height Profile (b) Initial Particle Concentration Profile

Figure 4.8: Initial Condition for h and c

Initial condition for h will be taken as spherical cap and adopted from different articles [1, 23] in the literature. This approach will be followed because of dominant surface tension in balance of normal stress due to slow inner flow and negligible gravity [20]. These criteria suits to current formulation.

Initial condition for c will be adopted from Karapetsas et al. [28]. Their initial condition will be modified in a way that c is 0 at contact line. Thus, there will be uniform profile in most of the geometry and near the contact line, profile will decrease to 0.

4.2.3 Results of the Base Case

In this section, results of the base case will be displayed. Following set of parameters will be used:

$$E = 1.0, \;\; K = 0.3, \;\; Ca = 0.001, \;\; M = 1.0, \;\; \tilde{\rho} = 1.0, \;\; \epsilon = 0.1$$
$$Da = 1.0, \;\; Pe = 10.0, \;\; \beta = 0.01, \;\; \eta^* = 0.03, \;\; \Theta_A = 0.1, \;\; \Theta_R = 0.1$$

This will be the base case. These parameters are set by doing some simulation and considering boundaries mentioned in Parameter Selection part. Chosen Ca is a little bit below the indicated value in table 4.2, however it can still be used because there is not big difference between these values. Limit for contact angle is selected as 2°. In this choice, experimental work of Hu and Larson [21] was considered. They indicated that for water droplet will start to recede around 2° to 4° on glass surface. Therefore, after contact angle goes below indicated value, simulation will switch to moving case. β value will be used only in moving case. In fixed contact line part, it will be taken as 0, because radius of droplet is not moving. Simulation will stop as long as 95 % of initial total particle mass is deposited. The time when simulation finished will be considered as t_{final}. Time step size will be decreased when limit related mass lass criterion of evaporation is exceeded. This condition is used in numerical algorithm which solve droplet with moving contact line in the absence of particle concentration. Limit for time step size will be 10^{-9}.

Temporal change of h, c, a, Θ, m_{dep} and m_{drop} will be presented. In particle deposition section deposited particle mass for point i in one time step is named

as $m_{i,dep}$. For result section, m_{dep} will be the density of accumulated particle in one of the deposition point:

$$m_{dep} = \frac{\sum_{k=0}^{t_{current}} m_{i,dep}^{k}}{\Delta x} \tag{4.16}$$

Superscript "k" represent time step and summation of $m_{i,dep}$ value for all time steps until current time step ($t_{current}$) gives accumulated value of particle deposition mass. This mass value is divided into Δx. This process is applied in order to having comparable variable which does not directly depend on Δx.

m_{drop} will be mass of two dimensional droplet and it will be calculated as area under h curve:

$$m_{drop} = \int_{0}^{a} h dx \tag{4.17}$$

In the calculation of this integral, Simpson's 1/3 rule will be used as explained before in this thesis. Density is not included in this calculation, because, focus is not getting dimensional mass of droplet but having some nondimensional indicator related to mass of the droplet.

For simulation, n is chosen as 50. In this selection, simulation with different n values was completed, then their h, c and m_{dep} profiles were compared. Figure 4.9 - 4.13 show the comparison for the results with $n = 30$, $n = 40$, $n = 50$ and $n = 60$.

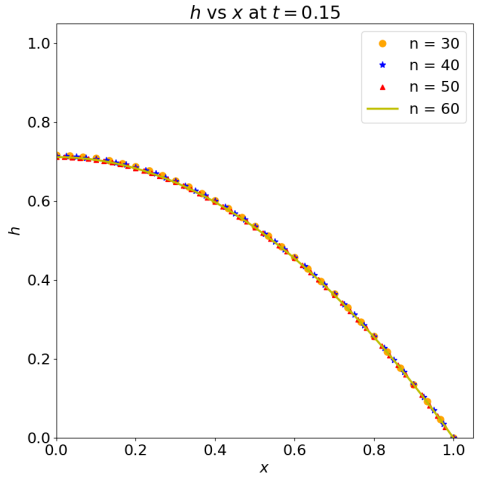

(a) $t = 0.15$

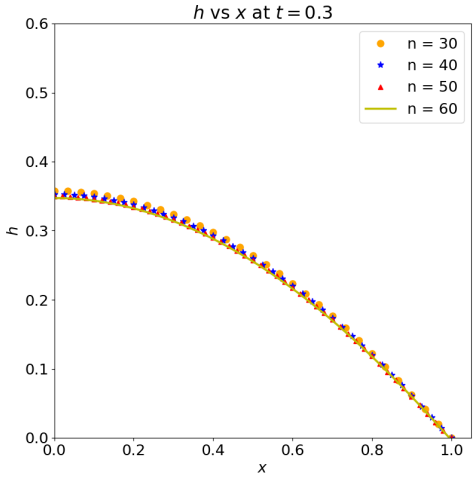

(b) $t = 0.3$

Figure 4.9: h vs x Profiles for Different n Values

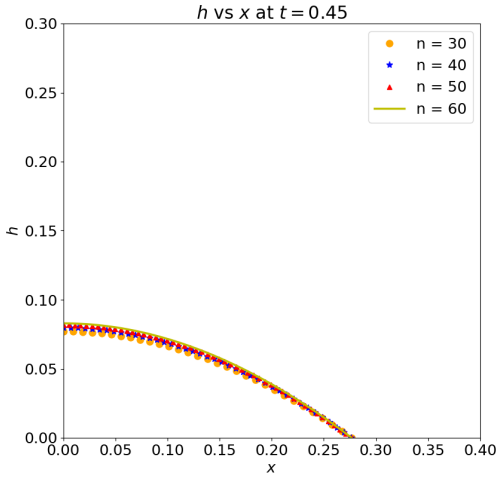

(a) $t = 0.45$

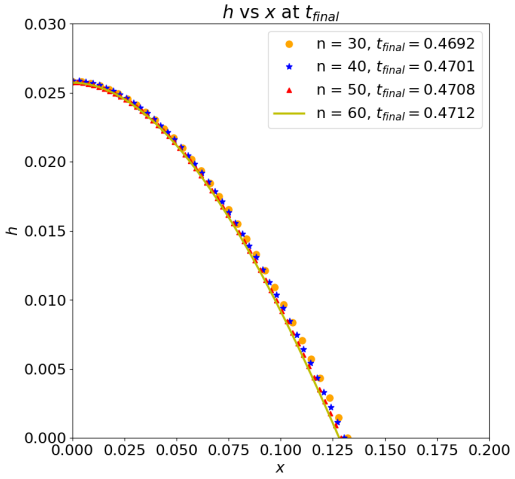

(b) t_{final}

Figure 4.10: h vs x Profiles for Different n Values

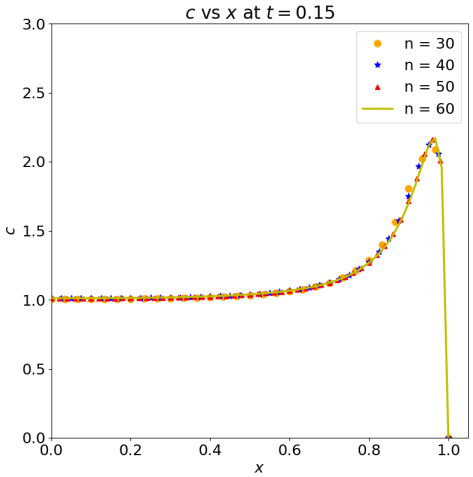

(a) $t = 0.15$

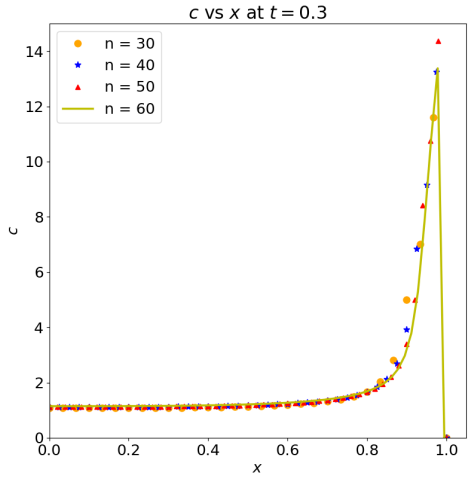

(b) $t = 0.3$

Figure 4.11: c vs x Profiles for Different n Values

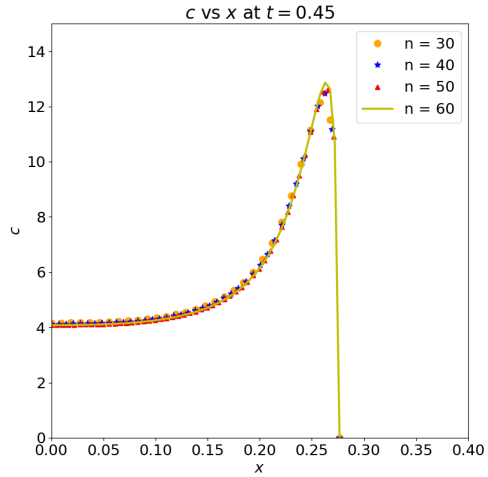

(a) $t = 0.45$

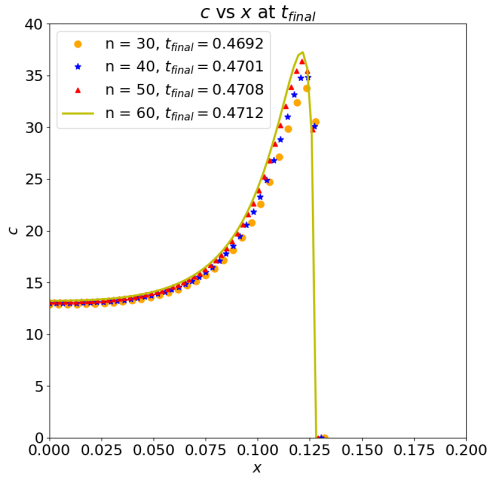

(b) t_{final}

Figure 4.12: c vs x Profiles for Different n Values

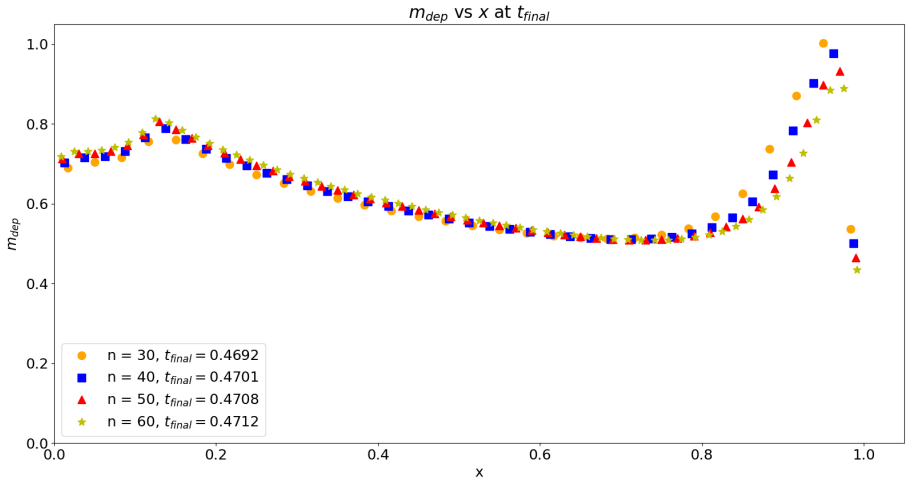

Figure 4.13: m_{dep} vs x at t_{final}

In most of the given figures, profiles are close to each other, however, $n = 50$ is much closer to $n = 60$. In addition, Figure 4.13 shows that deposited particle profiles are similar to each other and $n = 50$ is much closer to $n = 60$. As a result of this, $n = 50$ will be used in next simulations. For base case, temporal change of h,Θ, a and m_{drop} will be as followings:

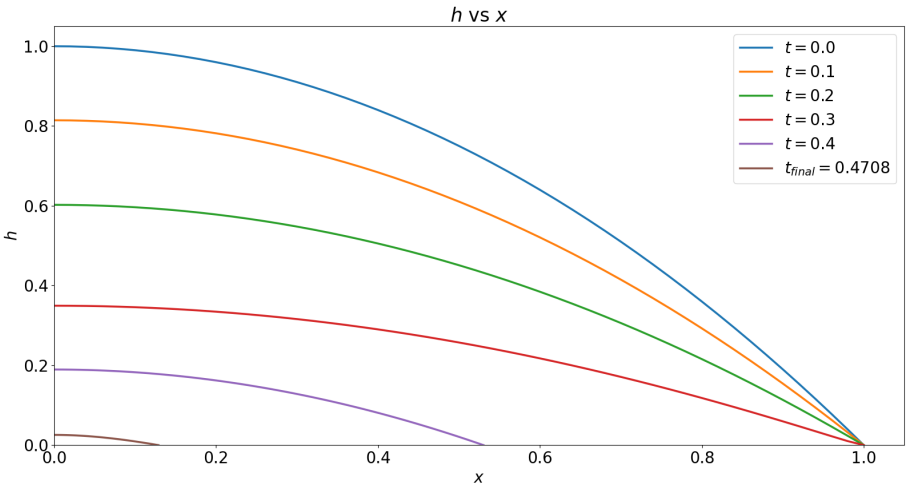

Figure 4.14: Temporal Change of h Profile

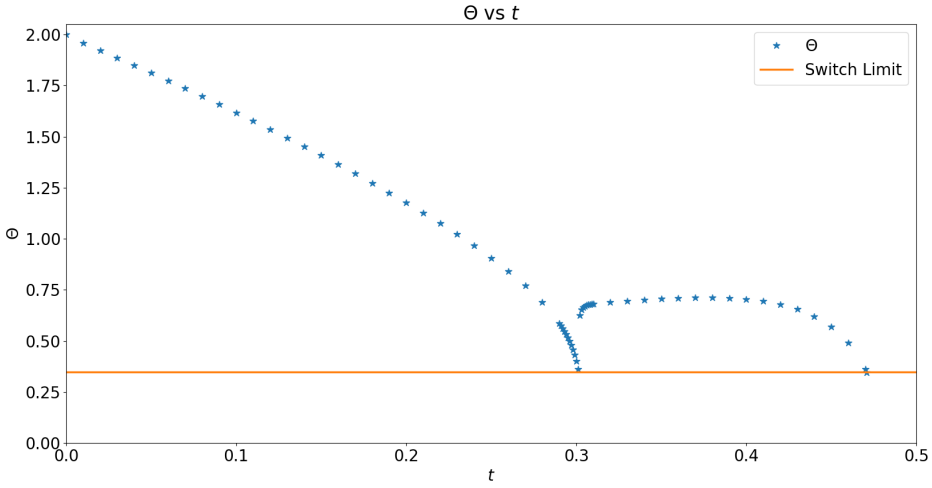

Figure 4.15: Temporal Change of Contact Angle

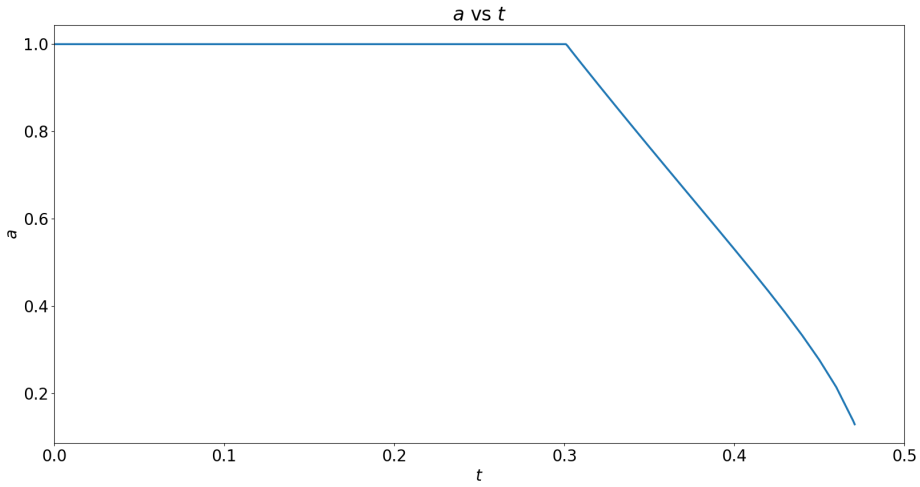

Figure 4.16: Temporal Change of Droplet Radius

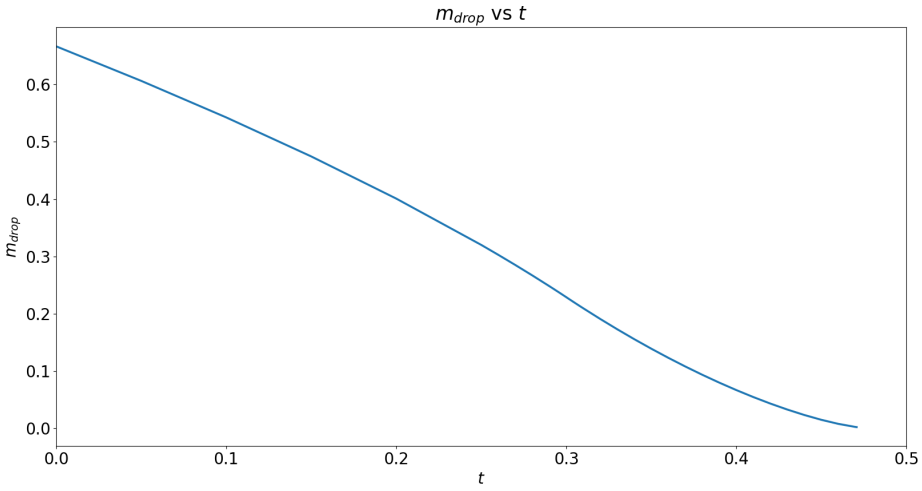

Figure 4.17: Temporal Change of Nondimensional Mass of Droplet

Figures 4.15, and 4.17 show linear change of contact angle and droplet mass in pinned part. Around $t = 0.3$, limit is exceeded and contact line starts to move. There is sharp increase in contact angle at indicated point. After this sharp increase, change of contact angle decreases and for some time it is not changing much. This can be considered as arranging to new regime. To make this transition more smoother, larger contact angle limit can be used. Figure 4.17 shows almost linear change of droplet mass and this situation matching with experimental study of Nguyen et al. [18] where they observed linear volume change for pinned droplet with small contact angle.

Particle concentration profile change through time is presented in Figure 4.18.

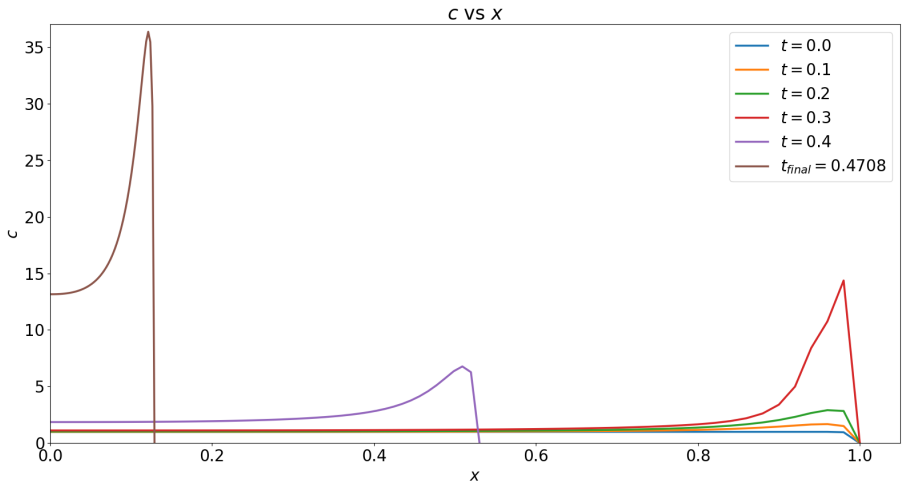

Figure 4.18: Temporal Change of c Profile

Because there is strong evaporation, particle concentration is increasing near the contact line. This induce coffee-ring effect and more particles accumulated near the contact line. Figure 4.19 shows that more particle is deposited near the contact line until $t = 0.3$. After this point, contact line is moving and remaining particles are deposited to other region of geometry. While contact line is moving, peak particle concentration is still close to contact line. At the end of simulation, peak particle concentration goes to 35, which is a little bit much for dilute solution. This situation can be caused by very small droplet volume in the end. However, this situation is not problem because it occurs at the very end of simulation.

At the end of simulation, in Figure 4.19, there is second peak deposition point near the center, however, peak deposition point close to contact line is still bigger than this. The appearance of second peak deposition point near the center can be caused by fast contact line movement at the beginning of moving regime. If contact line recedes fast at the beginning of moving contact line regime, then, there will be not much time for deposition near the contact line and remaining dispersed particle will mostly deposited near the center of droplet.

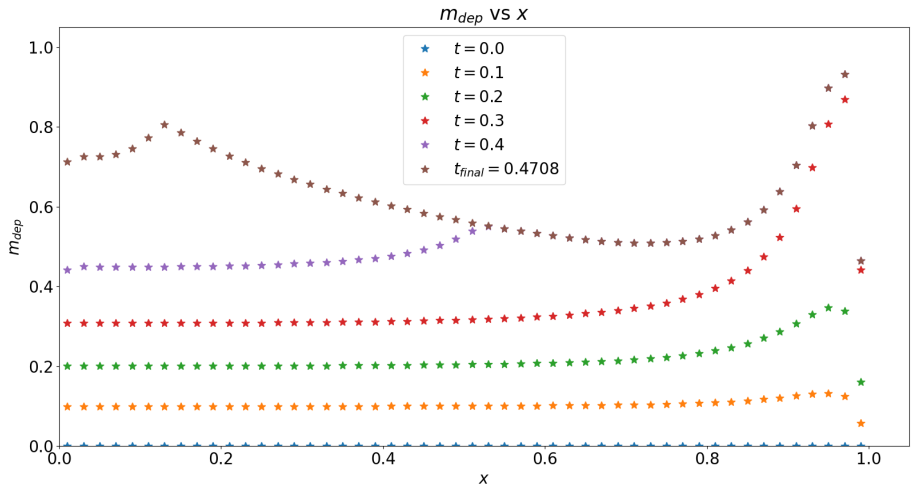

Figure 4.19: Temporal Change of m_{dep} Profile

For given simulation, total mass of particles can also be checked. Initial total mass of particles must be conserved through time. In this case, some of the particles are deposited to the surface, therefore, summation of total particle mass inside droplet and mass of deposited particle should be constant, because system only loses dispersed particle by deposition. Table 4.3 shows total particle mass inside droplet, total deposited mass and their summation. Total particle mass in droplet is calculated with $\int_0^a c(x,t)h(x,t)dx$ and total deposited particle mass is calculated with $\sum_{i=0}^{n-1} m_{dep}(x_i)\Delta x$.

Time	Total Particle Mass in Droplet	Total Deposited Particle Mass	Total Particle Mass
0.0	0.667	0.000	0.667
0.1	0.563	0.104	0.667
0.2	0.446	0.221	0.667
0.3	0.297	0.370	0.667
0.4	0.145	0.522	0.667
0.4708	0.033	0.633	0.666

Table 4.3: Particle Mass in Droplet and Deposited Area

In given table, mass values are rounded up to 3 digit, and these rounded values are summed. Therefore there can be small difference in some time steps. By looking at total particle mass value, it can be concluded that through whole simulation total mass of particles are conserved, therefore, algorithm for mass conservation of particles works well.

4.2.4 Parametric Study

After presenting results of the base case, parametric study can be done for different parameters. For this purpose, M, Da, E and Ca will be evaluated. Firstly, h, c and m_{dep} results will be presented. After this, results will be discussed in each subsection. In all cases, 4 different time steps will be presented for h, c and m_{dep}. In some of the graphs, range of specific axis can be changed rather than following the common one. This application is for demonstrating difference between results which are far smaller or bigger than common values.

4.2.4.1 Marangoni Number

In this section, Marangoni number will be increased, and its effects will be observed. 4 different Marangoni numbers will be compared and these values will be $1, 50, 100, 150$. c, m_{dep}, and h profiles will be compared for different Marangoni numbers.

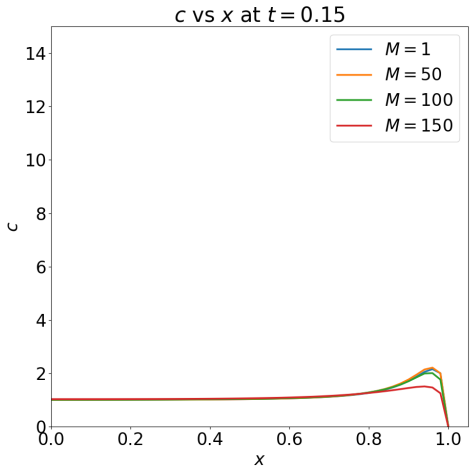

(a) Comparison at t = 0.15

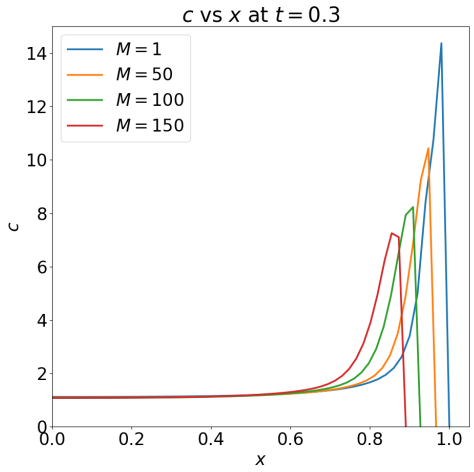

(b) Comparison at t = 0.3

Figure 4.20: Particle Concentration Profile Comparison for M

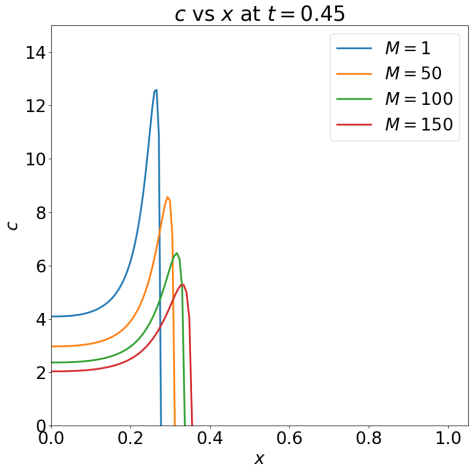

(a) Comparison at t = 0.45

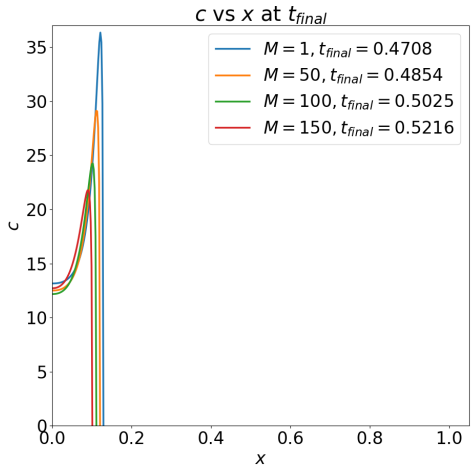

(b) Comparison at t_{final}

Figure 4.21: Particle Concentration Profile Comparison for M

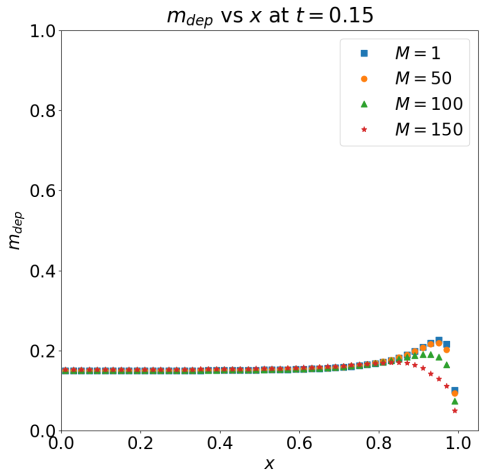

(a) Comparison at t = 0.15

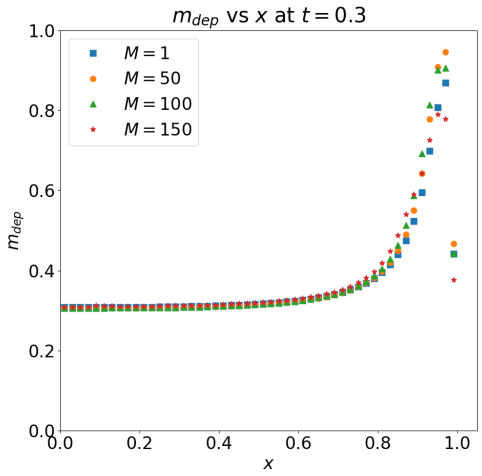

(b) Comparison at t = 0.3

Figure 4.22: Deposited Particle Profile Comparison for M

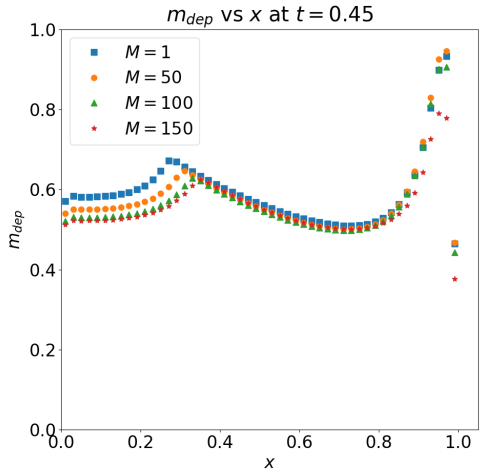

(a) Comparison at t = 0.45

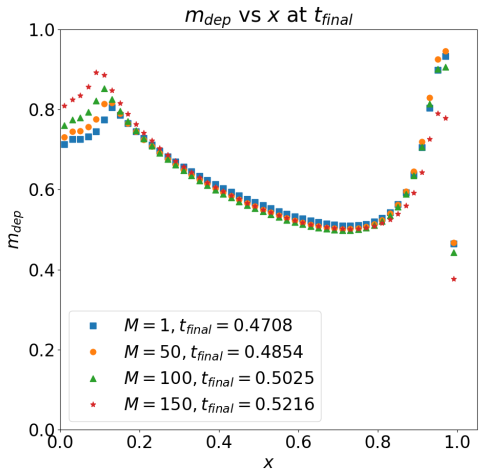

(b) Comparison at t_{final}

Figure 4.23: Deposited Particle Profile Comparison for M

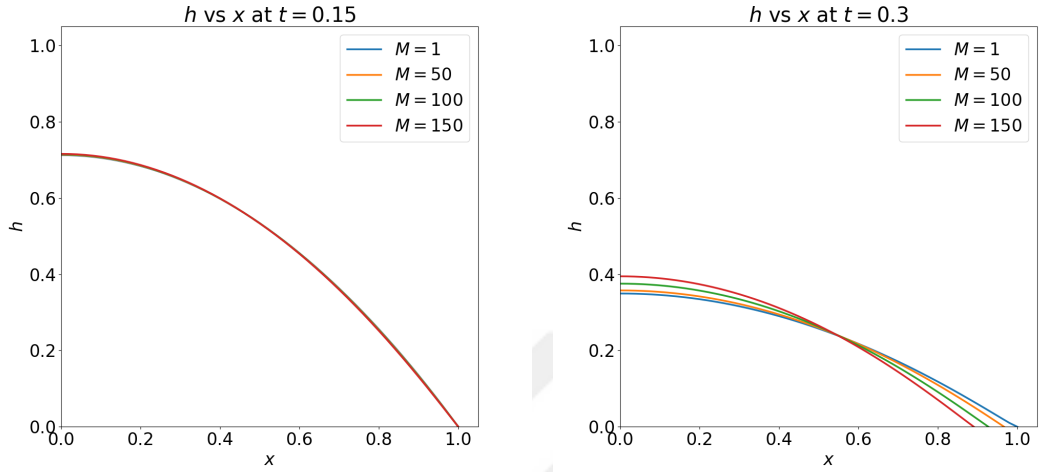

(a) Comparison at t = 0.15 (b) Comparison at t = 0.3

Figure 4.24: Droplet Interface Height Profile Comparison for M

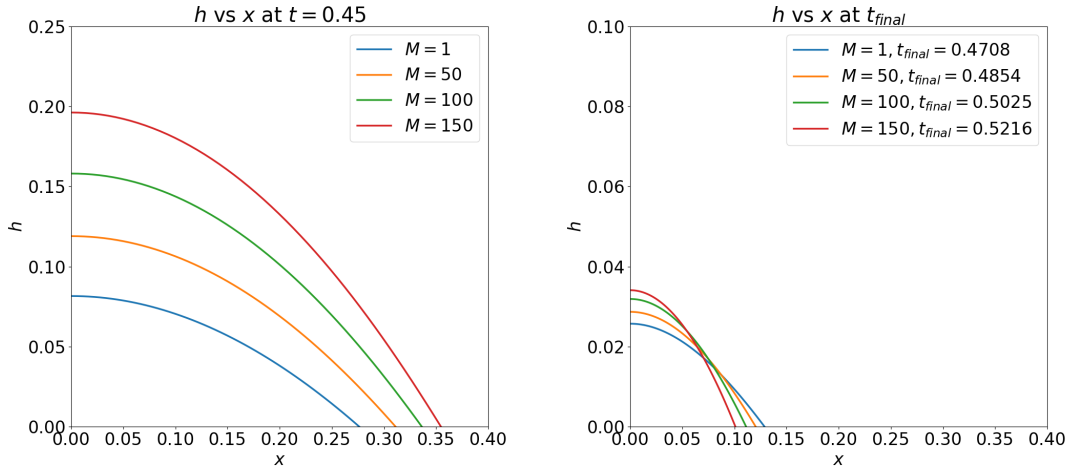

(a) Comparison at t = 0.45 (b) Comparison at t_{final}

Figure 4.25: Droplet Interface Height Profile Comparison for M

In Figure 4.20a, particle concentration values for $M = 1$, $M = 50$ and $M = 100$ are similar, however, $M = 150$ has lowest concentration among them. It is known that increasing Marangoni effect causes counter flow to center of droplet, therefore, at case with $M = 150$, particle concentration is lower than others.

Therefore, in the early stage at $t = 0.15$, $M = 150$ case deposits less particle. Increasing Ma number will increase the power of counter flow, therefore, the droplets with higher Marangoni number will switch to moving contact line regime earlier which can be seen in Figure 4.24b. As a result of this particle concentration behavior, in Figures 4.22, and 4.23, it can be seen that result with highest Ma has always lowest particle deposited near the contact line.

Particle concentration in moving contact line regime can be depend on size of the droplet. In Figure 4.25a, case with $M = 1$ has lowest droplet size. If particle concentration graph is evaluated for same time, in Figure 4.21a maximum peak particle concentration value belongs to case with $M = 1$. This situation can be related to particle concentration equation which is averaged in h. If particle mass is not changed a lot, while droplet size is getting smaller, this can cause high particle concentration value.

In Figure 4.23b, final deposit shapes are compared and it is seen that with increasing value of M, more particle deposited near the center of droplet. In Figure 4.23b, near the contact line maximum deposited particle mass is for $M = 50$ and after this, $M = 1$. This situation can be caused by h profile change in pinned case. Increasing Ma causes faster decrease of h profile, and this situation can boost height averaged evaporation term. As a result of this, particle concentration can increase much faster. If it is zoomed to contact line of Figure 4.24a, this will justify the previous argument:

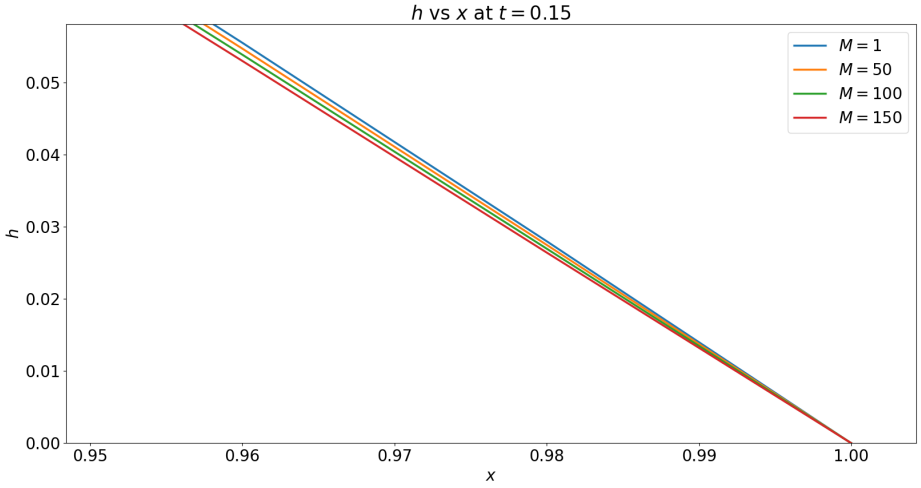

Figure 4.26: h Profile Near the Contact Line at t = 0.15

Figure 4.26 shows that h profile near the contact line decreases faster with increasing M. Even with this affect, higher M numbers will deposit more particle near the center at the end, because their contact line will move earlier and there can be more remaining particles in the droplet for deposition.

In order to get considerable Marangoni effects, base M value is increased 150 times. This much of increase can be considered as abnormal. In literature, Hu and Larson [10] compared octane and water in terms of Marangoni effect. Octane is demonstrating strong Marangoni effect, however, water is demonstrating weak Marangoni effects [10]. Theoretical Marangoni number for octane is found as 45800, and for water, it is found as 8 when there is contaminant [10]. The difference between them is around approximately 5000 to 6000 times. Although Marangoni number in this thesis is not same as Marangoni number in Hu and Larson [10], relative change can still be used to understand range. Therefore, 150 times increase in Marangoni number can be considered in reasonable range.

4.2.4.2 Damkohler Number

In this section, Damkohler number will be changed and its effects to h, c and m_{dep} will be observed. For this purpose $Da = 1.2$, $Da = 1.0$ and $Da = 0.9$ cases will be compared. When $\epsilon = 0.1$ and $Pe = 10$, $\frac{Da}{\epsilon Pe}$ will still be around one for $Da = 1.2$. Therefore choosing this value is not a problem. Firstly, c, m_{dep} and h profiles will be presented:

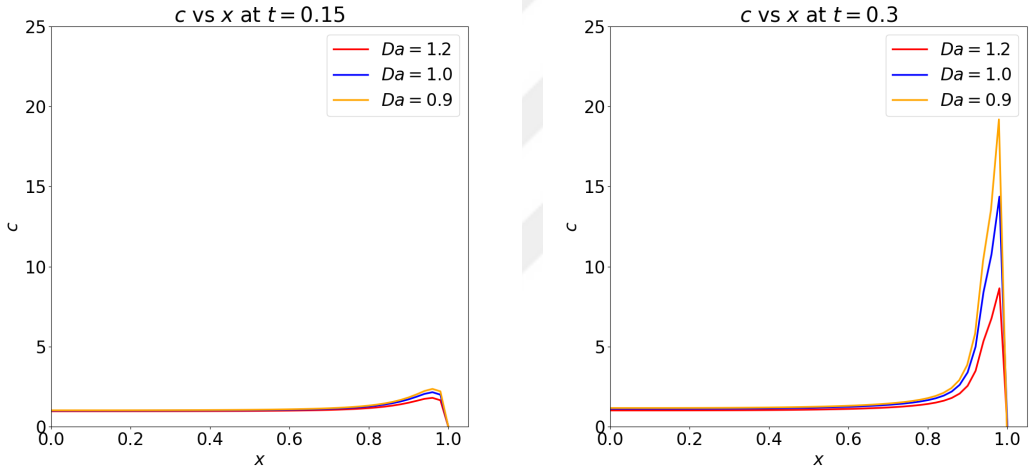

(a) Comparison at t = 0.15

(b) Comparison at t = 0.3

Figure 4.27: Particle Concentration Profile Comparison for Da

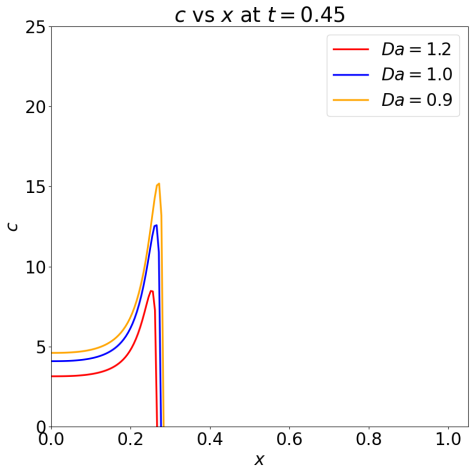

(a) Comparison at t = 0.45

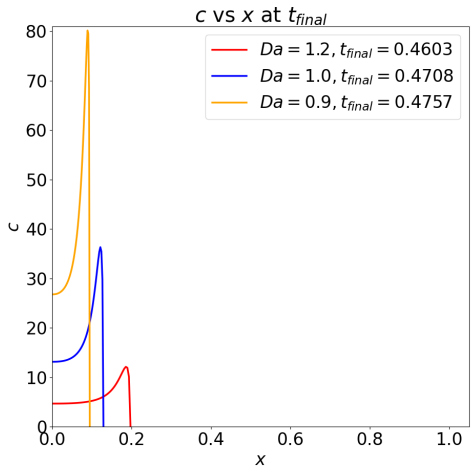

(b) Comparison at t_{final}

Figure 4.28: Particle Concentration Profile Comparison for Da

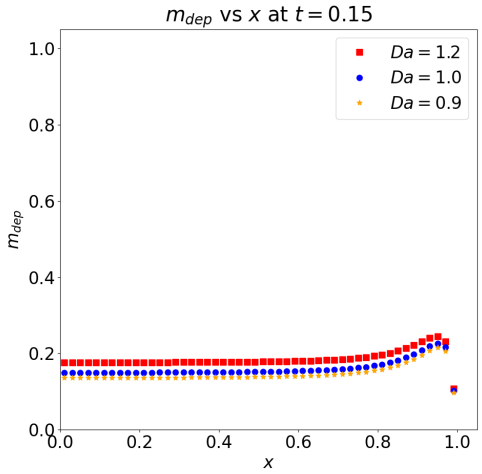

(a) Comparison at t = 0.15

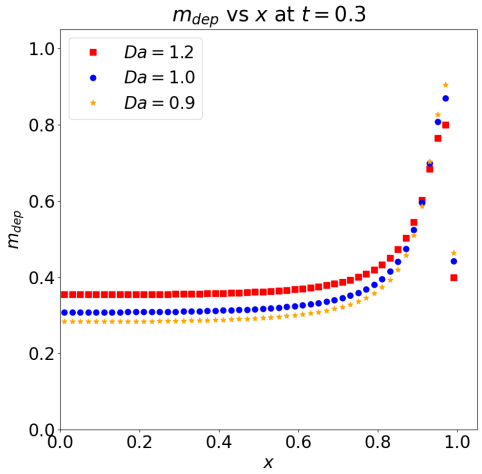

(b) Comparison at t = 0.3

Figure 4.29: Deposited Particle Profile Comparison for Da

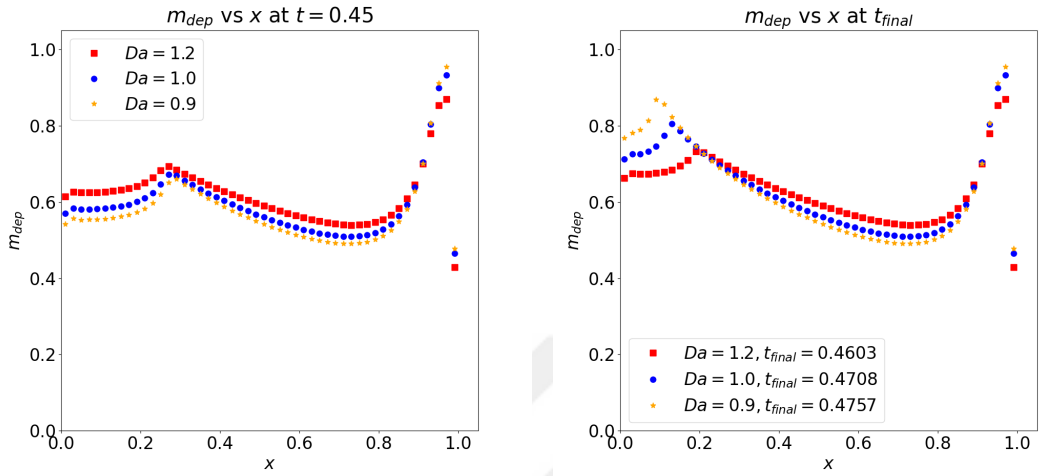

(a) Comparison at t = 0.45 (b) Comparison at t_{final}

Figure 4.30: Deposited Particle Profile Comparison for Da

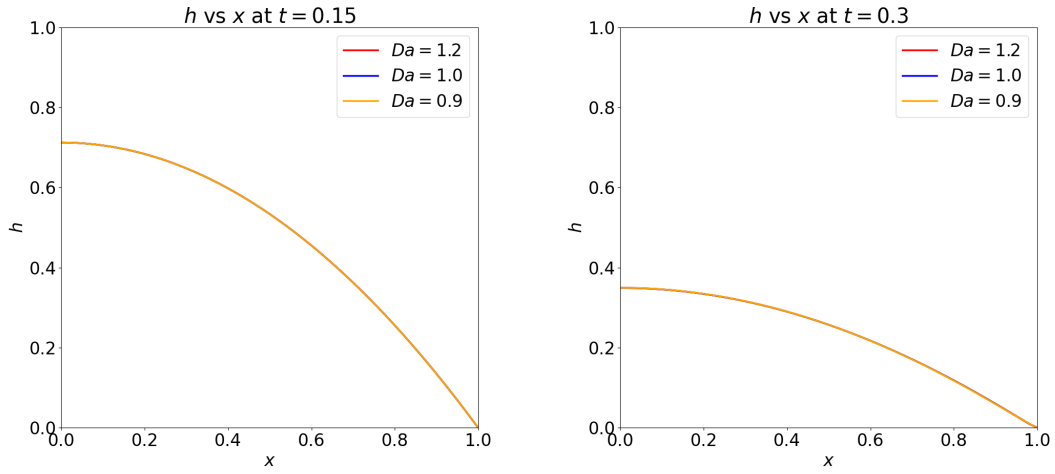

(a) Comparison at t = 0.15 (b) Comparison at t = 0.3

Figure 4.31: Droplet Interface Height Profile Comparison for Da

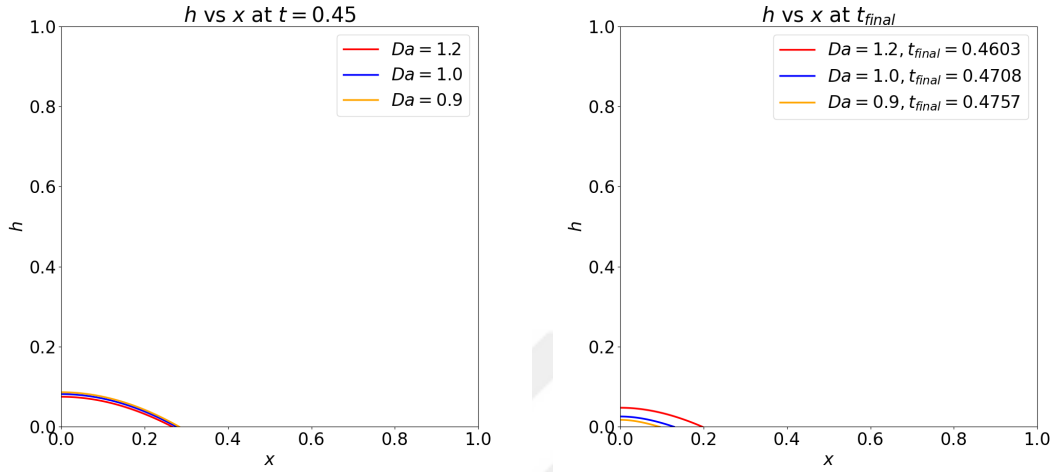

(a) Comparison at t = 0.45 (b) Comparison at t_{final}

Figure 4.32: Droplet Interface Height Profile Comparison for Da

Damkohler number measures ratio of particle deposition to diffusion [25]. When it is increased, more particle will be deposited, however, particle concentration will decrease more. Therefore, in Figures 4.27 and 4.28, for all time steps, cases with highest Da have lowest peak particle concentration. In Figure 4.28b, particle concentration of case with $Da = 0.9$ reaches almost 80. This situation can cause dilute approximation is invalid. However, this is not problem for given case because this occurs in very late time step.

For deposition profiles in early time step at $t = 0.15$, case with highest Da number deposited more particle. However, this situation changes in next time steps as in Figures 4.29b- 4.30b, because cases with lower Da numbers will have higher particle concentration value, therefore these cases will deposit more particle near the contact line. In Figure 4.30b, it can be seen that increasing Da number will cause less deposited particle near the center and contact line. Therefore, more particles will be deposited in the middle of the center and contact line. When Da is high, particles will be deposited more and they will diffuse less, therefore, deposited particle profile can be expected to more uniform, in comparison with other cases with lower Da number.

In Figures 4.31a, 4.31b, and 4.32a, h profiles are almost identical. In Figure 4.32b, final droplet sizes are different, and as expected case with $Da = 1.2$ deposits faster 95 % of initial particle mass, and with decreasing Da number this time is increasing.

4.2.4.3 Evaporation Number

In this section effects of evaporation number will be discussed. $E = 1.0$, $E = 0.75$ and $E = 0.5$ cases will be used to see effect of indicated numbers on c, h and m_{dep} profiles.

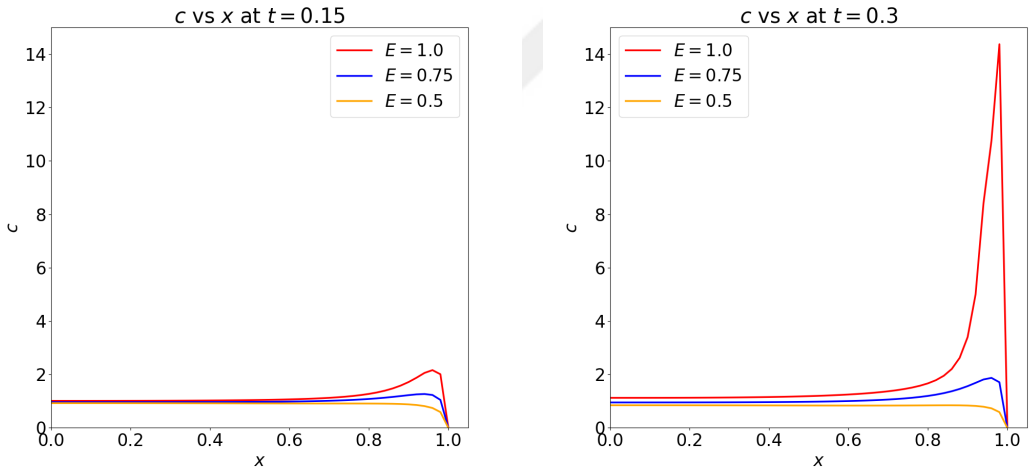

(a) Comparison at t = 0.15

(b) Comparison at t = 0.3

Figure 4.33: Particle Concentration Profile Comparison for E

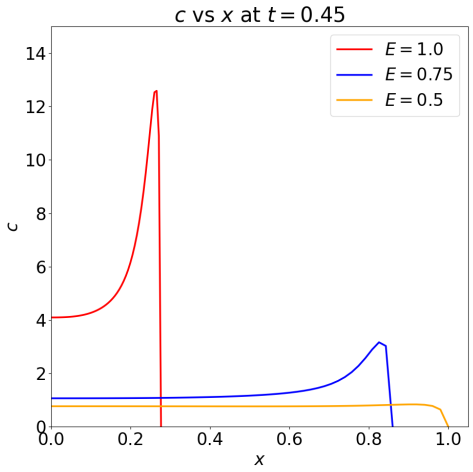

(a) Comparison at t = 0.45

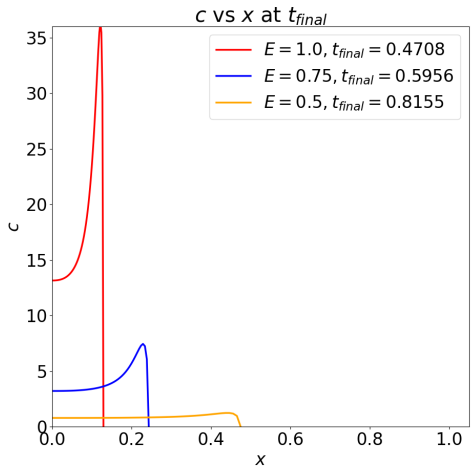

(b) Comparison at t_{final}

Figure 4.34: Particle Concentration Profile Comparison for E

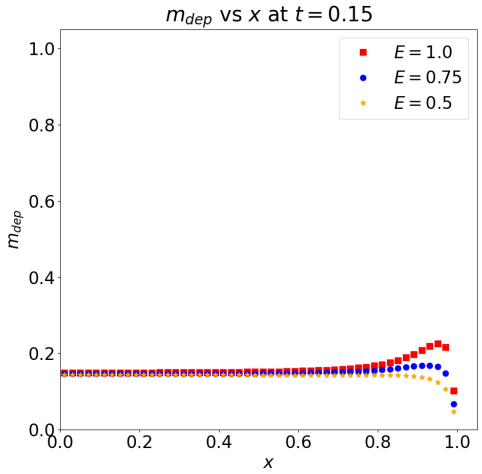

(a) Comparison at t = 0.15

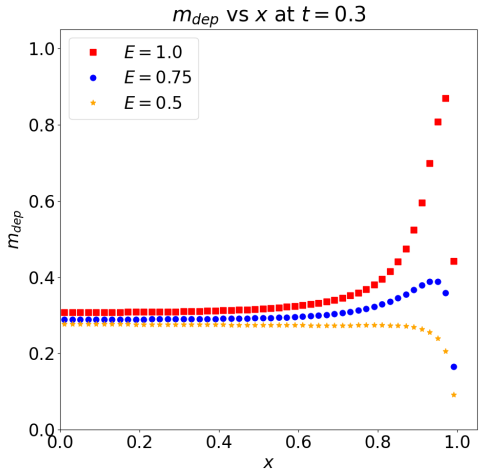

(b) Comparison at t = 0.3

Figure 4.35: Deposited Particle Profile Comparison for E

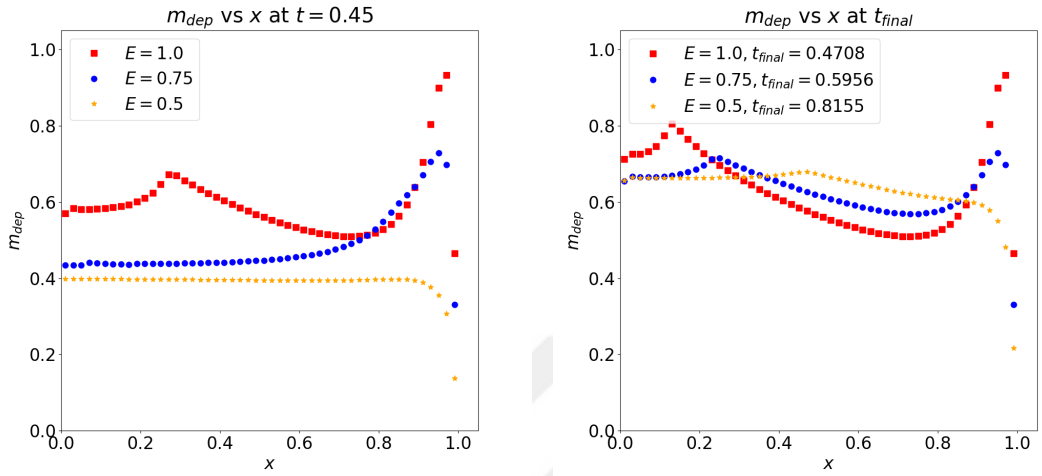

(a) Comparison at t = 0.45 (b) Comparison at t_{final}

Figure 4.36: Deposited Particle Profile Comparison for E

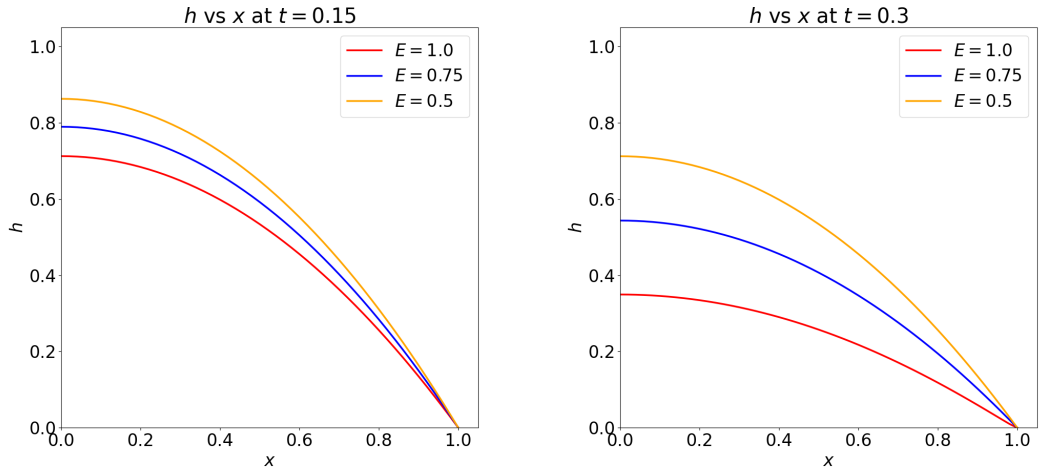

(a) Comparison at t = 0.15 (b) Comparison at t = 0.3

Figure 4.37: Droplet Interface Height Profile Comparison for E

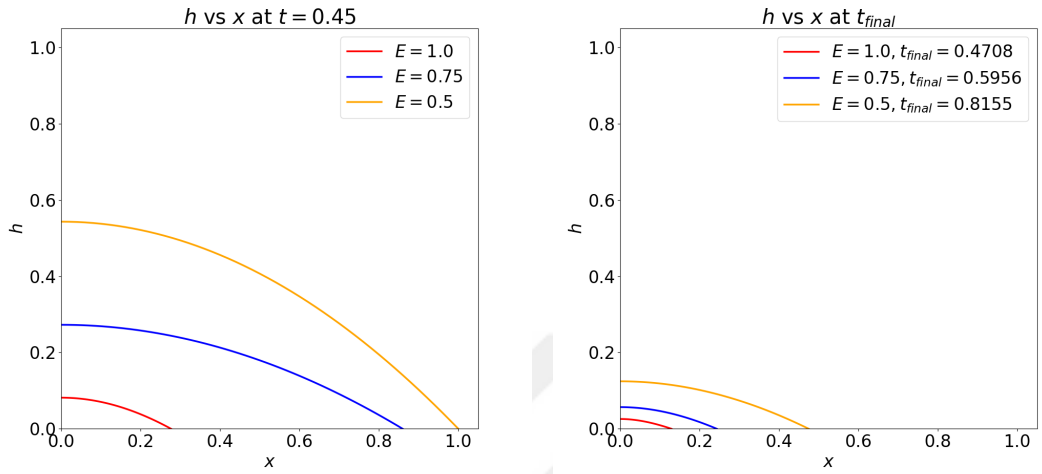

(a) Comparison at t = 0.45

(b) Comparison at t_{final}

Figure 4.38: Droplet Interface Height Profile Comparison for E

Evaporation number is an important parameter for droplet. It is a measure for power of evaporation process. Figures 4.33 and 4.34 show that decrease in E makes particle concentration profile more uniform. This situation also affects deposited particle profile. When particle concentration becomes uniform, deposition profile will follow the same behavior. Figures 4.35 and 4.36 show that decreasing E makes deposition more uniform.

At moving contact line regime, according to size of the droplet, peak particle concentration value is changing. This situation is explained in Marangoni part. In Figures 4.34a and 4.34b, the cases with $E = 1.0$ has minimum droplet size and maximum peak particle concentration. Figures 4.37 and 4.38 show that decreasing E number will increase the total evaporation time. This situation affects final size of the droplet, because algorithm stops when 95% of initial particle mass is deposited. Therefore, when E number decreased, same amount of particle will be deposited with less amount of mass loss.

4.2.4.4 Capillary Number

In this part, Ca will be changed and its effects on h, c, and m_{dep} will be observed. 3 different Ca number will be used in this comparison. These are $Ca = 0.001$, $Ca = 0.002$ and $Ca = 0.005$. Firstly, c, m_{dep} and h profiles will be presented:

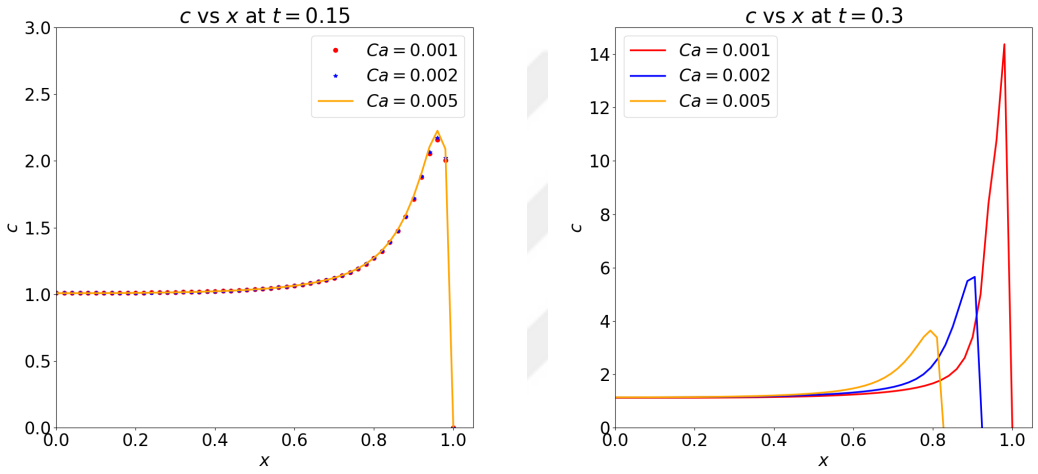

(a) Comparison at t = 0.15 (b) Comparison at t = 0.3

Figure 4.39: Particle Concentration Profile Comparison for Ca

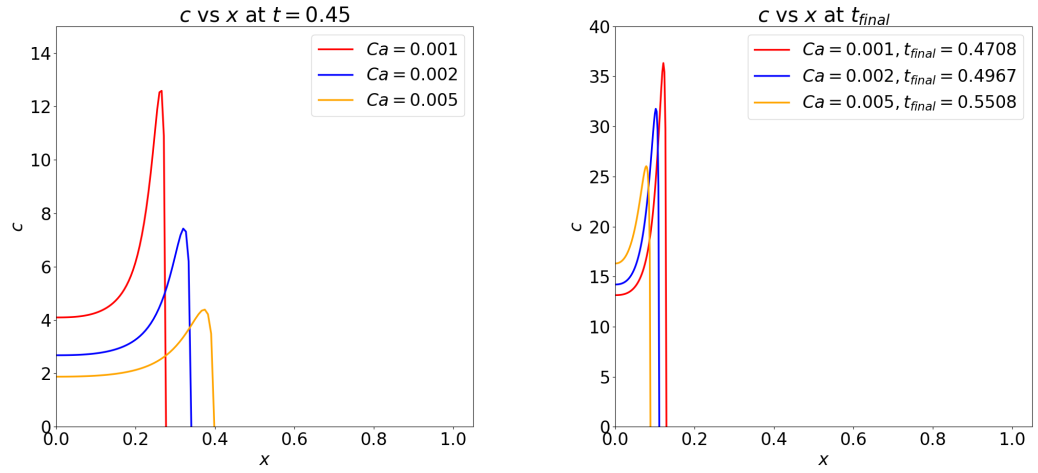

(a) Comparison at t = 0.45 (b) Comparison at t_{final}

Figure 4.40: Particle Concentration Profile Comparison for Ca

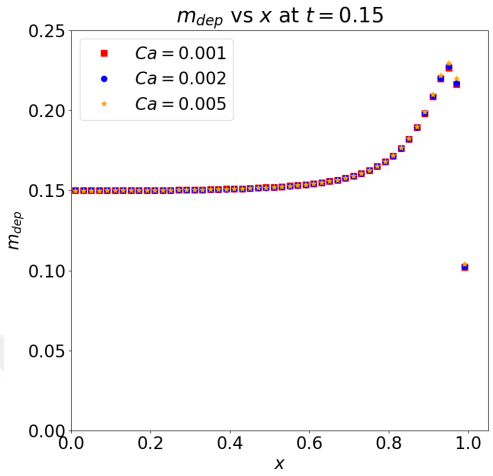

(a) Comparison at t = 0.15

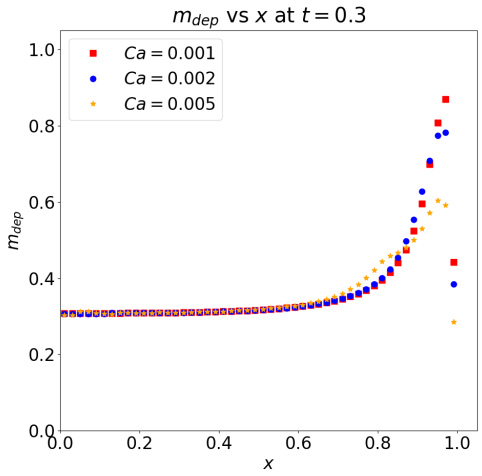

(b) Comparison at t = 0.3

Figure 4.41: Deposited Particle Profile Comparison for Ca

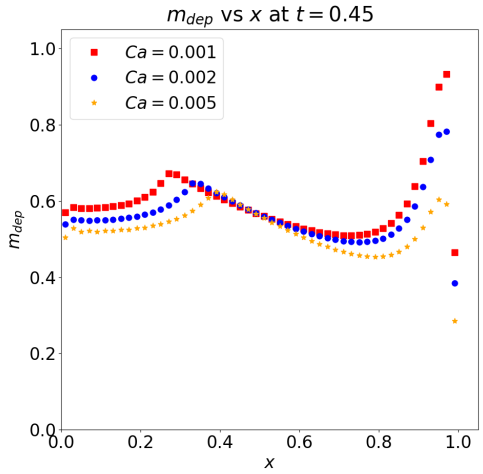

(a) Comparison at t = 0.45

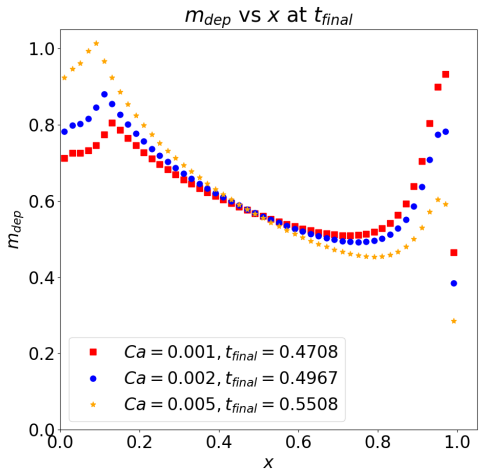

(b) Comparison at t_{final}

Figure 4.42: Deposited Particle Profile Comparison for Ca

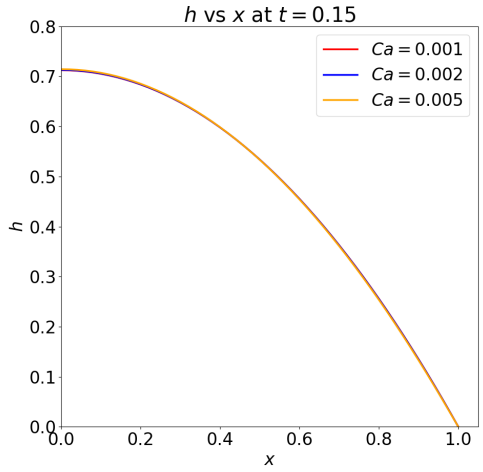

(a) Comparison at t = 0.15

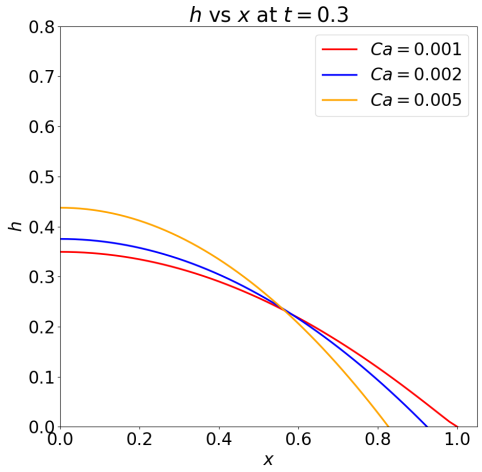

(b) Comparison at t = 0.3

Figure 4.43: Droplet Interface Height Profile Comparison for Ca

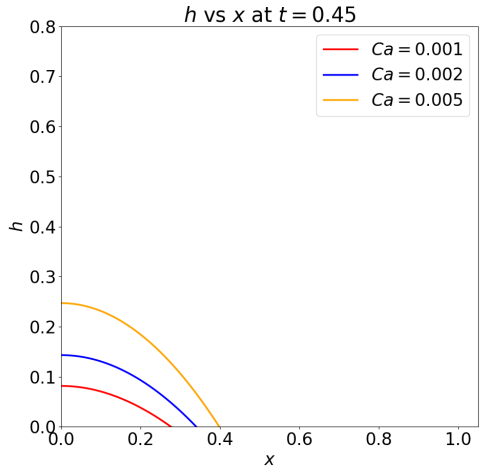

(a) Comparison at t = 0.45

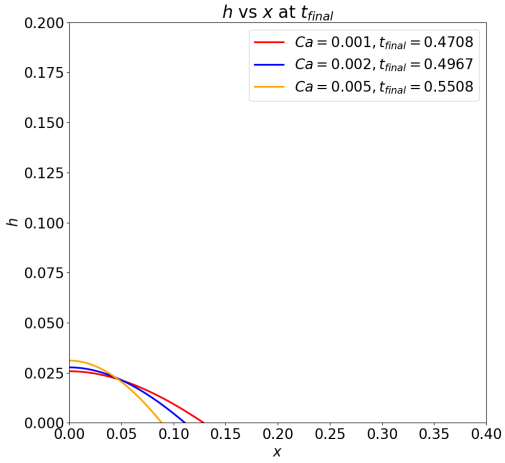

(b) Comparison at t_{final}

Figure 4.44: Droplet Interface Height Profile Comparison for Ca

Figure 4.39a, shows that increasing Ca, increased peak particle concentration slightly. This situation can be caused by faster decrease of h profile near the contact line for higher capillary number. This situation can be assessed by looking at contact angle value at $t = 0.15$. For $Ca = 0.001$ case, rounded contact

angle value is 1.408, for $Ca = 0.002$ case, rounded contact angle value is 1.392, and for $Ca = 0.005$ case, rounded contact angle value is 1.342. This situation shows that h profile near contact line decreases much faster with increasing Ca. Therefore, this fast decrease can boost height averaged evaporation and particle concentration can increase much faster. In Figure 4.39b, mentioned fast decrease of contact angle can also be seen because cases with larger capillary number switch to moving contact line regime earlier. In same figure, difference between particle concentration peak values can be explained by looking at h profile in Figure 4.43b. With increasing capillary number, maximum height to radius ratio is increasing therefore, peak particle concentration becomes lower as in Figure 4.43b. Similar fashion is also in Figures 4.40a and 4.40b. By looking at h and c profiles in Figures 4.40a, 4.40b, 4.44a and 4.44b, $Ca = 0.001$ case has always largest peak particle concentration and lowest ratio of maximum height to radius, in comparison with other cases. Therefore, in Figures 4.40a, and 4.40b, peak particle concentrations decreases with increasing Ca.

Deposited particle mass comparison in Figure 4.41a shows correlated result with c profile at $t = 0.15$ and cases with higher Ca number deposit more particles near the contact line. However, at later stages, in Figures 4.41b, 4.42a and 4.42b, case with $Ca = 0.001$ deposits more particle near the contact line because contact line will start to move much later than other cases. Therefore, this case will deposit more particles near the contact line in pinned regime. Figures 4.41b justifies this claim. At the t_{final} in Figure 4.42b , it can be concluded that, increasing Ca number will cause more particle deposition near the center of the droplet.

Chapter 5

Conclusion

Modeling dispersion and deposition of particles in evaporating droplet is a hard process, because there are many different parameters which must be solved together. Therefore, different assumptions are made to simplify problem and focus on one part of it. Many works in the literature uses either pinned or moving contact line assumptions. However, it is known that the droplet can exhibit both of the behavior in same lifetime of it. When one of the regime is ignored with some assumptions, whole process cannot be simulated. Therefore, in this work, numerical algorithm is derived for both regime and combined for special case of the droplet whose contact line is initially pinned then after some contact angle it starts to move.

In order to get mathematical model of current problem, different models from literature are combined. Current model contains particle dispersion, deposition, temporal evolution of droplet interface height and radius. Lubrication theory and rapid vertical diffusion assumptions are used for getting one dimensional equations for h, and c. Particle concentration model in Karapetsas et al. [28] is expanded by adding particle deposition boundary condition from Widjaja and Harris [25]. Thus current model can deposit particle while it is evaporating and particle concentration is affected by this deposition.

Numerical algorithms were developed for pinned and moving cases separately. In moving contact line case without particle concentration, numerical algorithm is validated with results of Anderson and Davis [1]. In order to adapt h profile to moving contact line case, an interpolation approach is used. In pinned case with particle concentration, numerical algorithm is validated for particle dispersion, droplet interface height change and particle concentration dependence of viscosity with results of Fischer [23] and Tarasevich et al. [26]. After validation, these algorithms were combined to simulate the droplets which are initially pinned then moving. In this combination, h and c profiles are adapted to dynamic mesh by doing linear interpolation. For contact line movement, model in Anderson and Davis [1] is used. For numerical solution, FDM is used.

After deriving numerical algorithm, numerical simulations are completed and parametric study is done by changing one parameter at once. With decided parameter set, deposition profile similar to coffee-ring deposit shape is obtained. After this, M is changed, and it is observed that increasing Marangoni number increases deposited particle amount near the center as expected. Decrease in evaporation number and increase in Damkohler number caused more uniform deposition profiles. Increasing capillary number results in more particle deposition near the center.

By considering features of presented model and literature review, combining pinned and moving contact line regimes with particle deposition provides some novelty to this work.

The model in this work can be improved with some future work. Firstly, model related to contact line movement can be improved by doing some experiment. The used model [1] is derived by mass balance at this point. In this relation, effects of evaporation and constitutive relation between contact angle and contact line speed are linearly summed [1]. Therefore, it is not enough for modeling droplet with dispersed particles. Conducting experiment for the droplet contains dispersed particles and finding new constitutive relation can increase the accuracy of current model.

In current model, particle dispersion is modeled with advection-diffusion equation and particle to particle interaction is not considered. Therefore, interactions between particle can be added to model to improve it.

The model in this work is validated by results using lubrication theory. Validation of current model can be improved by using Direct Numerical Simulations (DNS) because DNS is not limited with assumptions of lubrication theory and DNS can create good reference results.

Appendix A

Mathematical Derivations

In this chapter, related mathematical derivations will be presented for different parts of the model.

A.1 Scaling and Lubrication Theory

Nondimensionalization of governing equations, constitutive relations and boundary conditions are completed in this section. For dimensional parameters following substitutions will be made in this section:

$$x = x^* a_0, \quad a = a^* a_0, \quad z = z^* h_0, \quad h = h^* h_0, \quad \theta = \Theta\epsilon \tag{A.1}$$

$$u = u^* u_c, \quad w = w^* u_c \epsilon, \quad t = t^* \frac{a_0}{u_c} \tag{A.2}$$

$$p = p^* \frac{\rho \nu_0 u_c a_0}{h_0^2}, \quad J = J^* \frac{k\Delta T}{h_0 L}, \quad T = T^* \Delta T + T_S, \quad c = c^* c_i \tag{A.3}$$

To calculate x and z component of Navier-Stokes equation, $\bar{\tau}$ must be defined. Element of $\bar{\tau}$ is as following [9]:

$$\bar{\tau}_{ij} = \frac{1}{2}\left(\frac{\partial \tilde{u}_i}{\partial \tilde{x}_j} + \frac{\partial \tilde{u}_j}{\partial \tilde{x}_i}\right) \tag{A.4}$$

Where $\tilde{u}$ and $\tilde{x}$ are velocity and position vectors. Sub-indices show position at vector, therefore, $(\tilde{u}_1, \tilde{u}_2) = (u, w)$ and $(\tilde{x}_1, \tilde{x}_2) = (x, z)$. As a result $\bar{\tau}$ will be following:

$$\bar{\tau} = \begin{bmatrix} \frac{\partial u}{\partial x} & \frac{1}{2}\left(\frac{\partial u}{\partial z} + \frac{\partial w}{\partial x}\right) \\ \frac{1}{2}\left(\frac{\partial u}{\partial z} + \frac{\partial w}{\partial x}\right) & \frac{\partial w}{\partial z} \end{bmatrix} \tag{A.5}$$

X-component of Navier-Stokes equation for given case can be written as following:

$$\rho\frac{\partial u}{\partial t} + \rho u\frac{\partial u}{\partial x} + \rho w\frac{\partial u}{\partial z} = -\frac{\partial p}{\partial x} + \mu\left(\frac{\partial^2 u}{\partial x^2} + \frac{\partial^2 u}{\partial z^2}\right) + 2\frac{\partial \mu}{\partial x}\frac{\partial u}{\partial x} + \frac{\partial \mu}{\partial z}\left(\frac{\partial u}{\partial z} + \frac{\partial w}{\partial z}\right) \tag{A.6}$$

If variables in A.1-A.3 are substituted into equation A.6:

$$\frac{\rho\nu_0^2}{h_0^2 a_0}\frac{\partial u^*}{\partial t^*} + \frac{\rho\nu_0^2}{h_0^2 a_0}u^*\frac{\partial u^*}{\partial x^*} + \frac{\rho\nu_0^2}{h_0^2 a_0}w^*\frac{\partial u^*}{\partial z^*} + \frac{\rho\nu_0^2}{h_0^3}\frac{\partial p^*}{\partial x^*} =$$
$$\rho\nu_0\tilde{\mu}\left(\frac{\nu_0}{a_0^2 h_0}\frac{\partial^2 u^*}{\partial x^{*^2}} + \frac{\nu_0}{h_0^3}\frac{\partial^2 u^*}{\partial z^{*^2}}\right) + 2\frac{\rho\nu_0^2}{h_0 a_0^2}\frac{\partial \tilde{\mu}}{\partial x^*}\frac{\partial u^*}{\partial x^*} + \frac{\rho\nu^2}{h_0}\frac{\partial \tilde{\mu}}{\partial z^*}\left(\frac{1}{h_0^2}\frac{\partial u^*}{\partial z^*} + \frac{1}{a_0^2}\frac{\partial w^*}{\partial x^*}\right) \tag{A.7}$$

Where $\tilde{\mu} = \left(1 - \frac{c_i}{c_\infty}c^*\right)^{-2}$. If equation A.7 is multiplied by $\frac{h_0^3}{\rho\nu_0^2}$:

$$\epsilon\frac{\partial u^*}{\partial t^*} + \epsilon u^*\frac{\partial u^*}{\partial x^*} + \epsilon w^*\frac{\partial u^*}{\partial z^*} =$$
$$-\frac{\partial p^*}{\partial x^*} + \tilde{\mu}\left(\epsilon^2\frac{\partial^2 u^*}{\partial x^{*^2}} + \frac{\partial^2 u^*}{\partial z^{*^2}}\right) + 2\epsilon^2\frac{\partial \tilde{\mu}}{\partial x^*}\frac{\partial u^*}{\partial x^*} + \frac{\partial \tilde{\mu}}{\partial z^*}\left(\frac{\partial u^*}{\partial z^*} + \epsilon^2\frac{\partial w^*}{\partial x^*}\right) \tag{A.8}$$

With lubrication approximation, terms with ϵ and ϵ^2 can be canceled and as a result of this:

$$-\frac{\partial p^*}{\partial x^*} + \tilde{\mu}\frac{\partial^2 u^*}{\partial z^{*^2}} + \frac{\partial \tilde{\mu}}{\partial z^*}\frac{\partial u^*}{\partial z^*} = 0 \tag{A.9}$$

$$-\frac{\partial p^*}{\partial x^*} + \frac{\partial}{\partial z}\left(\tilde{\mu}\frac{\partial u^*}{\partial z^*}\right) = 0 \tag{A.10}$$

Z-component of Navier-Stokes equation for given case can be written as following:

$$\rho\frac{\partial w}{\partial t} + \rho u\frac{\partial w}{\partial x} + \rho w\frac{\partial w}{\partial z} = -\frac{\partial p}{\partial z} + \mu\left(\frac{\partial^2 w}{\partial x^2} + \frac{\partial^2 w}{\partial z^2}\right) + 2\frac{\partial \mu}{\partial z}\frac{\partial w}{\partial z} + \frac{\partial \mu}{\partial x}\left(\frac{\partial u}{\partial z} + \frac{\partial w}{\partial x}\right) \tag{A.11}$$

If variables in A.1-A.3 are substituted into equation A.11:

$$\frac{\rho\nu_0^2}{a_0^2 h_0}\frac{\partial w^*}{\partial t^*} + \frac{\rho\nu_0^2}{a_0^2 h_0}u^*\frac{\partial w^*}{\partial x^*} + \frac{\rho\nu_0^2}{a_0^2 h_0}w^*\frac{\partial w^*}{\partial z^*} + \frac{\rho\nu_0^2 a_0}{h_0^4}\frac{\partial p^*}{\partial z^*} =$$
$$\rho\nu_0\tilde{\mu}\left(\frac{\nu_0}{a_0^3}\frac{\partial^2 w^*}{\partial x^{*^2}} + \frac{\nu_0}{h_0^2 a_0}\frac{\partial^2 w^*}{\partial z^{*^2}}\right) + 2\frac{\rho\nu_0^2}{a_0 h_0^2}\frac{\partial \tilde{\mu}}{\partial z^*}\frac{\partial w^*}{\partial z^*} + \frac{\rho\nu_0^2}{a_0}\frac{\partial \tilde{\mu}}{\partial x^*}\left(\frac{1}{h_0^2}\frac{\partial u^*}{\partial z^*} + \frac{1}{a_0^2}\frac{\partial w^*}{\partial x^*}\right) \tag{A.12}$$

If equation A.12 is multiplied by $\frac{h_0^4}{\rho\nu_0^2 a_0}$:

$$\epsilon^3\frac{\partial w^*}{\partial t^*} + \epsilon^3 u^*\frac{\partial w^*}{\partial x^*} + \epsilon^3 w^*\frac{\partial w^*}{\partial z^*} =$$
$$-\frac{\partial p^*}{\partial z^*} + \tilde{\mu}\left(\epsilon^4\frac{\partial^2 w^*}{\partial x^{*^2}} + \epsilon^2\frac{\partial^2 w^*}{\partial z^{*^2}}\right) + 2\epsilon^2\frac{\partial \tilde{\mu}}{\partial z^*}\frac{\partial w^*}{\partial z^*} + \frac{\partial \tilde{\mu}}{\partial x^*}\left(\epsilon^2\frac{\partial u^*}{\partial z^*} + \epsilon^4\frac{\partial w^*}{\partial x^*}\right) \tag{A.13}$$

With lubrication approximation, terms with ϵ^2, ϵ^3 and ϵ^4 can be canceled and as a result of this:

$$-\frac{\partial p^*}{\partial z^*} = 0 \tag{A.14}$$

For incompressible fluid, continuity equation will be as following:

$$\frac{\partial u}{\partial x} + \frac{\partial w}{\partial z} = 0 \tag{A.15}$$

If variables in A.1-A.3 are substituted into equation A.15:

$$\frac{\nu_0}{a_0 h_0}\frac{\partial u^*}{\partial x^*} + \frac{\nu_0}{a_0 h_0}\frac{\partial w^*}{\partial z^*} = 0 \tag{A.16}$$

$\frac{\nu_0}{a_0 h_0}$ can be canceled, as a result of this:

$$\frac{\partial u^*}{\partial x^*} + \frac{\partial w^*}{\partial z^*} = 0 \tag{A.17}$$

Energy equation of Navier-Stokes can be written as following:

$$\frac{\partial T}{\partial t} + u\frac{\partial T}{\partial x} + w\frac{\partial T}{\partial z} = \frac{k}{\rho c_p}\left(\frac{\partial^2 T}{\partial x^2} + \frac{\partial^2 T}{\partial z^2}\right) \tag{A.18}$$

If variables in A.1-A.3 are substituted into equation A.18:

$$\frac{\nu_0 \Delta T}{a_0 h_0}\frac{\partial T^*}{\partial t^*} + \frac{\nu_0 \Delta T}{a_0 h_0}u^*\frac{\partial T^*}{\partial x^*} + \frac{\nu_0 \Delta T}{a_0 h_0}w^*\frac{\partial T^*}{\partial z^*} = \frac{k}{\rho c_p}\left(\frac{\Delta T}{a_0^2}\frac{\partial^2 T^*}{\partial x^{*^2}} + \frac{\Delta T}{h_0^2}\frac{\partial^2 T^*}{\partial z^{*^2}}\right) \tag{A.19}$$

If equation A.19 is multiplied by $\frac{h_0^2}{\nu_0 \Delta T}$:

$$\epsilon\frac{\partial T^*}{\partial t^*} + \epsilon u^*\frac{\partial T^*}{\partial x^*} + \epsilon w^*\frac{\partial T^*}{\partial z^*} = \frac{k}{\nu_0 \rho c_p}\left(\epsilon^2\frac{\partial^2 T^*}{\partial x^{*^2}} + \frac{\partial^2 T^*}{\partial z^{*^2}}\right) \tag{A.20}$$

If $\frac{k}{\nu_0 \rho c_p}\epsilon^2 << 1$ is assumed, with lubrication approximation, terms with ϵ and ϵ^2 can be canceled and as a result of this:

$$\frac{\partial^2 T^*}{\partial z^{*^2}} = 0 \tag{A.21}$$

After completing scaling of Navier-Stokes equation, advection-diffusion equation for particle concentration can be nondimensionalized. Dimensional form of this equation is as following:

$$\frac{\partial c}{\partial t} + \bar{U}.\nabla c = D_c \nabla^2 c \tag{A.22}$$

If terms in equation A.22 are opened up, equation A.22 will be as following:

$$\frac{\partial c}{\partial t} + u\frac{\partial c}{\partial x} + w\frac{\partial c}{\partial z} = D_c \left(\frac{\partial^2 c}{\partial x^2} + \frac{\partial c^2}{\partial z^2} \right) \tag{A.23}$$

If variables in A.1-A.3 are substituted into equation A.23:

$$\frac{c_i \nu_0}{a_0 h_0}\frac{\partial c^*}{\partial t^*} + \frac{c_i \nu_0}{a_0 h_0} u^* \frac{\partial c^*}{\partial x^*} + \frac{c_i \nu_0}{a_0 h_0} w^* \frac{\partial c^*}{\partial z^*} = D_c \left(\frac{c_i}{a_0^2}\frac{\partial^2 c^*}{\partial x^{*^2}} + \frac{c_i}{h_0^2}\frac{\partial^2 c^*}{\partial z^{*^2}} \right) \tag{A.24}$$

If equation A.24 is multiplied by $\frac{a_0 h_0}{\nu_0 c_i}$:

$$\frac{\partial c^*}{\partial t^*} + u^*\frac{\partial c^*}{\partial x^*} + w^*\frac{\partial c^*}{\partial z^*} = \frac{D_c \epsilon}{\nu_0} \left(\frac{\partial^2 c^*}{\partial x^{*^2}} + \frac{1}{\epsilon^2}\frac{\partial^2 c^*}{\partial z^{*^2}} \right) \tag{A.25}$$

Where Pe is $\frac{\nu_0}{D_c \epsilon}$. After completing scaling of advection-diffusion equation, radius equation can be nondimensionalized. Indicated equation is as following:

$$\frac{\partial a}{\partial t} = -\frac{J(a)}{\rho sin\theta} + \eta f(\theta) \tag{A.26}$$

If variables in A.1-A.3 are substituted into equation A.26:

$$\frac{\nu_0}{h_0}\frac{\partial a^*}{\partial t^*} = -\frac{-k\Delta T}{\rho h_0 L}\frac{J(a^*)}{\Theta \epsilon} + \eta \epsilon^3 f(\Theta) \tag{A.27}$$

In this derivation, $sin\theta$ will be approximated as θ with small angle approximation because θ is small. There is ϵ^3 in second term of right hand side, because f is order of θ^3 and θ is scaled with ϵ. Advancing and receding contact angle are also scaled with ϵ, therefore:

$$f(\Theta) = \left\{ \begin{array}{ll} (\Theta - \Theta_A)^3, & \text{if } \Theta > \Theta_A \\ 0 \quad , & \text{if } \Theta_A > \Theta > \Theta_R \\ (\Theta - \Theta_R)^3, & \text{if } \Theta_R > \Theta \end{array} \right\} \tag{A.28}$$

If equation A.27 is multiplied by $\frac{h_0}{\nu_0}$:

$$\frac{\partial a^*}{\partial t^*} = -\frac{k\Delta T}{\epsilon\rho\nu_0 L}\frac{J(a^*)}{\Theta} + \frac{\eta\epsilon^3 h_0}{\nu_0} f(\Theta) \tag{A.29}$$

$$\frac{\partial a^*}{\partial t^*} = -E\frac{J(a^*)}{\Theta} + \eta^* f(\Theta) \tag{A.30}$$

Where $E = \frac{k\Delta T}{\epsilon\rho\nu_0 L}$ and $\eta^* = \frac{\eta\epsilon^3 h_0}{\nu_0}$. After radius equation, boundary conditions can be nondimensionalized. Kinematic boundary condition is as following:

$$\left(w - \frac{\partial h}{\partial t} - \frac{\partial h}{\partial x}u\right)\left(\frac{1}{\sqrt{1 + \left(\frac{\partial h}{\partial x}\right)^2}}\right) = \frac{J}{\rho} \tag{A.31}$$

If variables in A.1-A.3 are substituted into equation A.31:

$$\left(\frac{\nu_0}{a_0}w^* - \frac{\nu_0}{a_0}\frac{\partial h^*}{\partial t^*} - \frac{\nu_0}{a_0}u^*\frac{\partial h^*}{\partial x^*}\right)\left(\frac{1}{\sqrt{1 + \epsilon^2\left(\frac{\partial h^*}{\partial x^*}\right)^2}}\right) = \frac{k\Delta T}{\rho h_0 L}J^* \tag{A.32}$$

If equation A.32 is multiplied by $\frac{a_0}{\nu_0}$ and term with ϵ^2 is canceled with lubrication theory:

$$w^* - \frac{\partial h^*}{\partial t^*} = u^* \frac{\partial h^*}{\partial x^*} + \frac{k\Delta T}{\epsilon \rho \nu_0 L} J^* \tag{A.33}$$

$$w^* - \frac{\partial h^*}{\partial t^*} = u^* \frac{\partial h^*}{\partial x^*} + E J^* \tag{A.34}$$

Normal boundary condition is as following:

$$-\frac{J^2}{\rho_v} - \bar{T}.\bar{n}.\bar{n} = (\nabla.\bar{n})\sigma \tag{A.35}$$

$\bar{T}.\bar{n}.\bar{n}$ must be calculated and $\bar{T}$ is as following:

$$\bar{T} = -p\bar{I} + 2\mu\bar{\tau} \tag{A.36}$$

If $\bar{T}$ is multiplied by $\bar{n}$ twice:

$$\bar{T}.\bar{n} = -p\bar{n} + 2\mu\bar{\tau}.\bar{n} \tag{A.37}$$

$$\bar{T}.\bar{n}.\bar{n} = -p + 2\mu\bar{\tau}.\bar{n}.\bar{n} \tag{A.38}$$

$\bar{\tau}.\bar{n}.\bar{n}$ will be as following:

$$\bar{\tau}.\bar{n}.\bar{n} = \frac{1}{1 + \left(\frac{\partial h}{\partial x}\right)^2} \left(\frac{\partial u}{\partial x} \left(\frac{\partial h}{\partial x} \right)^2 - \frac{\partial h}{\partial x} \left(\frac{\partial u}{\partial z} + \frac{\partial w}{\partial x} \right) + \frac{\partial w}{\partial z} \right) \tag{A.39}$$

$\nabla.\bar{n}$ will be as following:

$$\nabla.\bar{n} = \frac{-\frac{\partial^2 h}{\partial x^2}}{\sqrt{1 + \left(\frac{\partial h}{\partial x}\right)^2}} \tag{A.40}$$

As a result, normal stress boundary condition will be:

$$-\frac{J^2}{\rho_v}+p-2\mu\frac{\left(\frac{\partial u}{\partial x}\left(\frac{\partial h}{\partial x}\right)^2-\frac{\partial h}{\partial x}\left(\frac{\partial u}{\partial z}+\frac{\partial w}{\partial x}\right)+\frac{\partial w}{\partial z}\right)}{1+\left(\frac{\partial h}{\partial x}\right)^2}=\frac{-\frac{\partial^2 h}{\partial x^2}}{\sqrt{1+\left(\frac{\partial h}{\partial x}\right)^2}}(\sigma_0-\gamma(T-T_S)) \tag{A.41}$$

If variables in A.1-A.3 are substituted into equation A.41 and $1+\left(\frac{\partial h}{\partial x}\right)^2$ is taken as 1 because term $\left(\frac{\partial h}{\partial x}\right)^2$ will become $\epsilon^2\left(\frac{\partial h^*}{\partial x^*}\right)^2$ which can be canceled with lubrication approximation:

$$\begin{aligned}
&-\frac{k^2\Delta T^2}{\rho_v h_0^2 L^2}J^{*^2}+\frac{\rho\nu_0^2 a_0}{h_0^3}p^* \\
&-2\mu_0\tilde{\mu}\left(\epsilon^2\frac{\nu_0}{a_0 h_0}\frac{\partial u^*}{\partial x^*}\left(\frac{\partial h^*}{\partial x^*}\right)^2-\epsilon\frac{\nu_0}{h_0^2}\frac{\partial u^*}{\partial z^*}\frac{\partial h^*}{\partial x^*}-\epsilon\frac{\nu_0}{a_0^2}\frac{\partial w^*}{\partial x^*}\frac{\partial h^*}{\partial x^*}+\frac{\nu_0}{a_0 h_0}\frac{\partial w^*}{\partial z^*}\right) \\
&=-\frac{h_0}{a_0^2}\frac{\partial^2 h}{\partial x^2}(\sigma_0-\gamma T^*\Delta T)
\end{aligned} \tag{A.42}$$

If equation A.42 is multiplied by $\frac{h_0^3}{\rho\nu_0^2 a_0}$:

$$\begin{aligned}
&-\frac{k^2\Delta T^2}{\rho\rho_v\nu_0^2 L^2}\epsilon J^{*^2}+p^* \\
&-2\tilde{\mu}\left(\epsilon^4\frac{\partial u^*}{\partial x^*}\left(\frac{\partial h^*}{\partial x^*}\right)^2-\epsilon^2\frac{\partial u^*}{\partial z^*}\frac{\partial h^*}{\partial x^*}-\epsilon^4\frac{\partial w^*}{\partial x^*}\frac{\partial h^*}{\partial x^*}+\epsilon^2\frac{\partial w^*}{\partial z^*}\right) \\
&=-\frac{\epsilon^3 h_0}{\rho\nu_0^2}\frac{\partial^2 h}{\partial x^2}(\sigma_0-\gamma T^*\Delta T)
\end{aligned} \tag{A.43}$$

Terms with ϵ^2,ϵ^3 and ϵ^4 will be canceled, however term with σ_0 will stay. As a result of this:

$$-\frac{k^2\Delta T^2}{\rho\rho_v\nu_0^2 L^2}J^{*^2}+p^*=-\frac{\epsilon^2 h_0}{\rho\nu_0^2}\frac{\partial^2 h}{\partial x^2}\sigma_0 \tag{A.44}$$

If $E = \frac{1}{\epsilon}\frac{k\Delta T}{\rho\nu_0 L}$, $\tilde{\rho} = \frac{1}{\epsilon^3}\frac{\rho_v}{\rho}$ and $Ca = \frac{1}{\epsilon^3}\frac{\rho\nu_0^2}{h_0\sigma_0}$:

$$p^* = \frac{E^2}{\tilde{\rho}} J^{*^2} - Ca^{-1}\frac{\partial^2 h^*}{\partial x^{*^2}} \tag{A.45}$$

Shear stress boundary condition is as following:

$$\bar{T}.\bar{n}.\bar{t} = \nabla\sigma.\bar{t} \tag{A.46}$$

Term $\bar{T}.\bar{n}.\bar{t}$ will be as following:

$$\bar{T}.\bar{n}.\bar{t} = -p\bar{I}.\bar{n}.\bar{t} + 2\mu\bar{\tau}.\bar{n}.\bar{t} \tag{A.47}$$

$\bar{I}.\bar{n}.\bar{t}$ will be 0 because $\bar{n}$ and $\bar{t}$ are orthogonal. In this case, $\bar{T}.\bar{n}.\bar{t}$ will be following:

$$\bar{T}.\bar{n}.\bar{t} = 2\mu\bar{\tau}.\bar{n}.\bar{t} \tag{A.48}$$

$\bar{\tau}.\bar{n}.\bar{t}$ will be as following:

$$\bar{\tau}.\bar{n}.\bar{t} = \frac{\left(\frac{\partial h}{\partial x}\left(\frac{\partial w}{\partial z} - \frac{\partial u}{\partial x}\right) + \left(\frac{1}{2} - \frac{1}{2}\left(\frac{\partial h}{\partial x}\right)^2\right)\left(\frac{\partial u}{\partial z} + \frac{\partial w}{\partial x}\right)\right)}{1 + \left(\frac{\partial h}{\partial x}\right)^2} \tag{A.49}$$

$\nabla\sigma.\bar{t}$ will be as following:

$$\nabla\sigma.\bar{t} = -\frac{\gamma\left(\frac{\partial T}{\partial x} + \frac{\partial T}{\partial z}\frac{\partial h}{\partial x}\right)}{\sqrt{1 + \left(\frac{\partial h}{\partial x}\right)^2}} \tag{A.50}$$

When all the terms are plugged, shear stress boundary condition will be as following:

$$2\mu\frac{\left(\frac{\partial h}{\partial x}\left(\frac{\partial w}{\partial z}-\frac{\partial u}{\partial x}\right)+\left(\frac{1}{2}-\frac{1}{2}\left(\frac{\partial h}{\partial x}\right)^2\right)\left(\frac{\partial u}{\partial z}+\frac{\partial w}{\partial x}\right)\right)}{1+\left(\frac{\partial h}{\partial x}\right)^2}=-\frac{\gamma\left(\frac{\partial T}{\partial x}+\frac{\partial T}{\partial z}\frac{\partial h}{\partial x}\right)}{\sqrt{1+\left(\frac{\partial h}{\partial x}\right)^2}} \tag{A.51}$$

If variables in A.1-A.3 are substituted into equation A.51:

$$\begin{aligned}&2\mu_0\tilde{\mu}\frac{\left(\epsilon\frac{\nu_0}{a_0h_0}\frac{\partial h^*}{\partial x^*}\left(\frac{\partial w^*}{\partial z^*}-\frac{\partial u^*}{\partial x^*}\right)+\left(\frac{1}{2}-\frac{1}{2}\epsilon^2\left(\frac{\partial h^*}{\partial x^*}\right)^2\right)\left(\frac{\nu_0}{h_0^2}\frac{\partial u^*}{\partial z^*}+\frac{\nu_0}{a_0^2}\frac{\partial w^*}{\partial x^*}\right)\right)}{1+\epsilon^2\left(\frac{\partial h^*}{\partial x^*}\right)^2}\\&=-\frac{\frac{\gamma\Delta T}{a_0}\left(\frac{\partial T^*}{\partial x^*}+\frac{\partial T^*}{\partial z^*}\frac{\partial h^*}{\partial x^*}\right)}{\sqrt{1+\epsilon^2\left(\frac{\partial h^*}{\partial x^*}\right)^2}}\end{aligned} \tag{A.52}$$

If equation A.52 is multiplied by $\frac{h_0^2}{\mu_0\tilde{\mu}\nu_0}$:

$$\begin{aligned}&2\frac{\left(\epsilon^2\frac{\partial h^*}{\partial x^*}\left(\frac{\partial w^*}{\partial z^*}-\frac{\partial u^*}{\partial x^*}\right)+\left(\frac{1}{2}-\frac{1}{2}\epsilon^2\left(\frac{\partial h^*}{\partial x^*}\right)^2\right)\left(\frac{\partial u^*}{\partial z^*}+\epsilon^2\frac{\partial w^*}{\partial x^*}\right)\right)}{1+\epsilon^2\left(\frac{\partial h^*}{\partial x^*}\right)^2}\\&=-\frac{\frac{\gamma\Delta Th_0}{\mu_0\tilde{\mu}\nu_0}\epsilon\left(\frac{\partial T^*}{\partial x^*}+\frac{\partial T^*}{\partial z^*}\frac{\partial h^*}{\partial x^*}\right)}{\sqrt{1+\epsilon^2\left(\frac{\partial h^*}{\partial x^*}\right)^2}}\end{aligned} \tag{A.53}$$

Term with ϵ^2 will be canceled:

$$\frac{\partial u^*}{\partial z^*}=-\frac{M}{\tilde{\mu}}\left(\frac{\partial T^*}{\partial x^*}+\frac{\partial T^*}{\partial z^*}\frac{\partial h^*}{\partial x^*}\right) \tag{A.54}$$

Where $M=\frac{\gamma\Delta Th_0}{\mu_0\nu_0}\epsilon$.

Energy boundary condition is as following:

$$J\left(L+\frac{1}{2}\left(\frac{J}{\rho_v}\right)^2\right)=-k\nabla T.\bar{n} \tag{A.55}$$

Right hand side of the equation A.55 will be as following:

$$-k\nabla T.\bar{n} = \frac{k\frac{\partial h}{\partial x}\frac{\partial T}{\partial x} - k\frac{\partial T}{\partial z}}{\sqrt{1+\left(\frac{\partial h}{\partial x}\right)^2}} \tag{A.56}$$

As a result, energy boundary will be following:

$$J\left(L + \frac{1}{2}\left(\frac{J}{\rho_v}\right)^2\right) = \frac{k\frac{\partial h}{\partial x}\frac{\partial T}{\partial x} - k\frac{\partial T}{\partial z}}{\sqrt{1+\left(\frac{\partial h}{\partial x}\right)^2}} \tag{A.57}$$

If variables in A.1-A.3 are substituted into equation A.57:

$$\frac{k\Delta T}{h_0}J^* + \frac{1}{2}\frac{k^3\Delta T^3}{\rho_v^2 h_0^3 L^3}J^{*3} = \frac{\frac{kh_0\Delta T}{a_0^2}\frac{\partial h^*}{\partial x^*}\frac{\partial T^*}{\partial x^*} - \frac{k\Delta T}{h_0}\frac{\partial T^*}{\partial z^*}}{\sqrt{1+\epsilon^2\left(\frac{\partial h^*}{\partial x^*}\right)^2}} \tag{A.58}$$

If equation A.58 is multiplied by $\frac{h_0}{k\Delta T}$:

$$J^* + \frac{1}{2}\frac{k^2\Delta T^2}{\rho_v^2 h_0^2 L^3}J^{*3} = \frac{\epsilon^2\frac{\partial h^*}{\partial x^*}\frac{\partial T^*}{\partial x^*} - \frac{\partial T^*}{\partial z^*}}{\sqrt{1+\epsilon^2\left(\frac{\partial h^*}{\partial x^*}\right)^2}} \tag{A.59}$$

If terms with ϵ^2 is canceled and it is assumed that $\frac{k^2\Delta T^2}{\rho_v^2 h_0^2 L^3} << 1$:

$$J^* = -\frac{\partial T^*}{\partial z^*} \tag{A.60}$$

Assumption $\frac{k^2\Delta T^2}{\rho_v^2 h_0^2 L^3} << 1$ is made by looking at articles [1, 8], which are used for establishing current model. Constitutive equation for evaporative mass flux is as following:

$$K^*J = T_I - T_S \tag{A.61}$$

If variables in A.1-A.3 are substituted into equation A.61:

$$\frac{K^* k \Delta T}{h_0 L} J^* = \Delta T T^* \tag{A.62}$$

ΔT will be canceled:

$$K J^* = T^* \tag{A.63}$$

Where K is $\frac{K^* k}{h_0 L}$. Boundary condition for particle concentration at $z = h$ is as following:

$$D_c(\bar{n}.\nabla c) = \frac{J}{\rho} c \tag{A.64}$$

If terms in equation A.64 are opened, equation A.64 will be as following:

$$D_c \left(\frac{-\frac{\partial h}{\partial x}}{\sqrt{1 + \left(\frac{\partial h}{\partial x}\right)^2}} \frac{\partial c}{\partial x} + \frac{1}{\sqrt{1 + \left(\frac{\partial h}{\partial x}\right)^2}} \frac{\partial c}{\partial z} \right) = \frac{J}{\rho} c \tag{A.65}$$

If variables in A.1-A.3 are substituted into equation A.65:

$$D_c \left(\frac{h_0 c_i}{a_0^2} \frac{-\frac{\partial h^*}{\partial x^*}}{\sqrt{1 + \epsilon^2 \left(\frac{\partial h^*}{\partial x^*}\right)^2}} \frac{\partial c^*}{\partial x^*} + \frac{c_i}{h_0} \frac{1}{\sqrt{1 + \epsilon^2 \left(\frac{\partial h^*}{\partial x^*}\right)^2}} \frac{\partial c^*}{\partial z^*} \right) = \frac{c_i k \Delta T}{\rho h_0 L} J^* c^* \tag{A.66}$$

If equation A.66 is multiplied by $\frac{a_0^2}{h_0 c_i}$:

$$D_c \left(\frac{-\frac{\partial h^*}{\partial x^*}}{\sqrt{1 + \epsilon^2 \left(\frac{\partial h^*}{\partial x^*}\right)^2}} \frac{\partial c^*}{\partial x^*} + \frac{1}{\epsilon^2} \frac{1}{\sqrt{1 + \epsilon^2 \left(\frac{\partial h^*}{\partial x^*}\right)^2}} \frac{\partial c^*}{\partial z^*} \right) = \frac{1}{\epsilon^2} \frac{k \Delta T}{\rho L} \frac{J^*}{\rho} c^* \tag{A.67}$$

Terms $\epsilon^2 \left(\frac{\partial h^*}{\partial x^*}\right)^2$ can be canceled:

$$D_c \left(-\frac{\partial h^*}{\partial x^*}\frac{\partial c^*}{\partial x^*} + \frac{1}{\epsilon^2}\frac{\partial c^*}{\partial z^*} \right) = \frac{1}{\epsilon^2}\frac{k\Delta T}{\rho L}\frac{J^*}{\rho}c^* \tag{A.68}$$

Boundary condition for particle deposition at $z = 0$ is as following:

$$D_c(\bar{n}.\nabla c) = -k_d c \tag{A.69}$$

For equation A.69, unit normal vector at solid plate is taken as $\bar{n} = (0, -1)$:

$$-D_c\frac{\partial c}{\partial z} = -k_d c \tag{A.70}$$

If variables in A.1-A.3 are substituted into equation A.70:

$$\frac{D_c c_i}{h_0}\frac{\partial c^*}{\partial z^*} = k_d c^* \tag{A.71}$$

$$\frac{\partial c^*}{\partial z^*} = Da\epsilon c^* \tag{A.72}$$

Where Da is $\frac{k_d a_0}{D_c}$. After scaling of governing equations, constitutive equations and boundary conditions, application of rapid vertical diffusion to related particle concentration equations and boundary conditions can be presented.

A.2 Rapid Vertical Diffusion Assumption

Nondimensional version of expansion shown in second chapter in equation 2.47 will be as following:

$$c^* = c_0^* + \epsilon^2 Pe c_1^* \tag{A.73}$$

This expansion will be applied equations A.25, A.68 and A.72. After this application, equation A.25 will be as following:

$$\begin{aligned}&\frac{\partial c_0^*}{\partial t^*}+\epsilon^2 Pe\frac{\partial c_1^*}{\partial t^*}+u^*\frac{\partial c_0^*}{\partial x^*}+\epsilon^2 Peu^*\frac{\partial c_1^*}{\partial x^*}+w^*\frac{\partial c_0^*}{\partial z^*}+\epsilon^2 Pew^*\frac{\partial c_1^*}{\partial z^*}\\&=\frac{1}{Pe}\left(\frac{\partial^2 c_0^*}{\partial x^{*^2}}+\epsilon^2 Pe\frac{\partial^2 c_1^*}{\partial x^{*^2}}+\frac{1}{\epsilon^2}\frac{\partial^2 c_0^*}{\partial z^{*^2}}+Pe\frac{\partial^2 c_1^*}{\partial z^{*^2}}\right)\end{aligned}\tag{A.74}$$

In equation A.74, terms with $\epsilon^2 Pe$, ϵ^2, first and second derivative of c_0 can be canceled:

$$\frac{\partial c_0^*}{\partial t^*}+u^*\frac{\partial c_0^*}{\partial x^*}=\frac{1}{Pe}\frac{\partial^2 c_0^*}{\partial x^{*^2}}+\frac{\partial^2 c_1^*}{\partial z^{*^2}}\tag{A.75}$$

If equation A.75 is averaged in h:

$$\frac{1}{h}\int_0^h\frac{\partial c_0^*}{\partial t^*}dz+\frac{1}{h}\int_0^h u^*\frac{\partial c_0^*}{\partial x^*}dz=\frac{1}{Pe}\frac{1}{h}\int_0^h\frac{\partial^2 c_0^*}{\partial x^{*^2}}dz+\frac{1}{h}\int_0^h\frac{\partial^2 c_1^*}{\partial z^{*^2}}dz\tag{A.76}$$

As a result of averaging:

$$\frac{\partial c_0^*}{\partial t^*}+\bar{u^*}\frac{\partial c_0^*}{\partial x^*}=\frac{1}{Pe}\frac{\partial^2 c_0^*}{\partial x^{*^2}}+\frac{1}{h}\left(\left(\frac{\partial c_1^*}{\partial z^*}\right)_{z=h}-\left(\frac{\partial c_1^*}{\partial z^*}\right)_{z=0}\right)\tag{A.77}$$

Where $\bar{u^*}$ is nondimensional height averaged velocity in x direction. $\left(\frac{\partial c_1^*}{\partial z^*}\right)_{z=h}$ and $\left(\frac{\partial c_1^*}{\partial z^*}\right)_{z=0}$ can be found from boundary conditions at $z=h$ and $z=0$. Application of expansion to equations A.68 and A.72 will give first derivative of c_1^* in terms of z at indicated boundaries. After indicated application, equation A.68 will be as following:

$$\begin{aligned}&-\frac{\partial h^*}{\partial x^*}\frac{\partial c_0^*}{\partial x^*}-\epsilon^2 Pe\frac{\partial h^*}{\partial x^*}\frac{\partial c_1^*}{\partial x^*}+\frac{1}{\epsilon^2}\frac{\partial c_0^*}{\partial z^*}+Pe\frac{\partial c_1^*}{\partial z^*}\\&=\frac{1}{\epsilon^2}\frac{k\Delta T}{D_c\rho L}\frac{J^*}{\rho}c_0^*+\epsilon^2 Pe\frac{1}{\epsilon^2}\frac{k\Delta T}{D_c\rho L}\frac{J^*}{\rho}c_1^*\end{aligned}\tag{A.78}$$

In equation A.78, $\frac{1}{\epsilon^2}\frac{k\Delta T}{D_c \rho L} = EPe$. In addition, if equation equation A.78 is divided by Pe :

$$-\frac{1}{Pe}\frac{\partial h^*}{\partial x^*}\frac{\partial c_0^*}{\partial x^*} - \epsilon^2\frac{\partial h^*}{\partial x^*}\frac{\partial c_1^*}{\partial x^*} + \frac{1}{\epsilon^2 Pe}\frac{\partial c_0^*}{\partial z^*} + \frac{\partial c_1^*}{\partial z^*} = EJ^* c_0^* + E\epsilon^2 PeJ^* c_1^* \quad \text{(A.79)}$$

In equation A.79, term with ϵ^2, first derivative of c_0^* in terms of z can be canceled. In addition, if E is taken as $O(1)$ or lesser, second term in the right hand side of the equation can be canceled. As a result of this:

$$\left(\frac{\partial c_1^*}{\partial z^*}\right)_{z=h} = EJ^* c_0^* + \frac{1}{Pe}\frac{\partial h^*}{\partial x^*}\frac{\partial c_0^*}{\partial x^*} \quad \text{(A.80)}$$

If expansion is applied to equation A.68,result will be as following:

$$\frac{\partial c_0^*}{\partial z^*} + \epsilon^2 Pe\frac{\partial c_1^*}{\partial z^*} = Da\epsilon c_0^* + \epsilon^2 PeDa\epsilon c_1^* \quad \text{(A.81)}$$

If equation A.81 is divided by $\epsilon^2 Pe$:

$$\frac{1}{\epsilon^2 Pe}\frac{\partial c_0^*}{\partial z^*} + \frac{\partial c_1^*}{\partial z^*} = \frac{Da}{\epsilon Pe}(c_0^* + \epsilon^2 Pec_1^*) \quad \text{(A.82)}$$

In equation A.82, first derivative of c_0^* in terms of z can be canceled. In addition, if $\frac{Da}{\epsilon Pe}$ is taken as $O(1)$ or less, $\epsilon^2 Pec_1^*$ can be canceled. As a result of this:

$$\left(\frac{\partial c_1^*}{\partial z^*}\right)_{z=0} = \frac{Da}{\epsilon Pe}c_0^* \quad \text{(A.83)}$$

If equations A.80 and A.83 are applied to equation A.77:

$$\frac{\partial c_0^*}{\partial t^*} + \bar{u^*}\frac{\partial c_0^*}{\partial x^*} = \frac{1}{Pe}\frac{\partial^2 c_0^*}{\partial x^{*2}} + \frac{1}{h}\left(\frac{1}{Pe}\frac{\partial h^*}{\partial x^*}\frac{\partial c_0^*}{\partial x^*} + EJ^* c_0^* - \frac{Da}{\epsilon Pe}c_0^*\right) \quad \text{(A.84)}$$

A.3 Deriving X-Component of Velocity

In the equations, height averaged x-component of velocity is required. Therefore in this part, it will be derived. Process will start with indefinite integration of nondimensional simplified Navier-Stokes x-momentum equation in 2.51. It contains second derivative of velocity's x-component in terms of z. Integrating twice this equation will give expression for u:

$$\int\int \frac{\partial^2 u}{\partial z^2} dz dz = \int\int \frac{1}{\tilde{\mu}} \frac{\partial p}{\partial x} dz dz \tag{A.85}$$

Simplified z-momentum equation 2.29 shows that pressure is not changing in z direction because first derivative of pressure in terms of z is equal to 0. Therefore it can be assumed p and $\frac{\partial p}{\partial x}$ does not depend on z. In this case, equation A.85 will be integrated in following way:

$$\frac{\partial u(x,z,t)}{\partial z} = \frac{\partial p}{\partial x} \frac{z}{\tilde{\mu}} + C_1 \tag{A.86}$$

$$u(x,z,t) = \frac{\partial p}{\partial x} \frac{z^2}{2\tilde{\mu}} + C_1 z + C_2 \tag{A.87}$$

p can be found from normal stress boundary condition equation 2.38, because, p is not changing in z direction:

$$p(x,t) = \frac{E^2}{\tilde{\rho}} J^2 - Ca^{-1} \frac{\partial^2 h}{\partial x^2} \tag{A.88}$$

Then derivative of pressure in terms of x will be as following:

$$\frac{\partial p}{\partial x} = \frac{2E^2}{\tilde{\rho}} J \frac{\partial J}{\partial x} - Ca^{-1} \frac{\partial^3 h}{\partial x^3} \tag{A.89}$$

It is known that $J = \frac{1}{K+h}$. Therefore:

$$\frac{\partial J}{\partial x} = -\frac{\partial h}{\partial x}\frac{1}{(K+h)^2} \tag{A.90}$$

As a result of this:

$$\frac{\partial p}{\partial x} = -\frac{2E^2}{\tilde{\rho}}\frac{\partial h}{\partial x}\frac{1}{(K+h)^3} - Ca^{-1}\frac{\partial^3 h}{\partial x^3} \tag{A.91}$$

After finding $\frac{\partial p}{\partial x}$, integration constants C_1 and C_2 in equation A.87 can be found. At $z = h$, first derivative of u in terms of z is as following:

$$\frac{\partial u(x,h,t)}{\partial z} = \frac{\partial p}{\partial x}\frac{h}{\tilde{\mu}} + C_1 \tag{A.92}$$

$\frac{\partial u(x,h,t)}{\partial z}$ can be found from shear stress boundary condition equation 2.39 and as a result of this:

$$\frac{\partial p}{\partial x}\frac{h}{\tilde{\mu}} + C_1 = -\frac{M}{\tilde{\mu}}\left(\left(\frac{\partial T}{\partial x}\right)_{z=h} + \left(\frac{\partial T}{\partial z}\right)_{z=h}\frac{\partial h}{\partial x}\right) \tag{A.93}$$

$$C_1 = -\frac{\partial p}{\partial x}\frac{h}{\tilde{\mu}} - \frac{M}{\tilde{\mu}}\left(\left(\frac{\partial T}{\partial x}\right)_{z=h} + \left(\frac{\partial T}{\partial z}\right)_{z=h}\frac{\partial h}{\partial x}\right) \tag{A.94}$$

Temperature is calculated and can be found in equation 2.53, therefore, its derivatives can be calculated:

$$\frac{\partial T}{\partial x} = \frac{\partial h}{\partial x}\frac{z}{(K+h)^2} \tag{A.95}$$

$$\frac{\partial T}{\partial z} = -\frac{1}{K+h} \tag{A.96}$$

Then, C_1 will be as following:

$$C_1 = -\frac{\partial p}{\partial x}\frac{h}{\tilde{\mu}} - \frac{M}{\tilde{\mu}}\left(\frac{h}{(K+h)^2}\frac{\partial h}{\partial x} - \frac{1}{K+h}\frac{\partial h}{\partial x}\right) \tag{A.97}$$

$$C_1 = -\frac{\partial p}{\partial x}\frac{h}{\tilde{\mu}} + \frac{MK}{\tilde{\mu}(K+h)^2}\frac{\partial h}{\partial x} \tag{A.98}$$

After finding C_1, u can be updated:

$$u(x,z,t) = \frac{\partial p}{\partial x}\frac{z^2}{2\tilde{\mu}} - \frac{\partial p}{\partial x}\frac{zh}{\tilde{\mu}} + \frac{MKz}{\tilde{\mu}(K+h)^2}\frac{\partial h}{\partial x} + C_2 \tag{A.99}$$

$$u(x,z,t) = \frac{\partial p}{\partial x}\left(\frac{z^2}{2\tilde{\mu}} - \frac{zh}{\tilde{\mu}}\right) + \frac{MKz}{\tilde{\mu}(K+h)^2}\frac{\partial h}{\partial x} + C_2 \tag{A.100}$$

At $z = 0$, $u(x,0,t) = \beta\frac{\partial u}{\partial z}$. If equation A.100 is evaluated at $z = 0$:

$$u(x,0,t) = \beta\left(\frac{\partial u}{\partial z}\right)_{z=0} = C_2 \tag{A.101}$$

Expression for $\frac{\partial u}{\partial z}$ must be found and evaluated at $z = 0$ to find C_2. This expression is already derived in equation A.86 and C_1 is also found. As a result of this:

$$\frac{\partial u(x,z,t)}{\partial z} = \frac{\partial p}{\partial x}\frac{z}{\tilde{\mu}} - \frac{\partial p}{\partial x}\frac{h}{\tilde{\mu}} + \frac{MK}{\tilde{\mu}(K+h)^2}\frac{\partial h}{\partial x} \tag{A.102}$$

$$\left(\frac{\partial u}{\partial z}\right)_{z=0} = -\frac{\partial p}{\partial x}\frac{h}{\tilde{\mu}} + \frac{MK}{\tilde{\mu}(K+h)^2}\frac{\partial h}{\partial x} \tag{A.103}$$

After finding this, C_2 can be found:

$$C_2 = -\frac{\partial p}{\partial x}\frac{\beta h}{\tilde{\mu}} + \frac{MK\beta}{\tilde{\mu}(K+h)^2}\frac{\partial h}{\partial x} \tag{A.104}$$

Finally full expression of u will be as following:

$$\begin{aligned} u(x,z,t) &= \frac{\partial p}{\partial x}\left(\frac{z^2}{2\tilde{\mu}} - \frac{zh}{\tilde{\mu}}\right) + \frac{MKz}{\tilde{\mu}(K+h)^2}\frac{\partial h}{\partial x} - \frac{\partial p}{\partial x}\frac{\beta h}{\tilde{\mu}} + \frac{MK\beta}{\tilde{\mu}(K+h)^2}\frac{\partial h}{\partial x} \\ &= \frac{\partial p}{\partial x}\left(\frac{z^2}{2\tilde{\mu}} - \frac{h(z+\beta)}{\tilde{\mu}}\right) + \frac{MK(z+\beta)}{\tilde{\mu}(K+h)^2}\frac{\partial h}{\partial x} \end{aligned} \tag{A.105}$$

After deriving u, height averaged version of it can be found:

$$\begin{aligned}
\bar{u} &= \frac{1}{h}\int_0^h u(x,z,t)dz \\
&= \frac{1}{h}\int_0^h \left(\frac{\partial p}{\partial x}\left(\frac{z^2}{2\tilde{\mu}} - \frac{h(z+\beta)}{\tilde{\mu}}\right) + \frac{MK(z+\beta)}{\tilde{\mu}(K+h)^2}\frac{\partial h}{\partial x}\right)dz \\
&= \frac{1}{h}\frac{\partial p}{\partial x}\left(\frac{h^3}{6\tilde{\mu}} - \frac{h(\frac{h^2}{2}+\beta h)}{\tilde{\mu}}\right) + \frac{MK(\frac{h^2}{2}+\beta h)}{\tilde{\mu}(K+h)^2}\frac{\partial h}{\partial x} \\
&= -\frac{\partial p}{\partial x}\frac{h}{\tilde{\mu}}\left(\frac{h}{3}+\beta\right) + \frac{MK(\frac{h}{2}+\beta)}{\tilde{\mu}(K+h)^2}\frac{\partial h}{\partial x}
\end{aligned} \tag{A.106}$$

If $\frac{\partial p}{\partial x}$ is applied to equation A.106:

$$\bar{u} = 2\frac{\partial h}{\partial x}\frac{E^2 h\left(\frac{h}{3}+\beta\right)}{\tilde{\mu}\tilde{\rho}(K+h)^3} + \frac{\partial^3 h}{\partial x^3}\frac{h\left(\frac{h}{3}+\beta\right)}{\tilde{\mu}Ca} + \frac{\partial h}{\partial x}\frac{MK\left(\frac{h}{2}+\beta\right)}{\tilde{\mu}(K+h)^2} \tag{A.107}$$

Bibliography

[1] D. M. Anderson and S. H. Davis, "The spreading of volatile liquid droplets on heated surfaces," *Physics of Fluids*, vol. 7, no. 2, pp. 248 – 265, 1995.

[2] R. D. Deegan, O. Bakajin, T. F. Dupont, G. Huber, S. R. Nagel, and T. A. Witten, "Capillary flow as the cause of ring stains from dried liquid drops," *Nature*, vol. 389, pp. 827 – 829, 1997.

[3] M. Singh, H. M. Haverinen, P. Dhagat, and G. E. Jabbour, "Inkjet printing—process and its applications," *Advanced Materials*, vol. 22, pp. 673–685, 2010.

[4] M. Chopra, L. Li, H. Hu, M. A. Burns, and R. G. Larson, "Dna molecular configurations in an evaporating droplet near a glass surface," *Journal of Rheology*, vol. 47, no. 5, pp. 1111–1132, 2003.

[5] S. Ni, J. Leemann, I. Buttinoni, L. Isa, and H. Wolf, "Programmable colloidal molecules from sequential capillarity-assisted particle assembly," *Science Advances*, vol. 2, no. 4, 2016.

[6] N. Murisic and L. Kondic, "On evaporation of sessile drops with moving contact lines," *Journal of fluid mechanics*, vol. 679, p. 219–246, 2011.

[7] R. D. Deegan, "Pattern formation in drying drops," *Physical review E*, vol. 61, no. 1, pp. 475–485, 2000.

[8] J. P. Burelbach, S. G. Bankoff, and S. H. Davis, "Nonlinear stability of evaporating/condensing liquid films," *Journal of Fluid Mechanics*, vol. 195, pp. 463 – 494, 1988.

[9] P. K. Kundu, I. M. Cohen, and D. R. Dowling, *Fluid Mechanics*. Academic Press, 5 ed., 2012.

[10] H. Hu and R. G. Larson, "Marangoni effect reverses coffee-ring depositions," *The Journal of Physical Chemistry B*, vol. 110, no. 14, pp. 7090–7094, 2006.

[11] P.-G. D. Gennes, F. Brochard-Wyart, D. Quéré, *et al.*, *Capillarity and wetting phenomena: drops, bubbles, pearls, waves*. Alex Reisinger, Transl., Springer, 2004.

[12] Y.-J. Sheng, S. Jiang, and H.-K. Tsao, "Effects of geometrical characteristics of surface roughness on droplet wetting," *The Journal of Chemical Physics*, vol. 127, no. 23, 2007.

[13] E. B. Dussan V., "On the spreading of liquids on solid surfaces: static and dynamic contact lines," *Annual Review of Fluid Mechanics*, vol. 11, pp. 371–400, 1979.

[14] P. Ehrhard and S. H. Davis, "Non-isothermal spreading of liquid drops on horizontal plates," *Journal of Fluid Mechanics*, vol. 229, pp. 365 – 388, 1991.

[15] L. A. Spielman and S. K. Friedlander, "Role of the electrical double layer in particle deposition by convective diffusion," *Journal of Colloid and Interface Science*, vol. 46, no. 1, pp. 22–31, 1974.

[16] E. B. Dussan V., "The moving contact line: the slip boundary condition," *Journal of Fluid Mechanics*, vol. 77, no. 4, pp. 665 – 684, 1976.

[17] V. S. Ajaev, "Spreading of thin volatile liquid droplets on uniformly heated surfaces," *Journal of fluid mechanics*, vol. 528, p. 279–296, 2005.

[18] T. A. Nguyen, A. V. Nguyen, M. A. Hampton, Z. P. Xu, L. Huang, and V. Rudolph, "Theoretical and experimental analysis of droplet evaporation on solid surfaces," *Chemical Engineering Science*, vol. 69, p. 522–529, 2012.

[19] A. Amini and G. M. Homsy, "Evaporation of liquid droplets on solid substrates. i. flat substrate with pinned or moving contact line," *Physical Review Fluids*, vol. 2, no. 4, 2017.

[20] H. Hu and R. G. Larson, "Analysis of the microfluid flow in an evaporating sessile droplet," *Langmuir*, vol. 21, no. 9, pp. 3963–3971, 2005.

[21] H. Hu and R. G. Larson, "Evaporation of a sessile droplet on a substrate," *The Journal of Physical Chemistry B*, vol. 106, no. 6, pp. 1334–1344, 2002.

[22] R. D. Deegan, O. Bakajin, T. F. Dupont, G. Huber, S. R. Nagel, and T. A. Witten, "Contact line deposits in an evaporating drop," *Physical review E*, vol. 62, no. 1, pp. 756–765, 2000.

[23] B. J. Fischer, "Particle convection in an evaporating colloidal droplet," *Langmuir*, vol. 18, no. 1, pp. 60–67, 2002.

[24] Y. O. Popov, "Evaporative deposition patterns: Spatial dimensions of the deposit," *Physical review E*, vol. 71, no. 3, 2005.

[25] E. Widjaja and M. T. Harris, "Particle deposition study during sessile drop evaporation," *AIChE Journal*, vol. 54, no. 9, pp. 2250 – 2260, 2008.

[26] Y. Y. Tarasevich, I. V. Vodolazskaya, and O. P. Isakova, "Desiccating colloidal sessile drop: dynamics of shape and concentration," *Colloid and Polymer Science*, vol. 289, no. 9, p. 1015–1023, 2011.

[27] A. K. Thokchom, A. Gupta, P. J. Jaijus, and A. Singh, "Analysis of fluid flow and particle transport in evaporating droplets exposed to infrared heating," *International Journal of Heat and Mass Transfer*, vol. 68, p. 67–77, 2014.

[28] G. Karapetsas, K. C. Sahu, and O. K. Matar, "Evaporation of sessile droplets laden with particles and insoluble surfactants," *Langmuir*, vol. 32, pp. 6871 – 6881, 2016.

[29] F. Wang, M. Wu, X. Man, and Q. Yuan, "Formation of deposition patterns induced by the evaporation of the restricted liquid," *Langmuir*, vol. 36, no. 29, pp. 8520–8526, 2020.

[30] C. Zhang and P. Akcora, "Evaporation controlled particle patterns in a polymer droplet," *Rsc Advances*, vol. 7, no. 30, pp. 18321–18326, 2017.

[31] T. Pham and S. Kumar, "Drying of droplets of colloidal suspensions on rough substrates," *Langmuir*, vol. 33, no. 38, pp. 10061–10076, 2017.

[32] I. M. Krieger and T. J. Dougherty, "A mechanism for non-newtonian flow in suspensions of rigid spheres," *Transactions of the Society of Rheology*, vol. 3, pp. 137 – 152, 1959.

[33] H. A. Barnes, "The yield stress—a review or '$\pi\alpha\nu\tau\alpha\ \rho\epsilon\iota$'—everything flows?," *Journal of Non-Newtonian Fluid Mechanics*, vol. 81, pp. 133 – 178, 1999.

[34] G. Karapetsas, R. V. Craster, and O. K. Matar, "On surfactant-enhanced spreading and superspreading of liquid drops on solid surfaces," *Journal of Fluid Mechanics*, vol. 670, pp. 5 – 37, 2011.

[35] O. E. Jensen and J. B. Grotberg, "The spreading of heat or soluble surfactant along a thin liquid film," *Physics of Fluids A: Fluid Dynamics*, vol. 5, no. 1, pp. 58 – 68, 1993.

[36] A. Gilat and V. Subramaniam, *Numerical Methods for Engineers and Scientists: An Introduction with Applications using MATLAB®*. Wiley, 3 ed., 2014.

[37] S. C. Chapra and R. P. Canale, *Numerical Methods for Engineers*. McGraw-Hill Education, 7 ed., 2015.

[38] J. W. Thomas, *Numerical Partial Differential Equations: Finite Difference Methods*. Springer, 1995.